

Gravity modeling: Calculations based on porosity-density context

by

Anne Øvreeide

MASTER THESIS IN MARINE GEOLOGY AND GEOPHYSICS

June 2010



Department of Earth Science

University of Bergen

Abstract

A normal way to model the gravity from a layered model is to determine the densities from the velocities, and then adjusting the densities within acceptable ranges to get a satisfactory fit with the observed gravity. In this thesis the densities are determined from knowledge of lithology and porosity. A grid method is developed, where the 2D earth model is gridded in x- and z-direction, and the density of each grid cell is determined by the lithology and porosity in the cell's four corners.

The grid method was tested on some synthetic models, an OBS-line from the Vøring margin and two seismic sections from the Viking Graben in the North Sea. Different scenarios, such as the presence of overpressure, erosion or sill were modeled to test how they affect the gravity field and if their contribution could be significant.

The synthetic models show that the grid method gives a more detailed result of the gravity when modeling the sedimentary upper structures than if the modeling is done with constant densities. In the case of overpressure, the value of the gravity decreases above the area of overpressure. A more significant change may happen when erosion in an area is present. The value of gravity increases over the area compared to if erosion was not accounted for. If sill layers are present, the thickness of the sill is often so thin that it will give no significant contribution to the gravity field.

The gravity calculated along the OBS-line shows similar trends when using the grid method as using the densities determined from the seismic P-velocities, but there are some local differences. There is however a big gap between the calculated and observed gravity. This can be reduced by correcting the depth to Moho by using Cordell & Henderson's iterative method, and further reduced by changing the density in certain key layers and/or by making the mantle inhomogeneous.

The gravity modeled from the two interpreted seismic sections has trends that mainly reflect the varying depth to basement. The depth to Moho was calculated by Cordell & Henderson's method to make a good fit between the observed and calculated gravity and a realistic geometry of the Moho. This method was compared to Airy's isostasy method of calculating the Moho. The Cordell & Henderson's method made a better fit between the observed and calculated gravity, indicating that the crust is not in isostatic equilibrium in the area. Flexural response of the lithosphere due to sediment loading may explain the calculated lateral change in lithostatic pressure below Moho.

Acknowledgements

This thesis is a 30 ECTS thesis and was performed during 20 weeks at the Department of Earth Sciences, University of Bergen, under supervision by Associate Professor Atle Austegard.

I would first of all like to thank my supervisor Atle Austegard for good guidance and for always having his door open. I appreciate the help from Trond Kvarven, who helped me with the seismic data and maps. Further thanks to fellow students for good conversations and help during this period.

I also give great gratitude to my roommates Ragnhild, Stina and Kari for the nice evenings and the huge support they give.

Finally, I want to thank my family for always being there, supporting me both morally and economically.

Anne Øvreeide

Bergen, June 2010

Contents

Chapter 1: Introduction	1
Chapter 2: Gravity modeling	3
2.1 General.....	3
2.2 Polygon method.....	5
2.3 Parker’s method.....	7
2.4 Cordell & Henderson’s method.....	8
2.5 The grid method.....	9
2.5.1 Porosity and density based on lithology.....	9
2.5.2 Porosity and density adjusted by effective pressure.....	10
2.5.3 Gridding.....	13
Chapter 3: Testing the grid method	17
3.1 General.....	17
3.2 Comparing the grid method to other methods.....	17
3.2.1 Flat model.....	19
3.2.2. Dipping model.....	20
3.2.3 Synthetic “realistic” model.....	21
3.3 Grid size.....	21
3.4 Effekt of compensating for effective pressure.....	23
3.5 Influence of overpressure; an example.....	24
3.6 Influence of erosion; an example.....	27
Chapter 4: Grid method applied on an interpreted crustal section on Vøring	33
4.1 General	33
4.2 Calculating gravity using the grid method and given lithologies.....	35
4.3 Adjustments of Moho using Cordell & Henderson’s method.....	39
4.4 Other possible changes of the model that can decrease the difference between modeled and observed gravity.....	43
Chapter 5: Grid method applied on two seismic sections from the North Sea	49
5.1 General.....	49
5.2 Interpretation.....	49
5.3 Lithology and velocity.....	58
5.3.1 Lithology.....	58
5.3.2 Velocity.....	59
5.4 The depth model, density grid and calculated gravity.....	64

5.5 The observed gravity.....	68
5.6 Cordell & Henderson-calculated Moho and comparison with published Moho in the area.....	70
Chapter 6: Summary and discussion.....	85
References.....	89
Appendix A: Some MATLAB programs used in the modeling.....	93

Chapter 1: Introduction

The purpose of the Bouguer-anomaly is to find the density variations of the geology below a datum, without having the effects of latitude or topography (Musset, 2000).

Bouguer correction Δg_B in land areas is found by calculating the gravity attraction from the masses above a datum (usually the sea-level). This is subtracted from the observed gravity, and the result is a field that represents the density distribution below the datum. In marine areas, the water layer is substituted by a layer of sediments which have density of average of the sediments. The Bouguer anomaly is often used in a qualitative way. It is locally usually low over sedimentary basins, and high over basement highs. Variation in Moho-depth gives more regional effects, and is often used to localize the ocean-continental boundary.

We can consider the observed gravity field as a sum of the field from the more shallow structures, g_s , and the deeper ones, g_d . If the upper structures are known (for example from seismic and boreholes), g_s can be calculated, and the gravity field from the deeper structures (for example Moho) may be estimated by $g_d = g_{obs} - g_s$. If we assume that the density of the crystalline crust and mantle is constant, and the depth to the Moho is known at one point (anchor point), we can model the topography of the Moho along the profile, see figure 1.1.

One method to do this is by using the Bouguer plate formula by iteration:

$$\Delta g = 2\pi G \Delta \rho \Delta h$$

Δg is the difference between observed gravity and the modeled Bouguer corrected gravity

$\Delta \rho = (\rho_m - \rho_c)$, ρ_m is the density of the mantle and ρ_c is the density of the crust

Δh is the vertical adjustment of Moho

Then the gravity of the new model is calculated, and the procedure repeated until the change of the model is below a given level.

In this thesis, different ways to model g_s and Moho are used, and a “new” grid method based on lithology- and porosity parameters is tested.

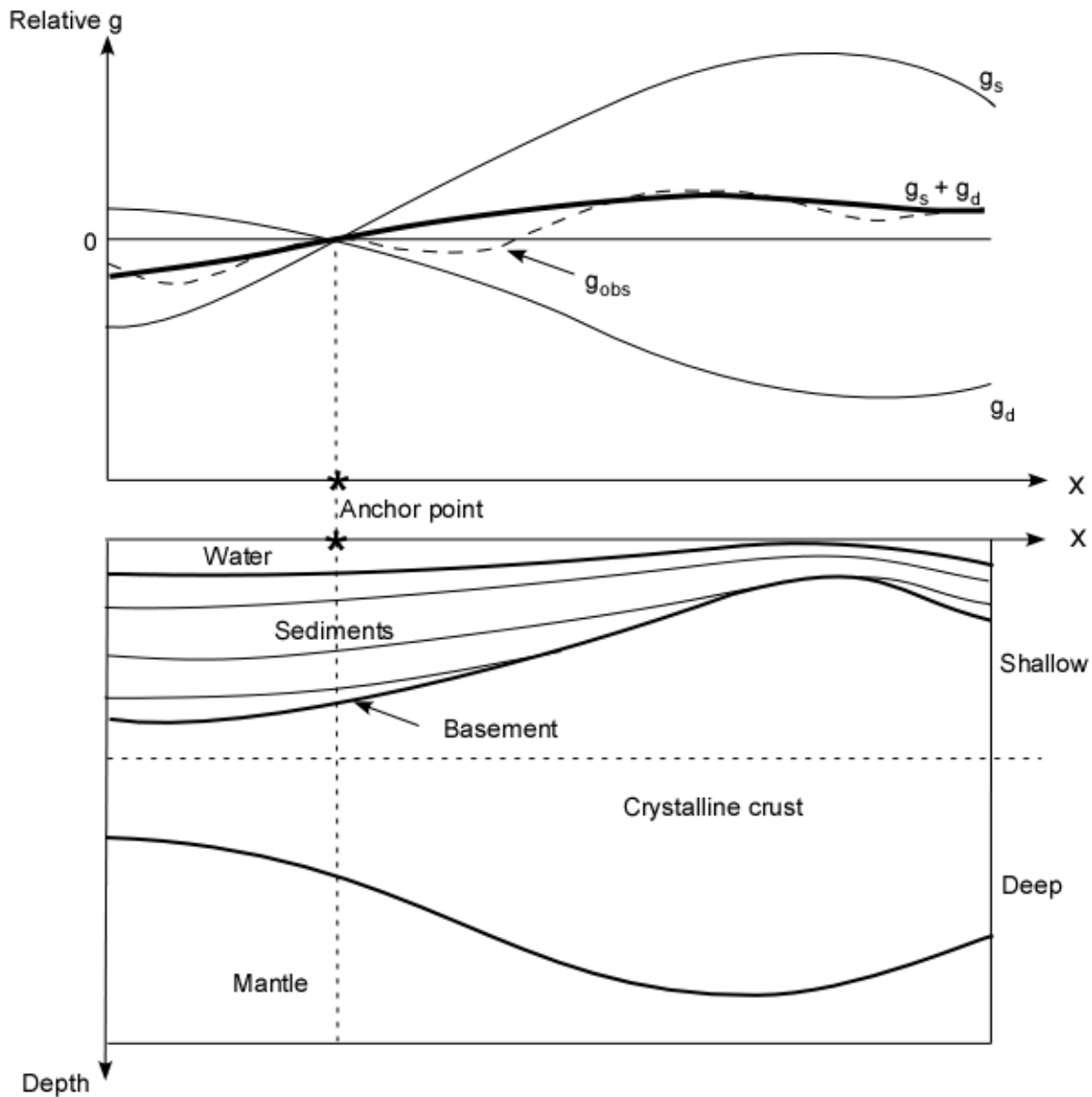


Figure 1.1: The relative gravity of an arbitrary geological model. The upper figure shows the modeled gravity, g_d , of the deep structures, the shallow structures, g_s , and from the entire model, $g_s + g_d$. The relative gravity of the whole structure can then be compared with the observed gravity, shown as a dotted line.

Chapter 2: Gravity modeling

2.1 General

Gravity modeling has its base in Newton's law of universal gravitation.

The law states that every point mass attract every single other point mass by a force pointing along the line intersecting both points. The force is directly proportional to the product of the two masses and inversely proportional to the square of the distance between the point masses.

$$F = G \frac{m_1 \cdot m_2}{r^2}$$

F is the magnitude of the gravitational force between the two point masses

G is the gravitational constant (approximately equal to $6.673 \times 10^{-11} \text{ N m}^2 \text{ kg}^{-2}$)

m_1 and m_2 are the first and second point mass

r is the distance between the two point masses

The gravitational acceleration has the unit m/s^2 , which is the SI unit for acceleration. However, the acceleration at various points on the earth does not differ that much and we use the unit mGal when we do gravity modeling. 1 mGal equals 10^{-5} m/s^2 .

In gravity modeling, the gravitational acceleration (g) is modeled, not the gravitational force. For a perfectly spherical Earth, with R_E as the radius and without any rotation, the acceleration would be,

$$g = \frac{F}{m_1} = \frac{GM_E}{R_E^2}$$

M_E is the mass of the Earth

R_E is the radius of the Earth

Since the reference Earth is a rotating ellipsoid, where the equatorial diameter is greater than the polar diameter, there need to be a correction for the latitude. The gravitational acceleration g is less at the equator because it is further away from the center of the Earth. Also because of its rotation, the Earth tends to fling bodies away from its rotation axis. The centrifugal force is dependent on the distance from the axis; the maximum is at the equator and decreases to zero at the poles.

Both effects vary with the latitude, λ , and can be combined in one formula; The international Gravity Formula (Musset, 2000):

$$g_{\lambda} = 978031(1 + 0.0053024 \sin^2 \lambda - 0.0000059 \sin^2 2\lambda) mGal$$

Forward and inverse modeling

Gravity modeling can be performed in two different ways; forward and inverse gravity modeling.

The forward modeling starts with an initial model for the geology of the area of interest. The model is made by using different available data, for example seismic data, borehole data and data from the field. Below Moho, the density is often assumed to be constant, which means that the gravity is only related to mass distributions shallower than the deepest point of the crust. After the initial model is made, densities (and porosity parameters) are set to the different layers. The gravity is then calculated from this model by using an appropriate algorithm. The next thing is to compare the observed and the calculated gravity. If there are differences between these two, the model has to be corrected to minimize the misfit by either changing densities or by changing the layering. Because the model is limited in depth, it is the trend of the relative gravity that is compared to the relative observed gravity.

The modeling method can be summed in four steps (Kearey, Brooks, & Hill, 2002)

1. Make a reasonable geological model (with densities). Use all available data.
2. Choose an appropriate algorithm to compute the gravity from the model.
3. Compare the calculated gravity and the observed gravity.

4. Correct the model to obtain a better fit between the observed and the calculated gravity. Repeat points 2-4 until a satisfactory result is obtained.

The inverse modeling method uses inversion methods that automatically determine the position, density contrast and geometry of a causative body. The requirement is that sufficient prior information about the source is incorporated by the method.

When modeling gravity, it is important to remember that there is no unique solution. The result should be as geological likely as possible and simultaneously fit with the observed gravity.

The different algorithm used in this modeling is the Polygon method, Parker's method and a "new" grid method, based on relationship between lithology, porosity and density. These are described in the following sub-chapters, and are all forward modeling methods. In addition an inverse method, here called Cordell & Henderson's method is used for calculating the topography of Moho.

2.2: Polygon method

The polygon method is described by Talwani, et al. (1959)

In this method, the two-dimensional body is approximated closely to a polygon, where the number of sides of the polygon is sufficiently large. The accuracy is only dependent on how well the polygon and the given body fit each other, and increases as the number of sides of the polygon increases.

A polygon ABCDEF (figure 2.1) with n sides is given and P is the point at the "surface" where the attraction between P and the polygon has to be determined. P and the polygon lie in a xz plane, where P is origo. If z is positive downwards and θ is measured from the positive x axis towards the positive z axis, then in P , Hubbert (1948) has shown that the vertical component of the gravitational attraction due to the polygon is equal to:

$$2G\rho \int z d\theta$$

G is the universal constant of gravitation

ρ is the density of the body

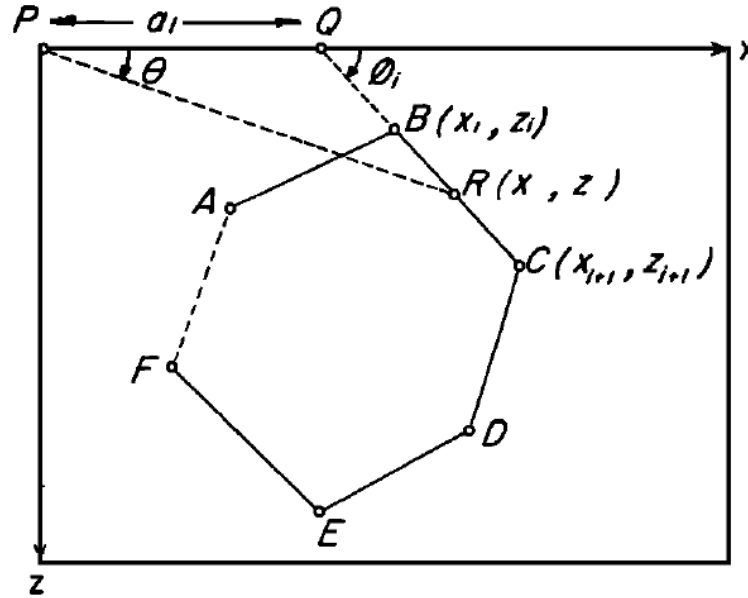


Figure 2.1: A sketch of the Polygon method and the geometrical elements involved (Talwani, et al., 1959)

The integral above is found by calculating the integral of every side of the polygon and find the sum of these. Considering the vertical component of the figure we get:

$$\oint z d\theta = \int_A^B z d\theta + \int_B^C z d\theta + \int_C^D z d\theta + \int_D^E z d\theta + \int_E^F z d\theta + \int_F^A z d\theta = Z_1 + Z_2 + Z_3 + Z_4 + Z_5 + Z_6$$

Then the general formula for the vertical component of gravitational attraction V is given by:

$$V = 2G\rho \sum_{i=1}^n Z_i,$$

where the summation is being made over the n sides of the polygon.

The Z_i component is calculated by this equation:

$$Z_i = a_i \sin \phi_i \cos \phi_i \left[\theta_i - \theta_{i+1} + \tan \phi_i \log_e \frac{\cos \theta_i (\tan \theta_i - \tan \phi_i)}{\cos \theta_{i+1} (\tan \theta_{i+1} - \tan \phi_i)} \right],$$

Where:

$$\theta_i = \tan^{-1} \frac{z_i}{x_i}, \quad \phi_i = \tan^{-1} \frac{z_{i+1} - z_i}{x_{i+1} - x_i}, \quad \theta_{i+1} = \tan^{-1} \frac{z_{i+1}}{x_{i+1}}, \quad \text{and } a_i = x_{i+1} + z_{i+1} \frac{x_{i+1} - x_i}{z_i - z_{i+1}}$$

The segments in the polygon have initial points given as x_i and z_i and endpoints given as x_{i+1} and z_{i+1} . If we know the coordinates of every corner points of the polygon, we can calculate the gravity of any two-dimensional body.

2.3: Parker's method

Parker(1973) describes a method to model the gravity in 3D, using 2D-Fourier transform:

$$F[\Delta g] = -2\pi G \exp\left(-|\vec{k}|z_0\right) \sum_{n=1}^{\infty} \frac{|\vec{k}|^{n-1}}{n!} F\left[\rho(\vec{r})h^n(\vec{r})\right]$$

$F[.]$ is the 2D-Fourier transform of the function in the bracket

k is the wavenumber, $k^2=k_x^2+k_y^2$

r is the distance, $r^2=x^2+y^2$

$\rho(r)$ is the density contrast across the boundary

$h(r)$ is the topography of the boundary

z_0 is the depth down to the deepest point of the boundary

G is Newtons gravitational constant

The result is a sum of Fourier transforms which can include the case of many layers and densities varying with position.

The sum converges fast when the depth to the deepest point of the boundary is shallow, and only a few terms are needed. The deeper the deepest point of the boundary is, the slower the sum converges and more terms are needed. By using the inverse Fourier transform we can find the relative gravity created by the boundary. This is repeated for all of the model's boundaries and to obtain the total gravity of the model the result from each boundary down to the compensation depth are summed.

In this thesis, 2D modeling is used. Parker's formula can also be used for 2D models if we modify it. We then use 1D-Fourier transform, and $h(r)=h$, $\rho(r)=\rho$ and $k=k_x$.

2.4: Cordell & Henderson's method

Cordell and Henderson(1968) describes an inverse, iterative method, which has three steps: 1) a “starter” model; 2) calculation of the gravity of the tentative model; and 3) a modification of the model, which is based on the Bouguer plate formula applied on the difference between the observed anomaly and the calculated anomaly. The last two steps are iterated until the observed and calculated anomalies give an acceptable fit.

Gravity anomaly is digitized on a regular grid. The causative body is assumed to be approximated to a bundle of vertical prisms, where each of the prisms has a cross-sectional area of one grid cell and a uniform density. Their vertical position is created using a systematic relationship to a horizontal reference plane.

If the density and the depth of the reference plane is specified, the effect of gravity at the pth grid point P: (x,y,0) due to the prism vertically beneath the qth grid point Q: (x',y',0) is a function only of prism thickness T_q and relative position:

$$\Delta g_{obs,p} \approx Gf(P, Q, T_q; \rho, D)$$

The gravity effect of the entire causative body at the pth grid point is then:

$$g_{obs,p} \approx \sum_{q=1}^M Gf(P, Q, T_q; \rho, D)$$

ρ is the density

D is the depth to the reference plane

M is total number of grid points

They define $t_{n,q}$ as the thickness of the prism element beneath the qth grid point at the nth iteration.

As a “starter” model they use a thickness at each grid point which is found from the Bouguer slab formula:

$$t_{1,q} = Kg_{obs,q}, \text{ where } K = \frac{1}{2\pi G\rho}$$

The input to the computer program is the gravity anomaly digitized on a grid, density contrast and the depth to the reference plane.

The practical usefulness of the iterative technique depends on how efficient we get a model which is satisfactory and stable. “Goodness of fit” is how the model is judged; a measure of how efficient the process is; the rate of how much the goodness of the fit improves through the iterations.

The goodness of fit is the largest error E_n , where:

$$E = \sup \{ |g_{obs,p} - g_{calc,n,p}| \} : \text{for all } p.$$

Then the rate of decrease of $\{E_n\}$ through the iterations is a measure of the efficiency.

Cordell-Henderson’s method can also be used in 2D-modeling, as shown in this thesis.

2.5: The grid method

In this method the geometric model is gridded in the x,z-plane, and the density in each grid cell is calculated from lithology and porosity.

2.5.1 Porosity and density based on lithology

We may find the porosities in the subsurface by using Athy’s law, which expresses the porosity-depth distribution within a layer:

$$\phi(z) = \phi_0 e^{-az}$$

ϕ_0 is the surface porosity (%)

a is the compaction coefficient (km^{-1})

z is the depth (km)

The constants ϕ_0 and a are dependent on lithology, and therefore requires Athy’s law that the lithology in each layer is known. Representative parameters for the North Sea (table 2.1) are found by Sclater and Christie(1980). These parameters are also used in this thesis.

Table 2.1: The porosity parameters representative for the North Sea

Lithology	ϕ_0	a	$\rho_g(\text{g/cm}^3)$
Sand	0.49	0.27	2.65
Shale	0.63	0.51	2.72
Chalk	0.70	0.71	2.71

If the lithologies are mixed, then the porosities can be estimated by weighting the porosity parameters. An example is a lithology of 60 % shale, 30 % sand and 10 % chalk. Then $\phi_0 = 0.6 \times 0.63 + 0.3 \times 0.49 + 0.1 \times 0.70 = 0.595$. Similarly, the constant a and the density can be estimated.

2.5.2: Porosity and density adjusted by effective pressure

When incompressible pore fluid is assumed, the effective pressure σ is defined as the difference between the lithostatic pressure S (weight of the overburden) and the pore pressure P . Smith(1971) proposed that porosity is a function of the effective pressure:

$$\phi = \phi_0 e^{-b\sigma}$$

The lithostatic pressure is given by $S = \rho_b g z$, where ρ_b is the average bulk density above the depth z . The pore pressure, when hydrostatic pressure prevails in the pores, is given by $P = \rho_f g z$, where ρ_f is the density of the pore fluid. If ρ_b and ρ_f are constants, there is a relationship between the parameters a and b :

$$b = \frac{a}{(\rho_b - \rho_f)g}$$

The lithostatic pressure at depth z is given by:

$$S = g \int_0^z (\phi \rho_f + (1 - \phi) \rho_g) dz$$

By using Athy's law, we get:

$$S = \left(\frac{1000 \phi_0}{a} \right) \left(e^{\left(\frac{-az}{1000} \right)} - 1 \right) (\rho_g - \rho_f) + g \rho_g z, P = g \rho_f z$$

ρ_g is the grain density (kg/m³)

ρ_f is the pore fluid density (kg/m³)

$g = 9.81 \text{ m/s}^2$

z is here in m.

S and P have Pascal as their units.

As the porosity will be affected by the effective pressure, Athy's law can only be applied with some confidence for uniform sediments under normal pressure. If we have a section with different layers with different porosities, the porosities in the deeper layers will be moved relative to their Athy-curves. We have to compensate for the effective pressure at the top of the layers. An example is shown in figure 2.2. Here the porosity and density are computed by using Athy's law, with and without compensation for the effective pressure at the top of each layer. The model consists of 5 layers with lithology and porosity parameters given in table 3.1 and the thickness of the layers are respectively 206, 517, 354, 523 and 400 m.

The curves have the same trend, but there are small differences. Up to 3 % in the porosity curve and the difference in the density curve varies from 0.015 to 0.04 g/cm³. Layer 1 is always the same as it is the first layer and the same for both methods. The curves in layer 4 seem to overlap each other, but there is a small difference of approximately 0.5 % in the porosity curve and approximately 0.005 g/cm³ in the density curve.

The effective pressure at a depth z_0 is represented by the total grain mass m above z_0 , if normal pressure is assumed. For a pure lithology, the grain mass-depth function can be derived from the porosity-depth function using the following equation:

$$m(z) = \int_0^z \rho_g [1 - \phi(z)] dz$$

By using Athy's law and integrating, we get:

$$m(z) = \rho_g \phi_0 e^{-az} + \rho_g (z - \phi_0 / a)$$

Figure 2.3 shows how the grain-mass at the bottom of one layer determines the starting point of the porosity curve in the next layer. The left figure shows the grain-mass curves for lithologies in layer 1, 2 and 3, while the dotted curves in the right figure shows the Athy-curves in the same layers. The effective pressure at top of layer 2 determines the vertical shift, Δh_2 downward, of the Athy-curve in layer 2, resulting in an increased porosity in that layer compared to its Athy-curve. Similarly, the effective pressure at the top of layer 3 is

higher than the pressure at this depth for a homogenous layer 3 – lithology, and this result in a lower porosity in layer 3 (the Athy-curve is vertically shifted Δh_3 upward).

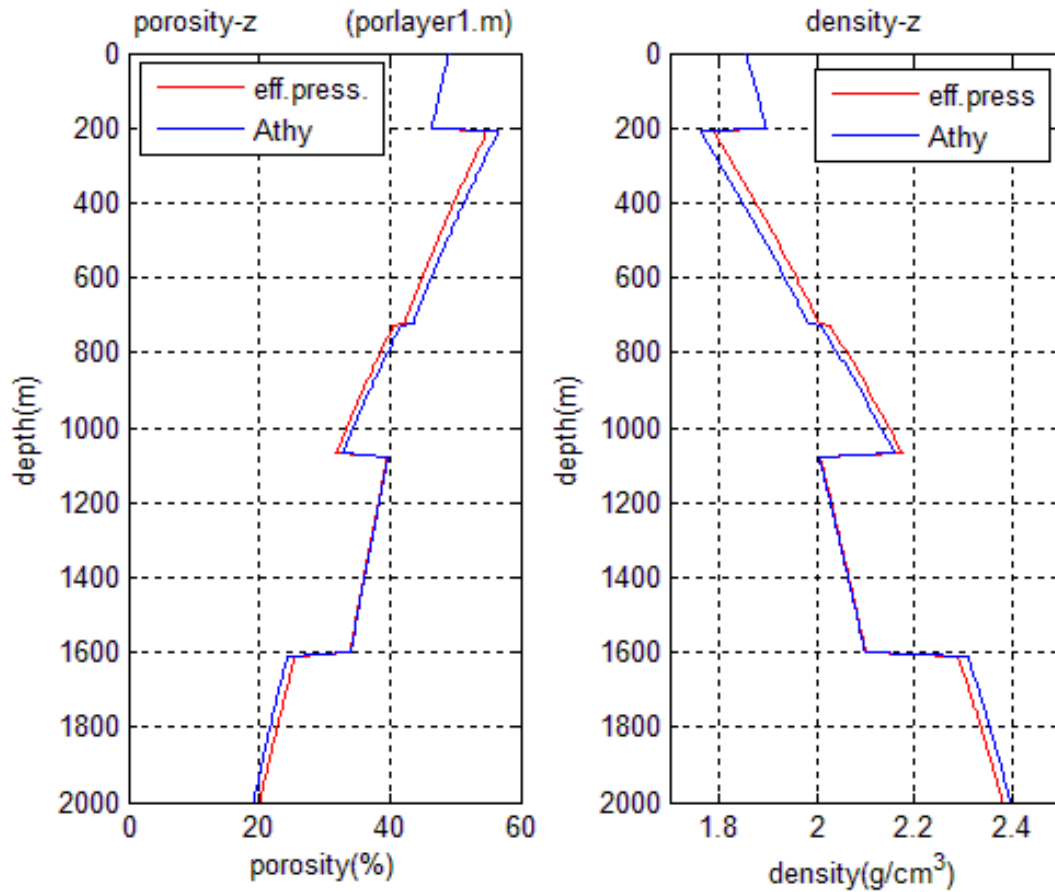


Figure 2.2: Porosity and density versus depth for a 5-layered model (see text), with and without compensating for effective pressure at the top of the layers.

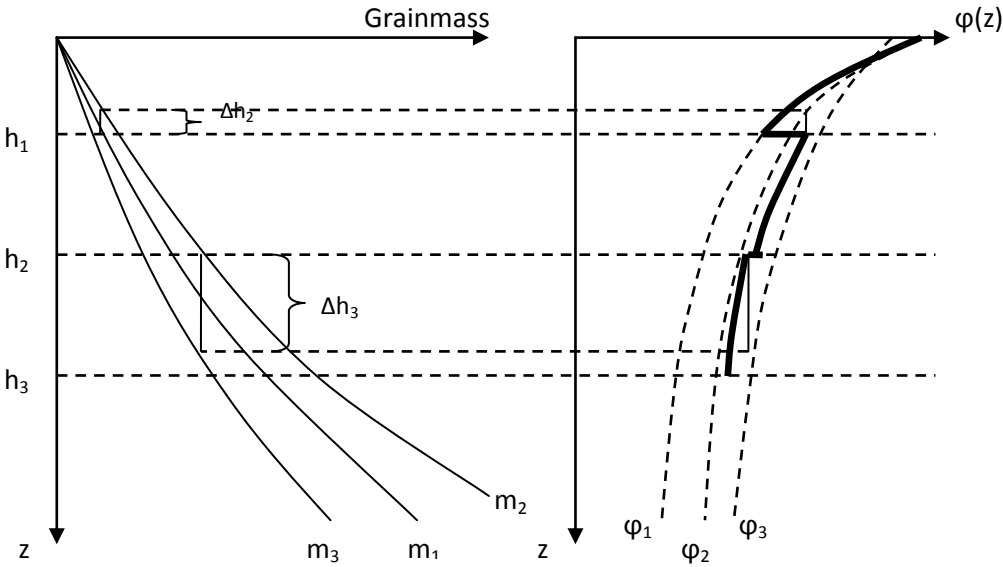


Figure 2.3: A porosity-depth distribution together with mass-depth curves of a model of three layers. The $\phi(z)$ -curve is found by shifting the $\phi_2(z)$ - and $\phi_3(z)$ -curve vertically a distance Δh_2 and Δh_3 , which are found from the mass-depth curves. For details, see text.

2.5.3 Gridding

If we know the density of pore fluid and the grain density from lithology, and the porosity-depth is found as described above, the bulk density ρ_b is found by using the formula:

$$\rho_b = \phi \rho_f + (1 - \phi) \rho_g$$

By gridding the model in the x- and z-direction, the porosity in each grid point can be estimated. The bulk density representing the grid cell is found by averaging the four density values in the corners of the cell, see figure 2.4. The gravity along the profile can then be calculated using the formula for a rectangle.

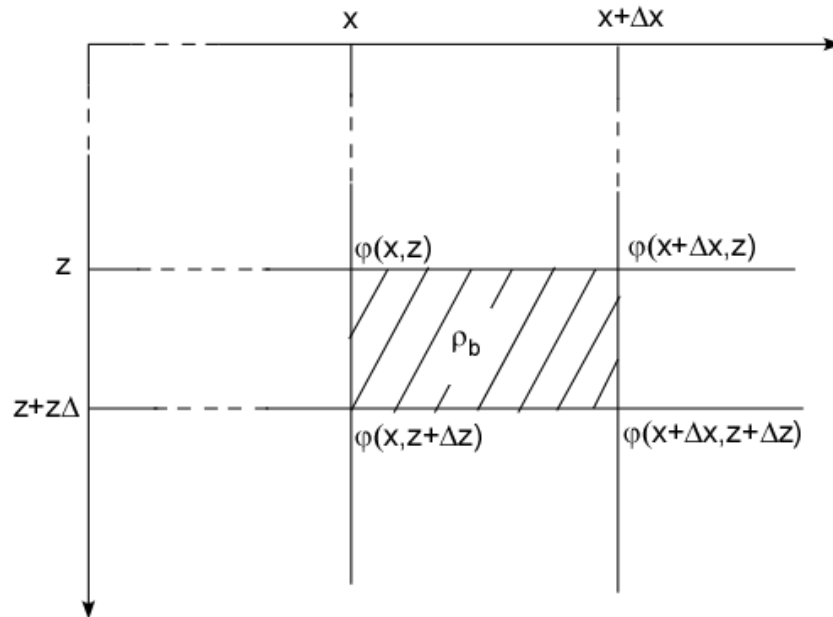


Figure 2.4: Knowing the porosity ϕ at the four corners of the cell, the bulk density at the corners are calculated by $\rho_b = \phi\rho_r + (1-\phi)\rho_g$. The bulk density representing the cell is the average of the bulk density at the corners.

The following formula (Jung, 1961) says that the gravity Δg at a point $P=(x,0)$ from a two-dimensional block of rectangular shape, where the upper edge is fixed at the surface $z=0$, is:

$$\Delta g = G\rho \left(a \ln \frac{a^2 + z^2}{a^2} - b \ln \frac{b^2 + z^2}{b^2} + 2z \left(\tan^{-1} \frac{a}{z} - \tan^{-1} \frac{b}{z} \right) \right)$$

Geometrical parameters are shown in figure 2.5.

The (relative) gravity profile is found by summing the gravity contribution from all grid cells at different observation points along the surface. The model must be elongated to reduce end effects.

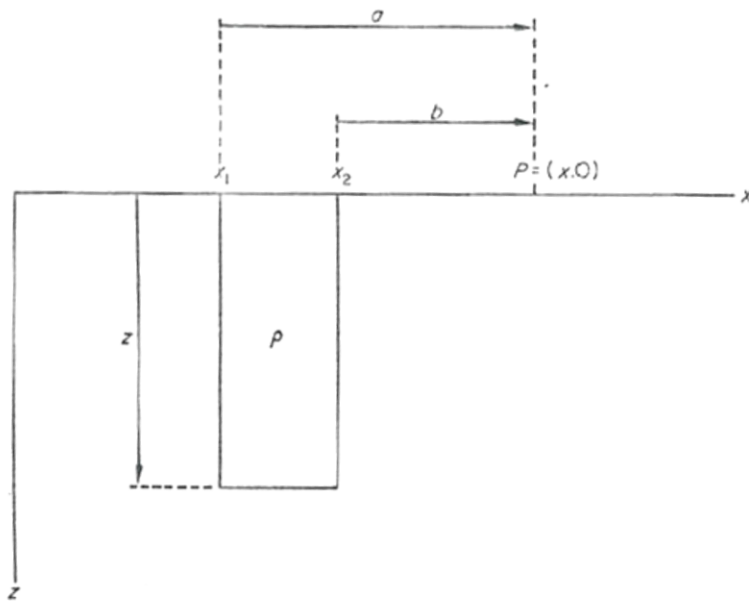


Figure 2.5: Two-dimensional rectangular block (Dyrelus & Vogel, 1972).

Chapter 3: Testing the grid method

3.1 General

In this chapter the grid model will be tested and applied on simple 2D models. The calculated gravity is first of all dependent on lithology and geometry of the model, but will also be dependent on the grid size in x- and z-direction, and eventual deviations from normal porosity, due to overpressure, erosion, etc.

The results of all the synthetic models here are model-dependent. They are included to illustrate some effects the grid model may create.

An example of a gridded geological model is shown in figure 3.1. Figure 3.2 shows the density and porosity distribution for this model at some x-positions along the profile, calculated using the grid method.

3.2 Comparing models with constant density with the grid method

Three simple synthetic models of the subsurface were made. They all have 5 different layers and the lithology of the layers in each model remains the same. The models differ as they have different structure; one with horizontal layers, one with dipping layers and one variable (figure 3.3-5). The lithology and porosity parameters used in the modeling are given in table 3.1.

The models are all modeled with two different density determinations; one with density varying within the layers according to the porosity estimated from the lithology, and one where the layers have constant bulk density equal to the mean density of the gridded density in the layers. In this modeling, the grid size used are: $dx=5$ km, $dz=100$ m.

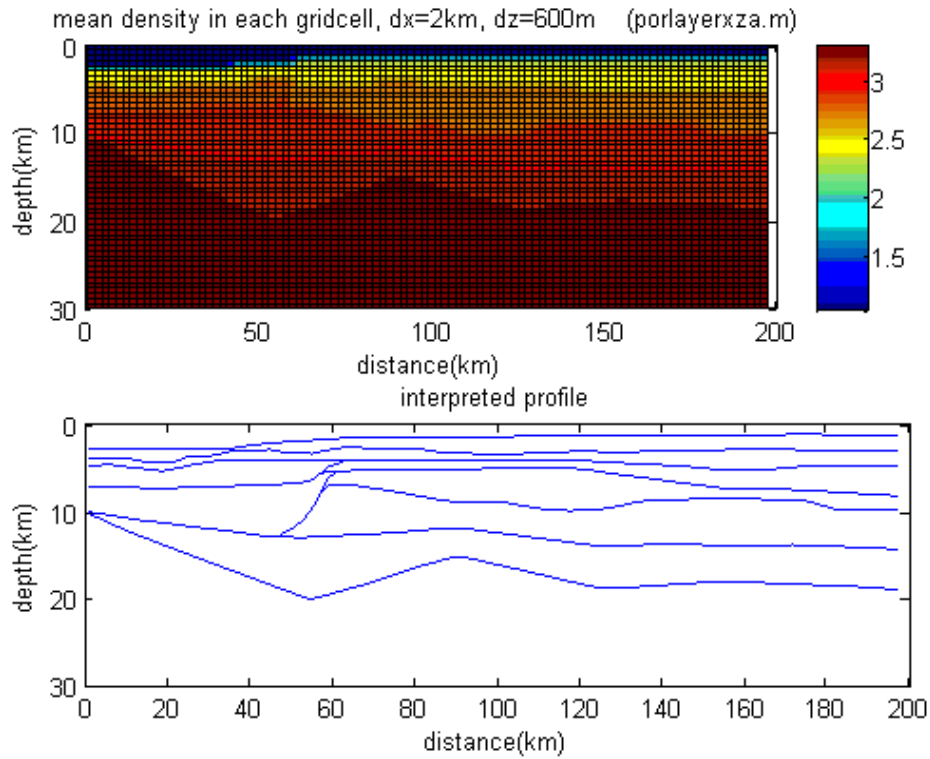


Figure 3.1: The gridded geological model from the interpretation.

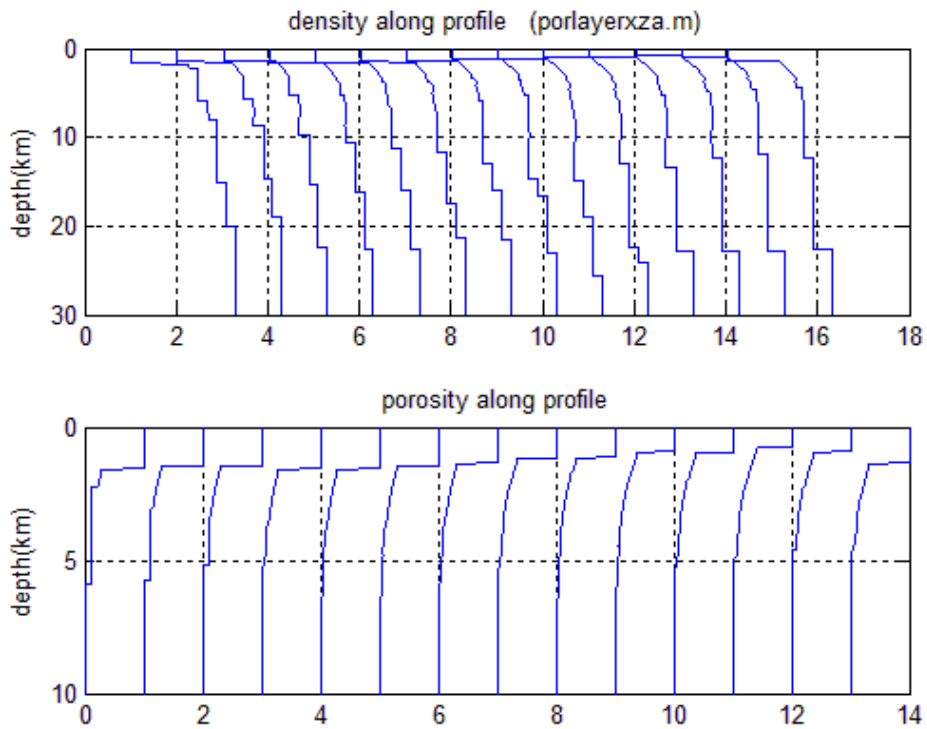


Figure 3.2: The density and porosity along the profile of the model in figure 3.1

Table 3.1: The porosity parameters used in the modeling of the synthetic models in figure 3.3-5

Layer	Lithology	ϕ_0	a	ρ_f	ρ_g
1	Sand	0.49	0.27	1.03	2.65
2	Shale	0.63	0.51	1.03	2.72
3	Chalk	0.70	0.71	1.03	2.71
4	Sand/shale	0.55	0.30	1.03	2.65
5	Shale/Chalk	0.65	0.61	1.03	2.72

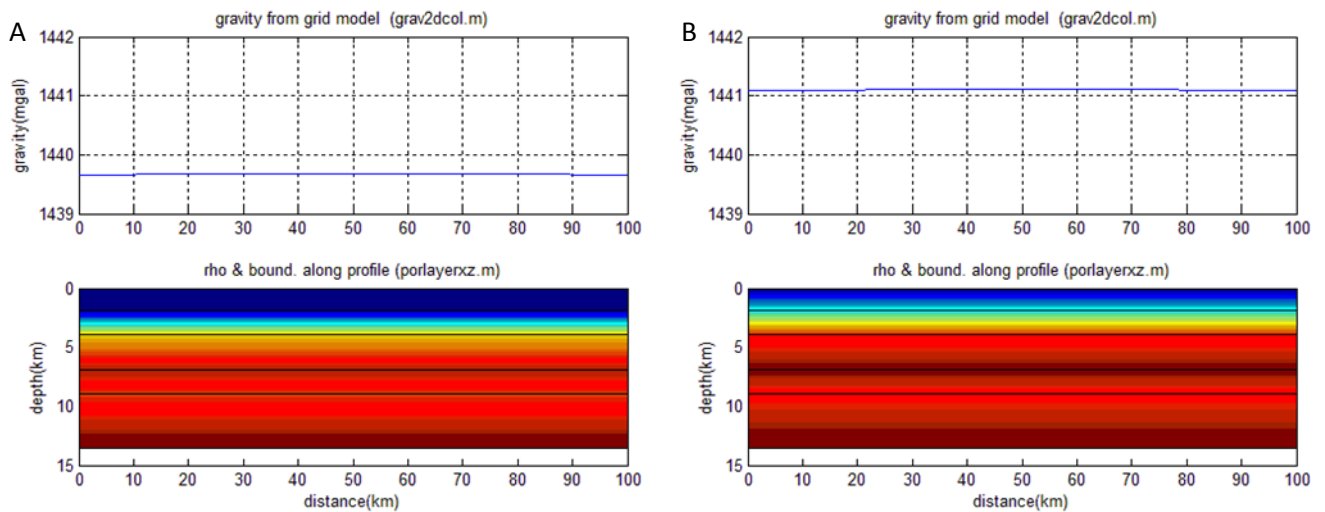


Figure 3.3: A: The modeled gravity when the density is constant within the layers. B: The modeled gravity when the density is varying within the layers.

3.2.1 Flat model

The flat model (figure 3.3) shows the same horizontal gravity in both cases. However, the total gravity from the two differs slightly (1.5 mgal) due to the gridding.

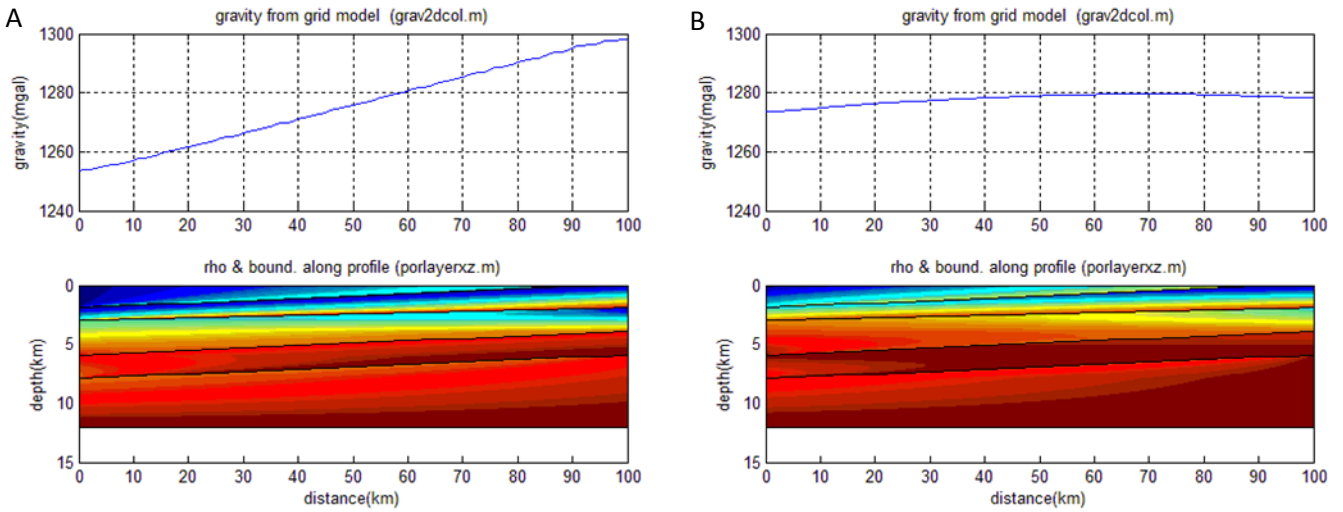


Figure 3.4: A: The modeled gravity when density is constant within the layers. B: The modeled gravity when the density is varying within the layers.

3.2.2 Dipping model

The difference between the two models in where the layers are dipping (figure 3.4) is that the model with constant porosity and density gives a much steeper gravity curve than the model with varying density, which is smoother and doesn't vary that much. The reason for the steep curve in figure 3.4A, where the porosity and density is constant, is that a vertical column's weight is increasing from left to right in the constant-density case, while it is fairly constant in the gridded case.

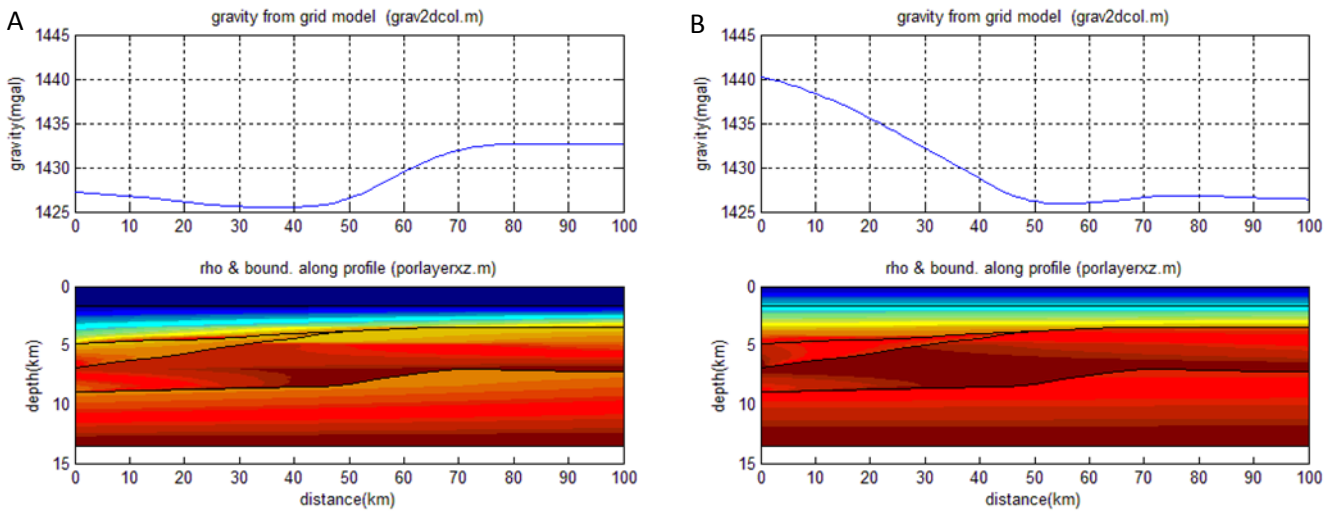


Figure 3.5: A: The modeled gravity where the density is constant within the layers. B: the modeled gravity where the density is varying within the layers.

3.2.3 Synthetic “realistic” model

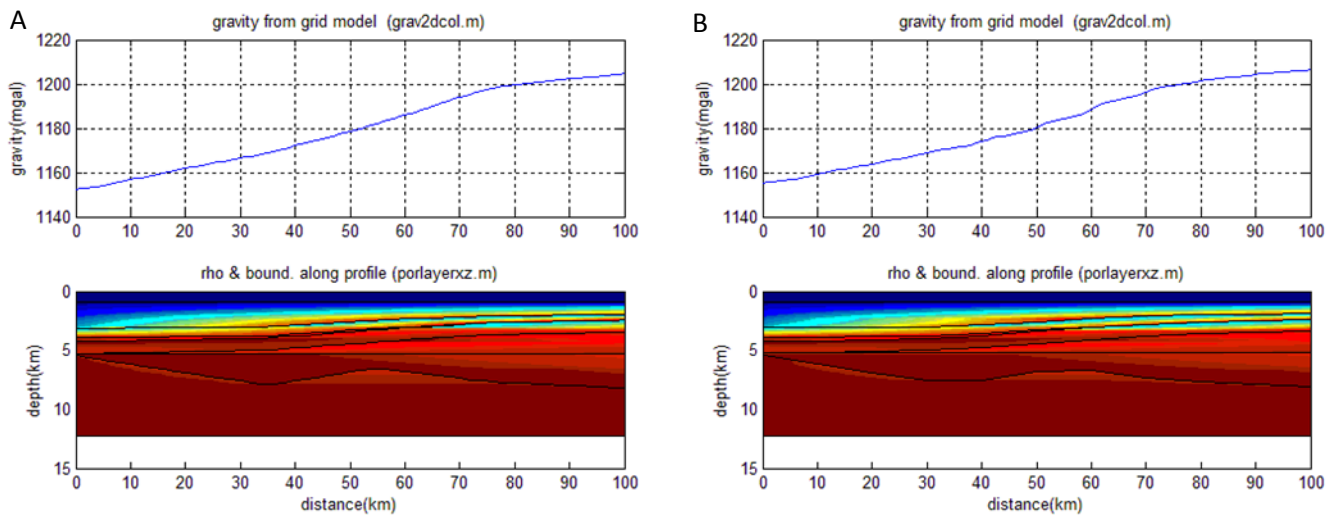
In the chosen “realistic” model, you can see a large difference in the gravity curves. They give almost an opposite trend (figure 3.5), and the model with varying porosity and density within the layers give a steeper gravity curve to the left (figure 3.5B) compared to the model with constant density within the layers (figure 3.5A). This opposite trend can again be explained by the varying weight of the vertical columns along the profile in the two cases.

3.3 Grid-size

If there is a considerably distance between the data points, interpolation may exclude some geological structures from the model. This can lead to significant errors in the gravity calculations. If there is an area with little change in the geology, the effect of large distances between the data points will be less significant. To see how coarse the grid could be without missing too much information, several grid sizes were tried. The influence of the grid size was tested by using a synthetic geological model with 8 layers and a more complex structure than the structure used in the simple synthetic models above. The lithology and porosity parameters are given in table 3.2. In figure 3.6, the gravity is modeled with two different grid sizes to show how it affects the gravity curve. The most suitable fit for the grid size is dependent on the topographic changes of the boundaries. The computation time for calculating the gravity field from a model is proportional to the number of cells, while the accuracy will decrease with increasing cell size. In this case a cell of length 2 km and thickness 50 m was sufficient (figure 3.6A). Using smaller cells did not improve the calculations.

Table 3.2: The lithology and porosity parameters used in testing the grid size in figure 3.6

Layer	Lithology	Φ_0	\mathbf{a}	ρ_f	ρ_g
1	Water	1	0	1.03	1.03
2	Sand	0.49	0.27	1.03	2.65
3	Chalk	0.70	0.71	1.03	2.71
4	Sand	0.49	0.27	1.03	2.65
5	Shale	0.63	0.51	1.03	2.72
6	Shale/Sand	0.55	0.40	1.03	2.67
7	Shale	0.63	0.51	1.03	2.72
8	Sand	0.49	0.27	1.03	2.65

Figure 3.6: A: Grid size of $dx=2$ km, $dz=50$ m. B: Grid size of $dx=10$ km, $dz=100$ m.

This grid size gives a fast computation of the gravity ($50 \times 250 = 12500$ cells, about 1 s computation time on my laptop (Pentium 4, 3.2 GHz)).

In figure 3.6B, the gravity curve has the same trend as the gravity curve in figure 3.6A, but as the grid is coarser it gives a rougher curve and may miss out on some information. To show how a coarser grid may miss out on some information, a more extreme geometric model was made (figure 3.7). Here one can clearly see the loss of information by having a too coarse grid. The parameters used in this modeling are listed in table 3.3.

Table 3.3: The porosity parameters used in modeling the case in figure 3.7 and figure 3.8

Layer	Lithology	Φ_0	a	ρ_f	ρ_g
1	Sand	0.49	0.27	1.03	2.65
2	Shale	0.63	0.51	1.03	2.72
3	Chalk	0.70	0.71	1.03	2.71
4	Sand/Shale	0.55	0.30	1.03	2.68
5	Shale/Chalk	0.65	0.61	1.03	2.72
6	Shale/Chalk	0.66	0.60	1.03	2.80

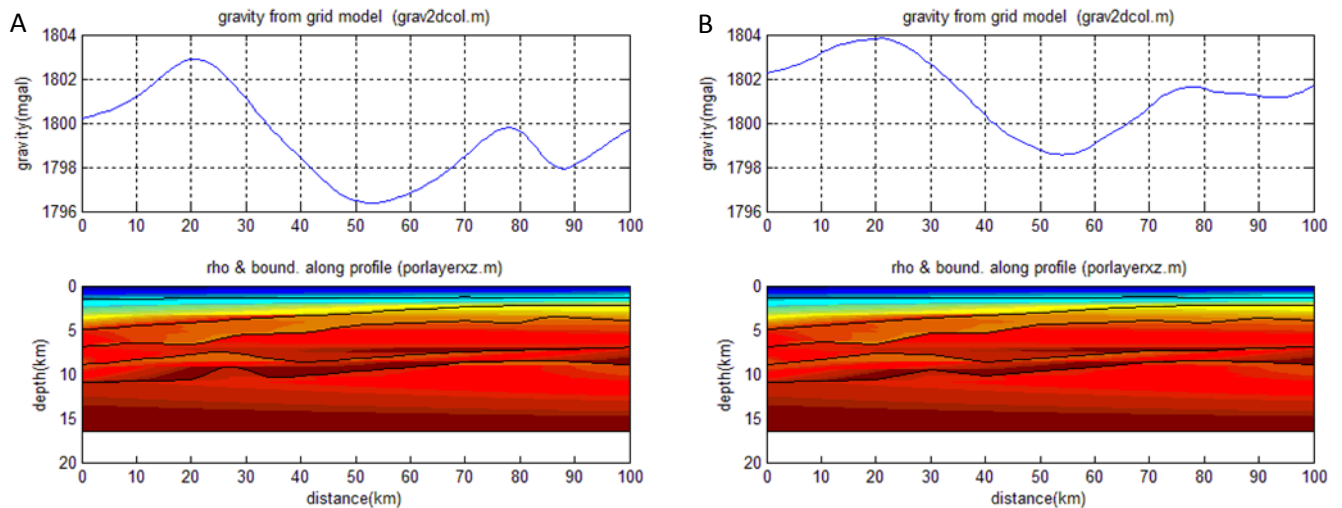


Figure 3.7: A: Grid size dx=2 km, dz=50 m. B: Grid size dx=10 km, dz=100 m

3.4 Effect of compensating for effective pressure

Figure 3.8 shows the gravity field for a model by using Athy's law with and without compensating for effective pressure. The porosity parameters used in the model are the five first layers listed in table 3.3.

The result gives the same trend at the left in the figures where the difference in mGal is up to 5. To the right, the difference is more significant. Here, there is an up to 15 mGal difference when comparing the two methods.

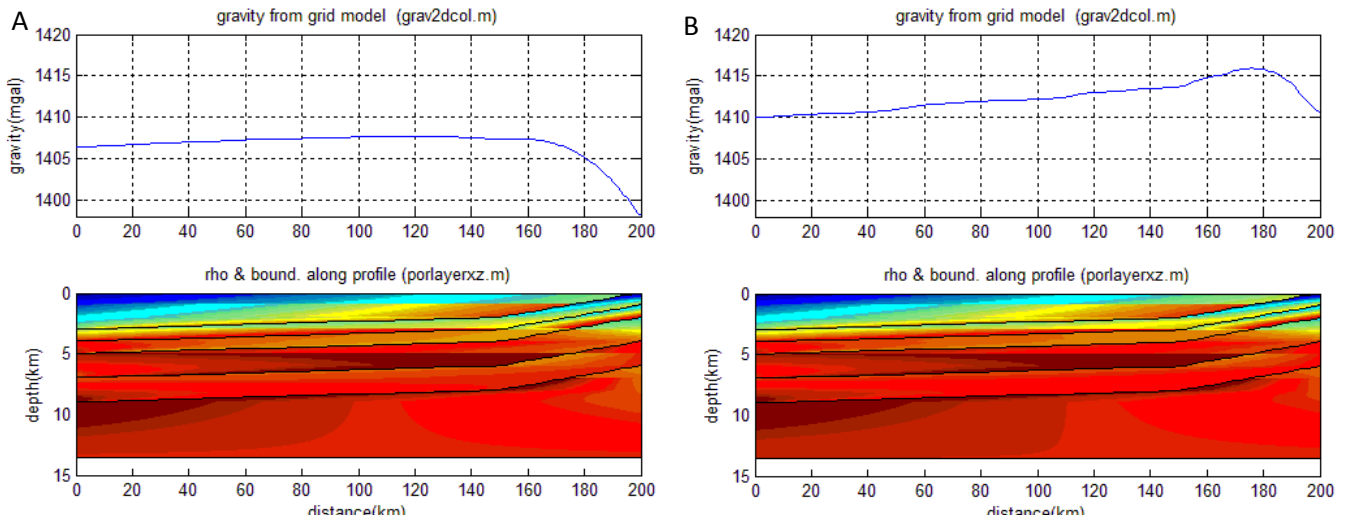


Figure 3.8: A: Gravity curve by using Athy's law, without compensating for the effective pressure. B: Gravity curve by compensating for the effective pressure

3.5 Influence of overpressure: an example

In the case where pore fluids can't be squeezed out of the rocks due to the fluids being trapped by impermeable rocks, it can result in overpressure. This means that the porosity remains high even at great depths. Such zones may therefore have a normal low density compared to its depth.

Overpressure is common in the Norwegian Sea, and especially on the Halten Terrace. There, the pore-fluid overpressure is increasing from east to west stepwise across the faults (van Balen & Skar, 2000). Skar (1999) proposed that the high overpressure at the Halten Terrace has its origin from the Rås Basin within the Vøring Basin. Overpressure is also present in the North Sea; in the Central Graben, Viking Graben, East Shetland Basin and Bergen High. Here, especially the Jurassic sandstones are overpressured as they are present at depths between 3700 m to 4500 m (Lindberg, 1980).

As overpressure is common along the Norwegian margin, a case with overpressure was modeled to see how it may affect the gravity. Here, I chose a simple model, where the subsurface is similar to the Norwegian margin with a deeper basin to the left where the overpressure is present within the third layer (figure 3.9).

When overpressure is present within a layer, the overpressured area has a nearly constant porosity as the pore fluid cannot escape from the pores. The transition to constant porosity is shown in figure 3.9 in a porosity-depth distribution.

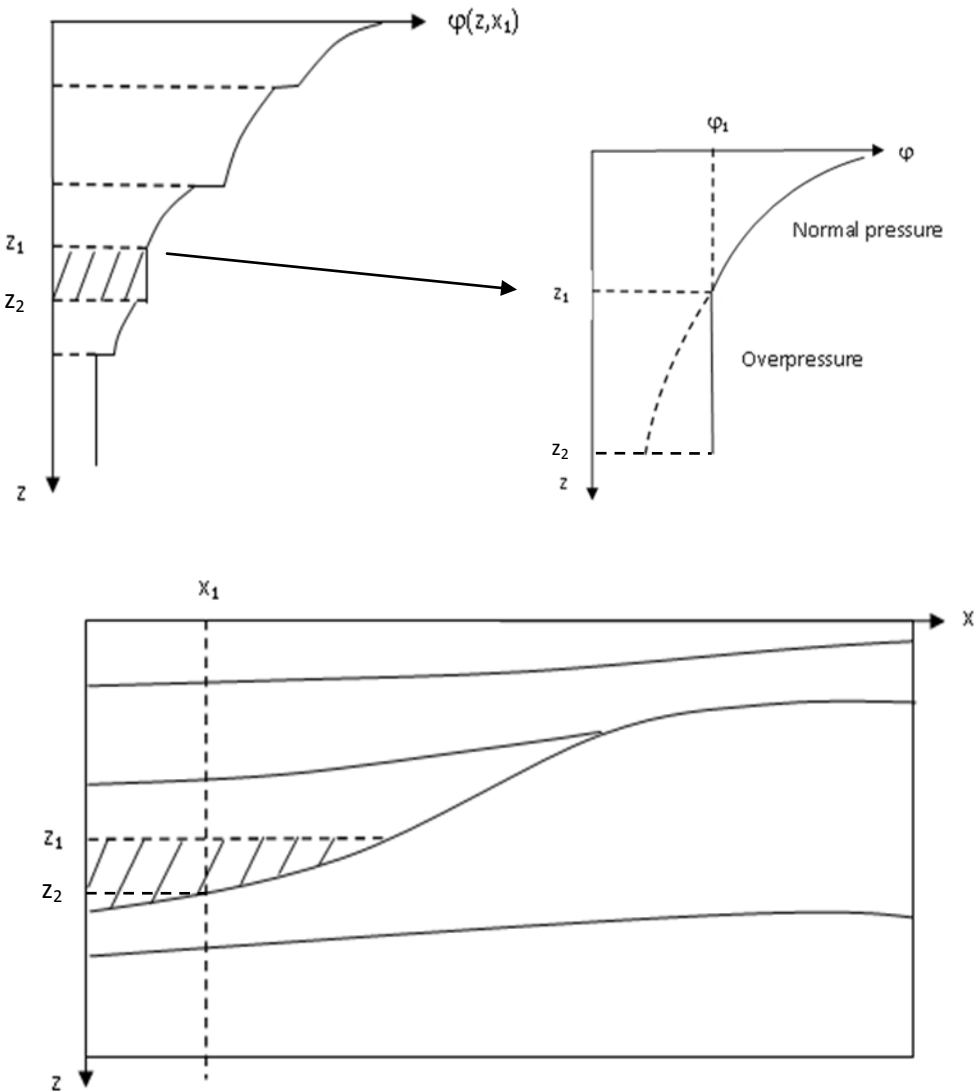


Figure 3.9: A: Porosity-depth distribution at $x=x_1$. The layer below z_1 is the area with overpressure. In this layer the porosity is constant. B: A figure which show how the overpressure affects the porosity-depth curve with constant porosity within that layer. C: The layering. The marked layer is the area with overpressure.

To see the effect of constant porosity within a layer, four models were made; the two first have an upper solid layer, and are different only in the third layer, where one has overpressure and the other has normal pressure. The next two models are the same as the

first two, but have water as upper layers (figure 3.10 and figure 3.11). The difference is as expected; the gravity has a lower value in the case of overpressure as the area with overpressure is lighter than if overpressure is absent.

The difference between the gravity from overpressured and non-overpressured models is dependent on the depth at which the overpressure is present. The greater the depth of the overpressured layer, the smaller the difference in the density between overpressured and non-overpressured model, and the smaller the difference in gravity. A deeper overpressured layer will result in a more low-frequency difference than a shallower overpressured layer. The difference in gravity will also be dependent on the thickness of the overpressured zone; the thicker the zone, the bigger will the difference be.

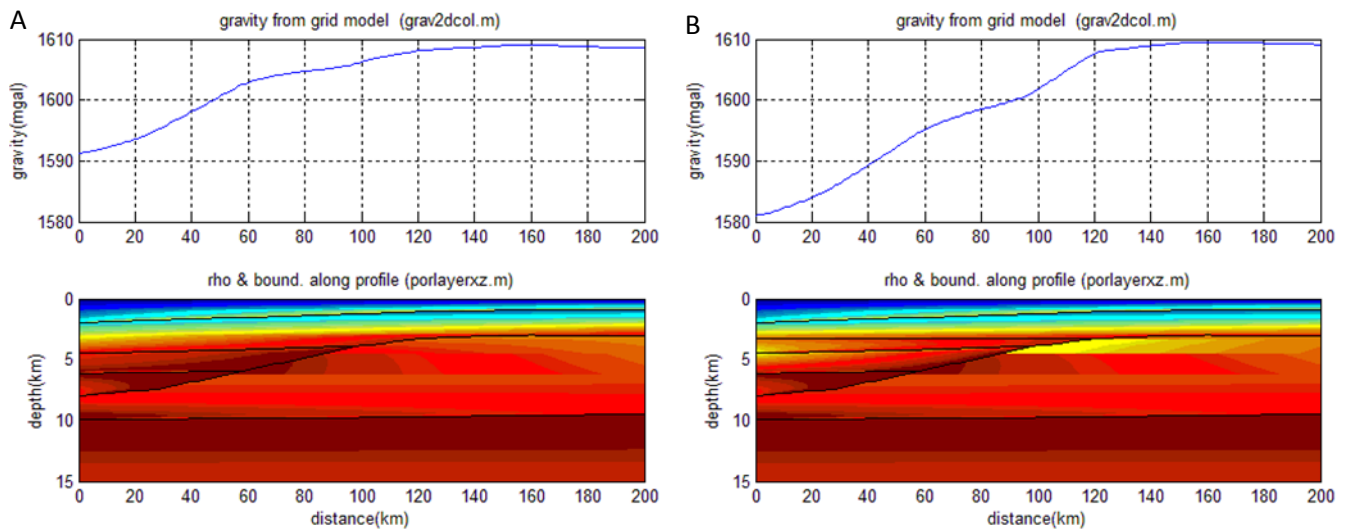


Figure 3.10: Models with solid layer as the upper layer. A show the model without any overpressure, while B shows the model with overpressure in the third layer

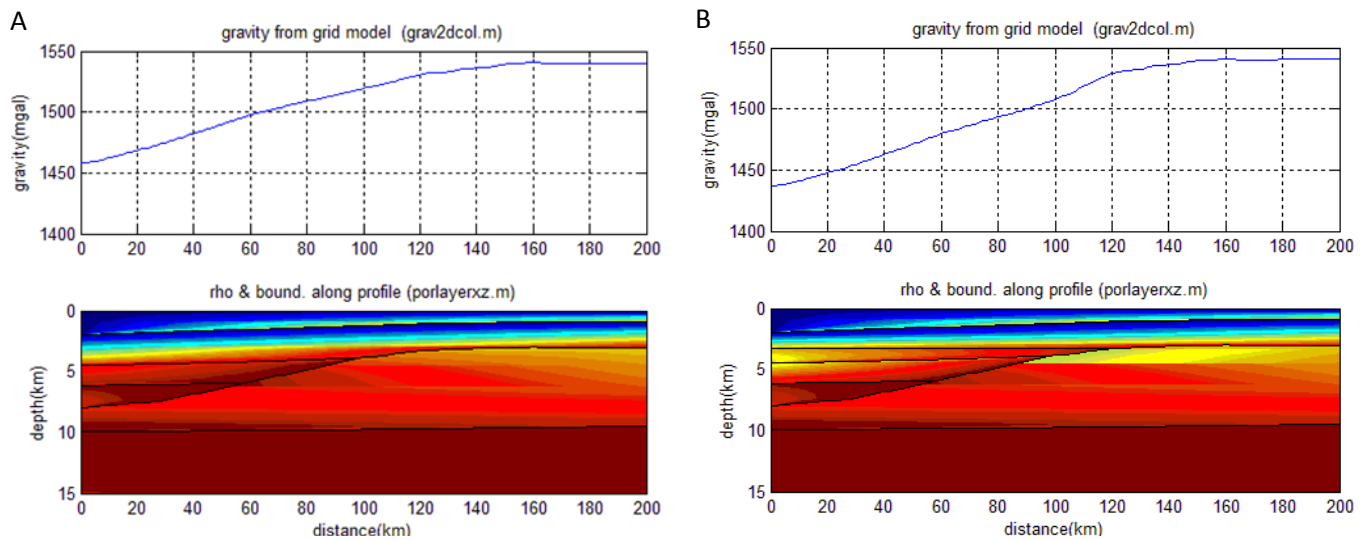


Figure 3.11: Models with water as the upper layer. A is without any overpressure, while B right has overpressure in the third layer

3.6 Influence of erosion: an example:

The Norwegian margin has suffered a considerable amount of erosion. At the Vøring margin, especially during the Northern Hemisphere glaciation after a time of intra plate tectonic uplift, there was an increase in erosion in the coastal area and sedimentation further out.

To show how the erosion may affect the gravity in such cases, a hypothetical profile is modeled (see figure 3.12 and 3.13). We assume that the layers are deposited more or less horizontal, then part of the layers is uplifted and the porosities are kept as they were. Erosion happens, but the porosity-depth distribution curve remains the same underneath the erosion surface (figure 3.14 and 3.15).

The gravity from the eroded model is shown in figure 3.16.

In figure 3.18 the gravity from a model with the same geometry as the eroded model but with no influence on porosity from erosion (figure 3.17) is calculated. By comparing figure 3.18 with figure 3.16 we see that in this case a difference of almost 70 mGal is calculated at the end of the profile. We can therefore conclude that in similar cases it will be important to interpret the erosion in a correct way.

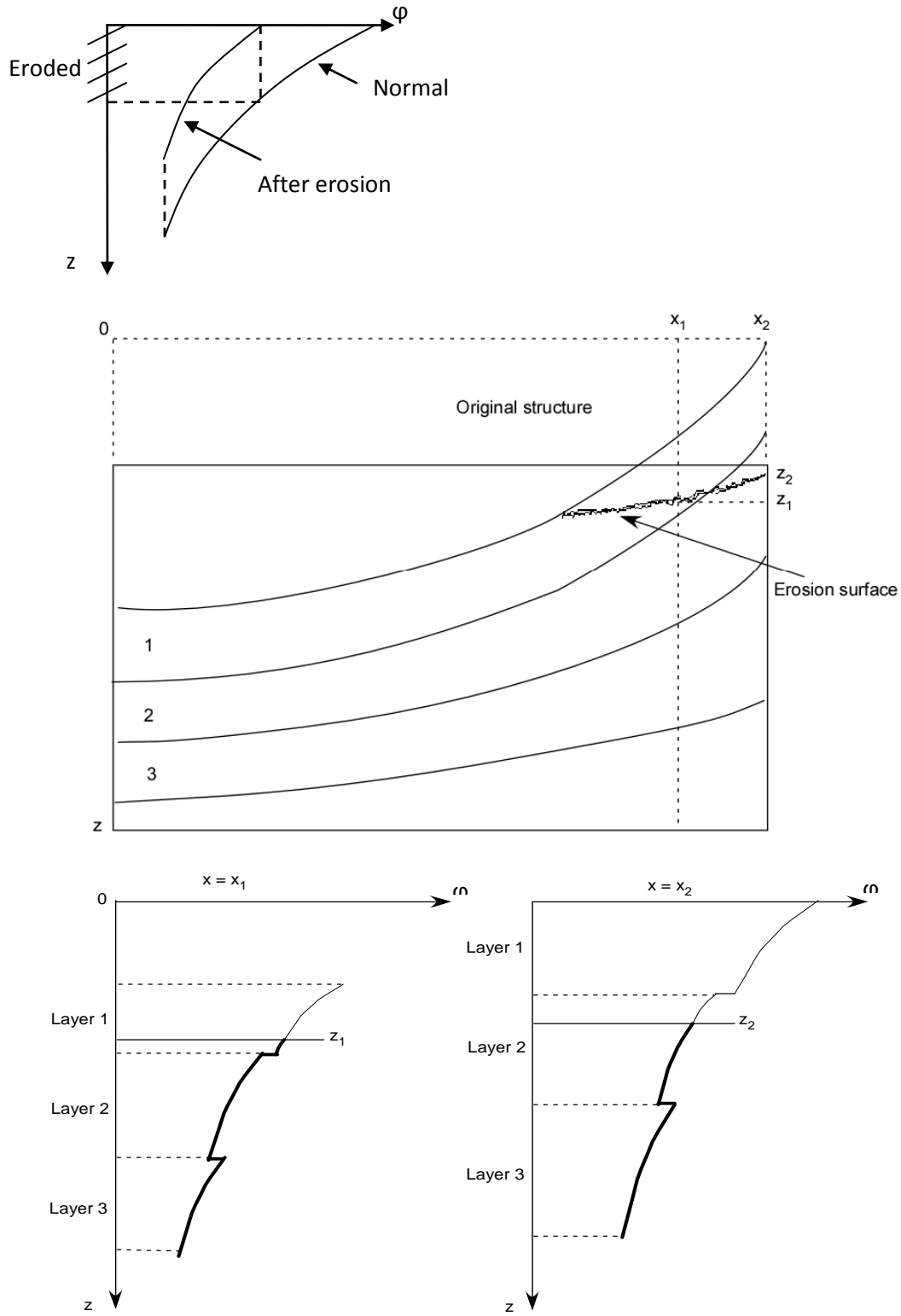


Figure 3.12: The upper figure shows a porosity-depth distribution curve of an arbitrary case pre- and post- erosion. The middle figure shows a geological model where the layers have been uplifted and eroded. The eroded structure is the structure above the erosion surface. The lower figure shows two porosity-depth distribution curves at x_1 and x_2 . The erosion surface at the two intersections is respectively z_1 and z_2 . The curve beneath the erosion surface is the new curve starting from the point at zero depth.

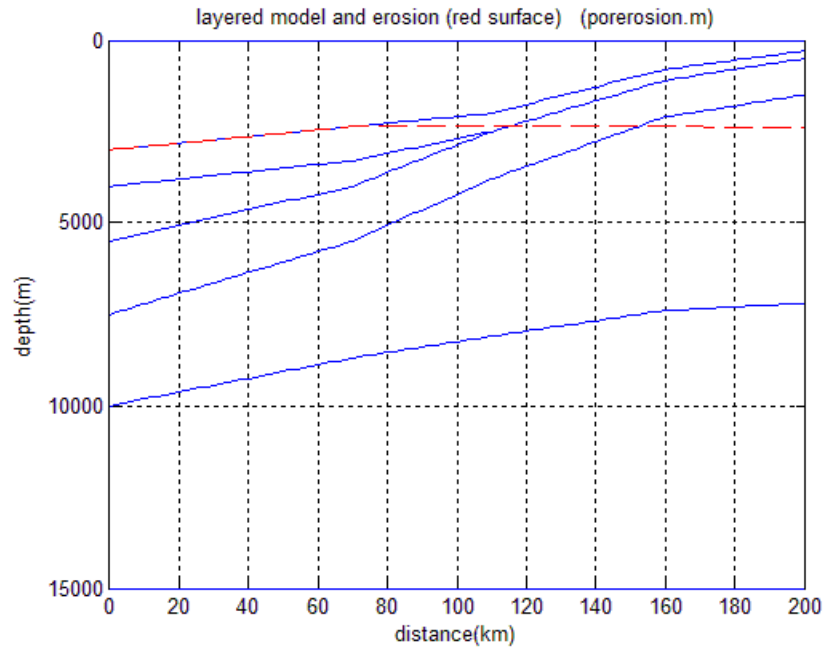


Figure 3.13: The geological model with the red line as the erosion surface.

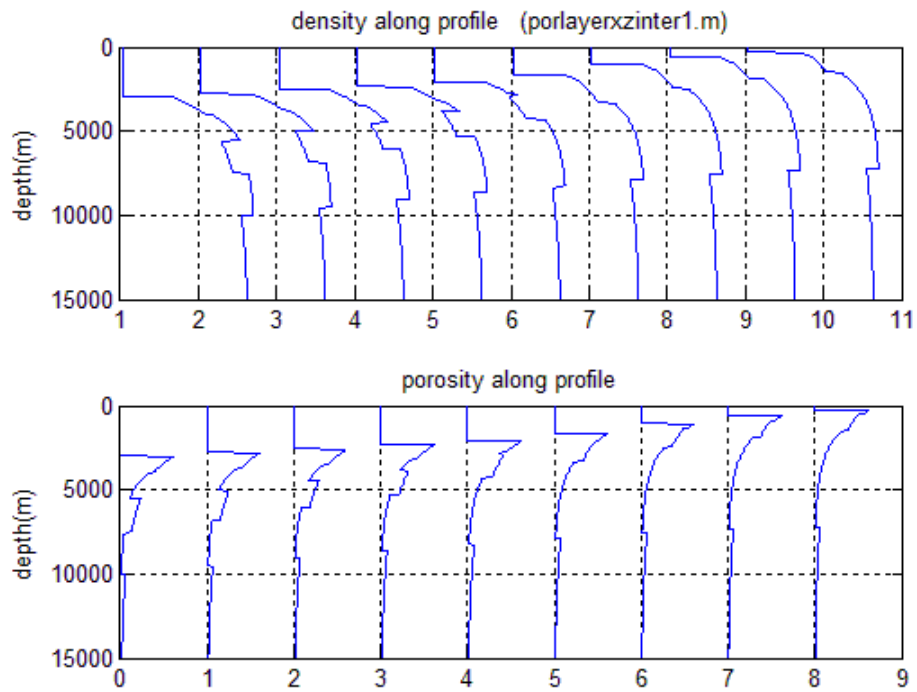


Figure 3.14: Porosity and density along the profile pre erosion

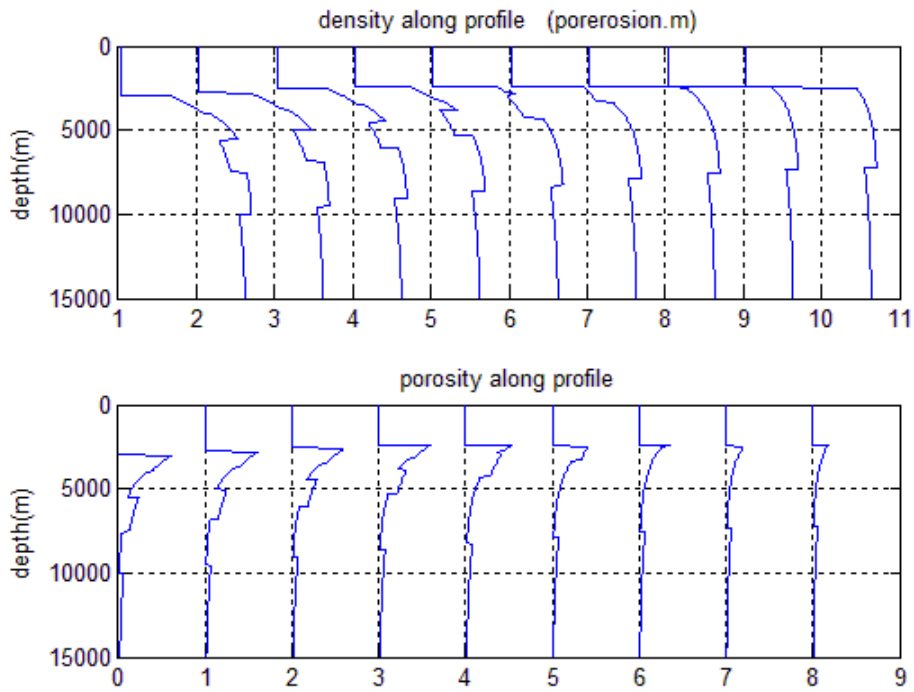


Figure 3.15: Porosity and density along the profile of the eroded model in figure 3.13

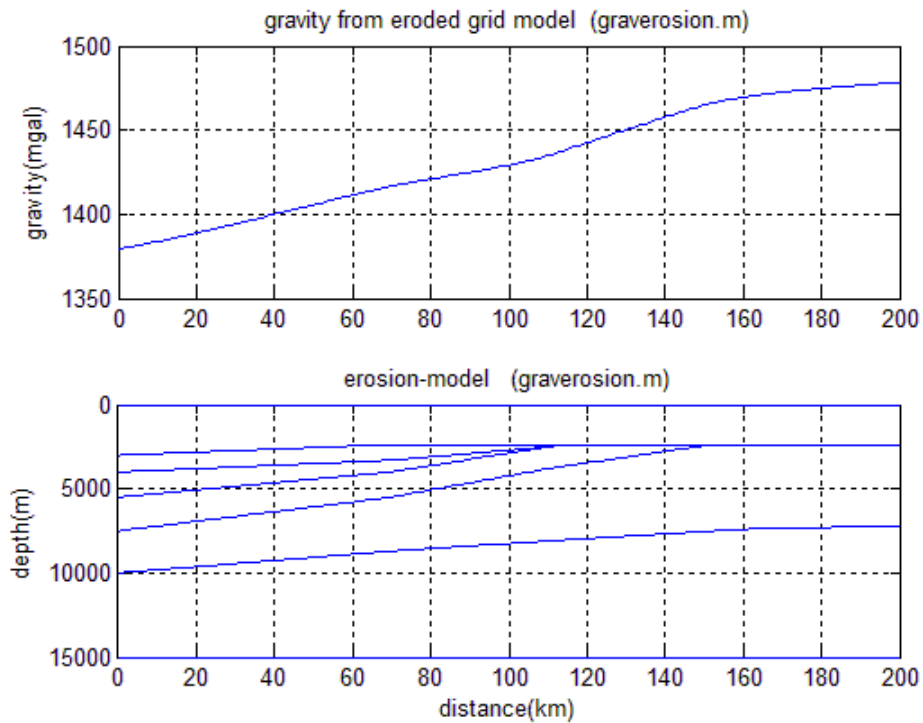


Figure 3.16: Gravity modeled from the eroded grid model

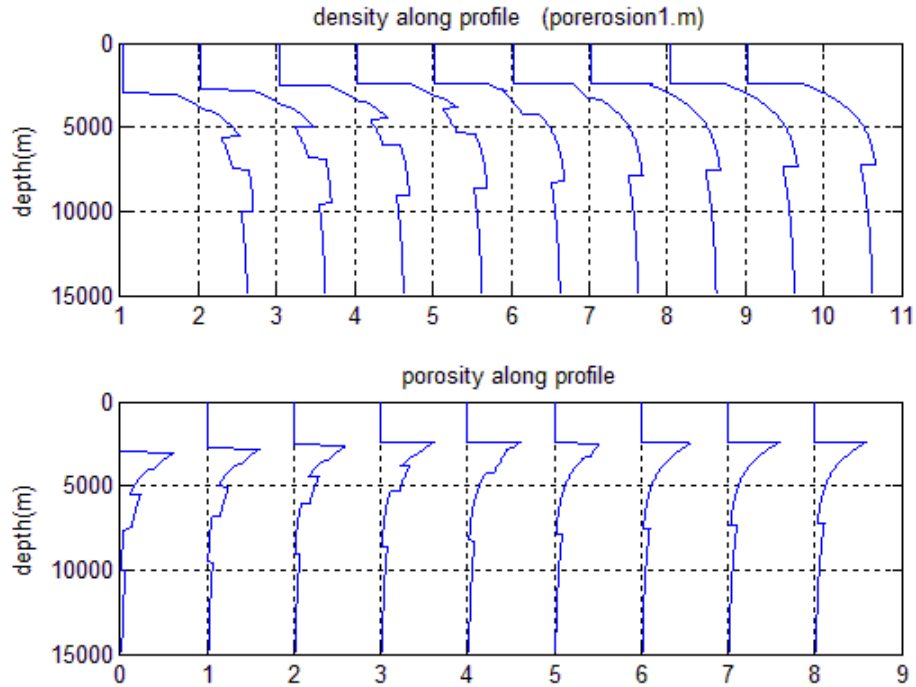


Figure 3.17: Porosity and density along a profile for a model with the same geometry as the eroded model in figure 3.13, but with no influence on the porosity from erosion.

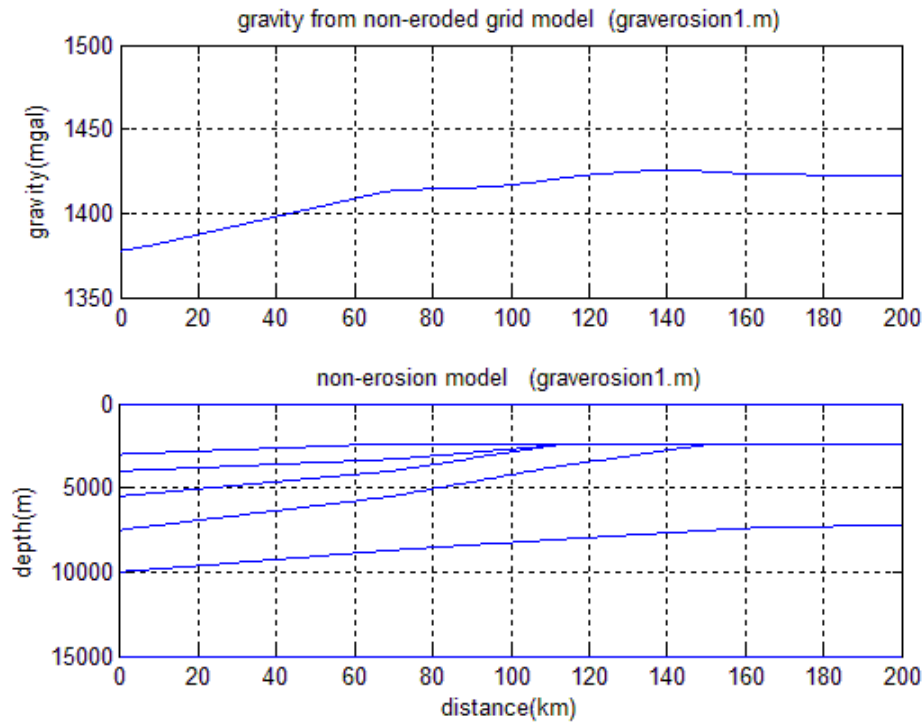


Figure 3.18: Gravity modeled from the model in figure 3.17

Chapter 4: Grid method applied on an interpreted crustal section on Vøring

4.1 General

Two different methods were applied to model the gravity of a digitized OBS-line from the thesis of Libak(2008). The first method was to use constant densities to model the gravity, as done by Libak. The second method used was the grid method described in chapter 3. The OBS-line that was modeled is OBS-line L10-96, which goes through the Vøring Basin (figure 4.1). The interpretation and layering used by Libak(2008) was also used here (see figure 4.2).

The main focus in this chapter is to examine the difference in modeling based on the grid method compared to modeling with constant densities, and to adjust the position of Moho and the lower crustal layer to fit the model with the observed gravity along the profile.

First the gravity was modeled using the density from the thesis of Libak(2008) (table 4.1). The result of modeling the gravity with constant densities is shown in figure 4.2A.

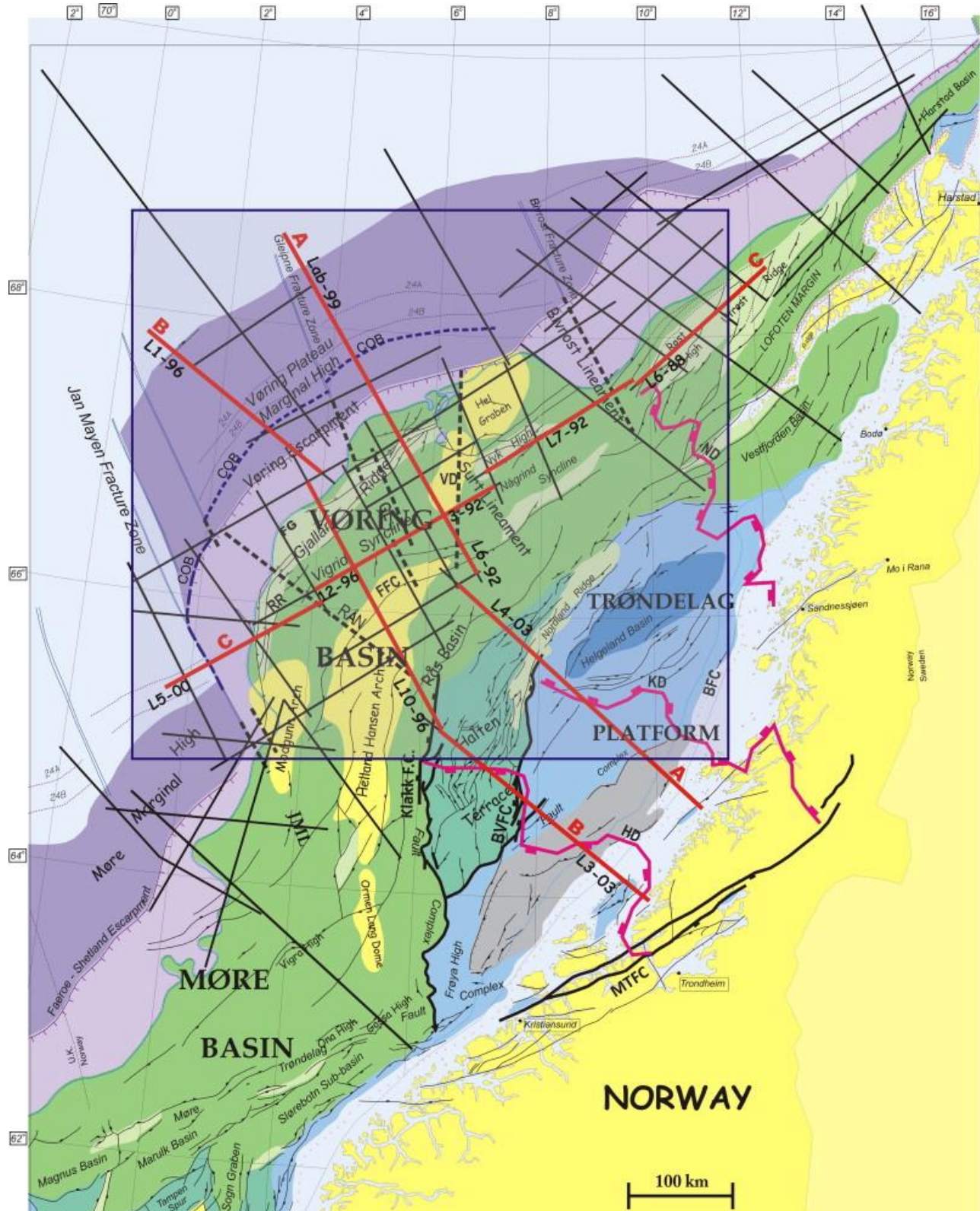


Figure 4.1: Overview of the modeling area, where the red line L10-96 is the one that is modeled (Mjelde, Faleide, Breivik, & Raum, 2009) modified from (Blystad P., 1995)

Table 4.1: The layering and densities (Libak, 2008) used in modeling with constant density.

Nr.	Layer	Bulk density (g/cm ³)
1	Water	1.03
2	Tertiary	2.13
3	Basaltic extrusives	2.63
4	Upper-Cretaceous	2.40
5	Mid-Cretaceous	2.47
6	Ocean layer 2B	2.77
7	Lower-Cretaceous	2.60
8	Ocean layer 3A	2.88
9	Pre-Cretaceous	2.69
10	Crystalline crust	2.83
11	HVL/Ocean layer 3B	3.10
12	Mantle	3.33

4.2 Calculating the gravity using the grid method and given lithologies

In the second method, the gravity modeling was done with varying densities within the layers. The lithology of the different layers was found from a report from well 6506/11-2 at Vøring margin together with other adjacent wells (NPD) as 6704/12-1, 6504/5-1S, 6506/3-1, 6605/8-1 and 6505/10-1. The report (Jensen, 1992) from well 6506/11-2 presents the percentage of the different lithologies section by section down the length of the borehole. From the lithology the porosity parameters a , ϕ_0 , and the densities could be calculated as described in the grid method in chapter 2.

The most uncertain sedimentary layer is the Upper-Jurassic layer, as the thickness of this layer varies within the Vøring Basin. There is a minimum thickness of 3 km of pre-Cretaceous sedimentary rocks regionally, and locally the thickness may be as much as 10 km (Raum, et al., 2006). Here, in this line, the thickness is approximately up to 5.5 km. The age of the pre-Cretaceous sedimentary layer is from the late mid-Jurassic (Brekke, 2000), and therefore the chosen formations from the pre-Cretaceous layer is the Spekk-, Melke-, Garn-, Not- and Ile-formations. The V_p/V_s ratio was also studied to help find these formations. The V_p/V_s ratio in this pre-Cretaceous layer was a bit lower than in the lower Cretaceous, 1.65-1.67 compared to 1.70-1.73 (Mjelde, et al., 2003), which may indicate a higher sand/shale ratio here. The parameters from the other layers, which are not sedimentary rocks, are found from Libak(2008).

All the parameters used in modeling the grid method are listed in table 4.2.

The result of the modeling the grid method is shown in figure 4.2B together with the result from the first method (figure 4.2A). When comparing the two methods, one can see that the trend of the relative gravity is similar. The gravity curve, where the densities are constant, show a higher value of up to 140 mGal compared to the gravity curve from the grid method. The gravity curve from the grid method is smoother and the only abrupt change in relative gravity is to the north-west part of the profile compared to the constant density method, where the gravity curve has a more gradually change.

Table 4.2: An overview of the different layers in the digitized line and the parameters used in the modeling

Nr.	Layer	Formations (and %).10	Sand (%)	Shale (%)	Chalk (%)	a	ϕ_0	ρ_f	ρ_g
1	Water					0	1	1.03	1.03
2	Tertiary	Naust (51)	50	50		0.44	0.59	1.03	2.70
		Kai (14)	50	25	25				
		Brygge (26)		100					
		Tare (4)		100					
		Tang (6)		100					
3	Basaltic extrusion					0.10	0.00	1.03	2.63
4	Upper- cretaceous	Springar (50)		100		0.51	0.63	1.03	2.71
		Nise (50)	6	90	4				
5	Mid- Cretaceous	Delfin (13)	100			0.45	0.58	1.03	2.69
		Kvitnos (80)	30	60	10				
		Lysing (7)	70	20	10				
6	Ocean layer 2B					0.05	0.00	1.03	2.77
7	Lower- Cretaceous	Lange (97)	15	75	10	0.50	0.62	1.03	2.71
		Lyr (3)		50	50				
8	Ocean layer 3A					0.05	0.00	1.03	2.88
9	Upper- Jurassic	Spekk (13)		100		0.44	0.59	1.03	2.69
		Melke (45)		90	10				
		Garn (17)	95		5				
		Not (7)	50	50					
		Ile (18)	90	10					
10	Crystalline crust					0.05	0.00	1.03	2.90
11	Ocean layer 3B					0.05	0.00	1.03	3.10
12	Mantle					0.05	0.00	1.03	3.3

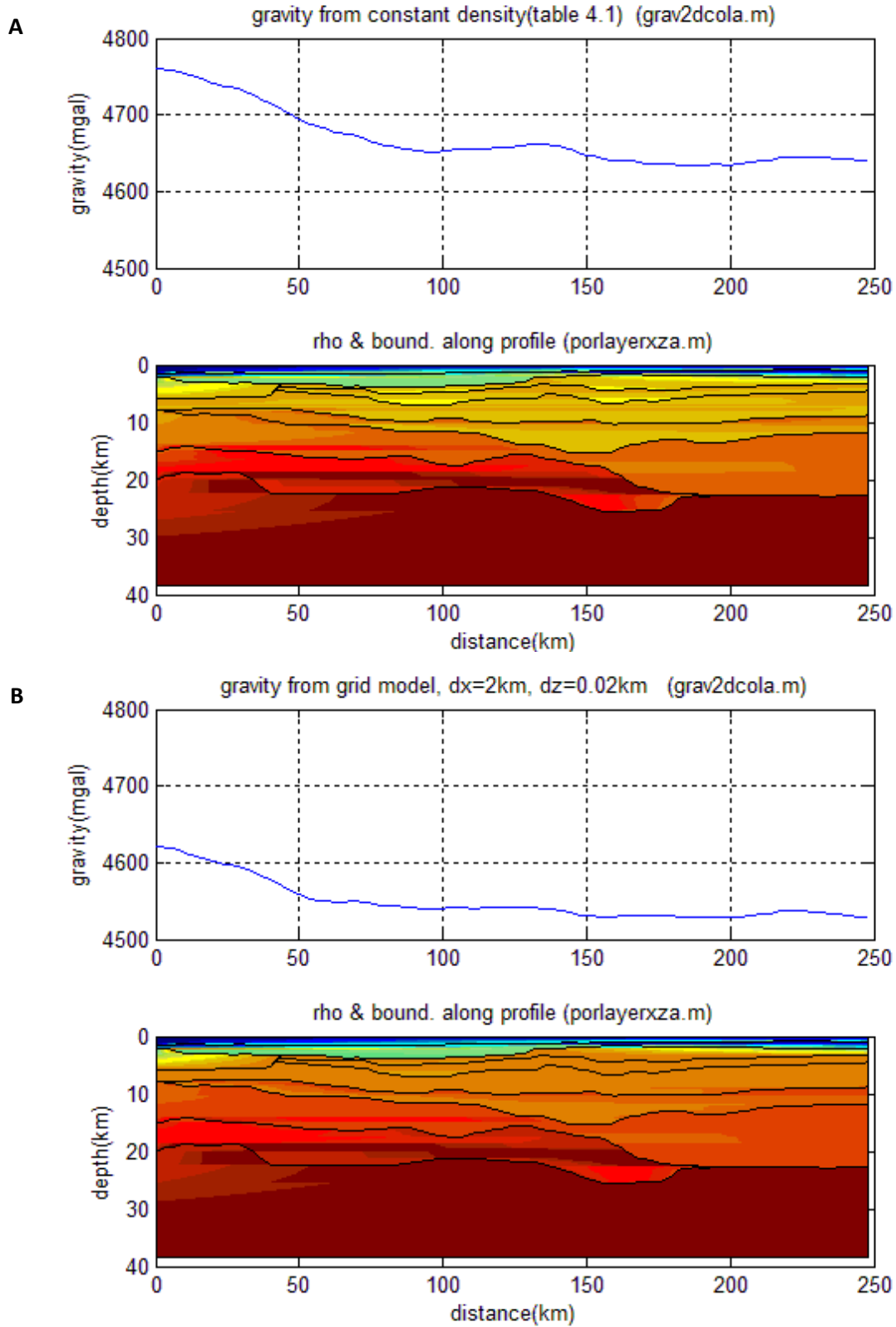


Figure 4.2: A: The modeled gravity when constant densities. B: the modeled gravity using the grid method, with varying densities.

4.3 Adjustments of Moho using Cordell & Henderson's method

The observed g along the OBS-line L10-96 is taken from Sandwell and Smith(1997)(more details in chapter 5.5), and differ significant from the modeled gravity, see figure 4.3 and figure 4.4.

To make a better fit between the modeled and the observed gravity, correction of the Moho is one possibility. The most uncertain part of the Moho is under the north-western part of the line, where the OBS-data is uncertain. If we look at the observed gravity, it would be more reasonable if the Moho lies deeper in that area. A program based on Cordell-Henderson's iterative method (see chapter 2.4) was developed to improve the fit between the observed and the calculated gravity. The observed and the calculated relative gravity is first set equal at an anchor point, and then Moho is adjusted based on this anchor point. I used an anchor point at 52 km to correct the Moho, and 5, 10 and 20 iterations were used for both methods (figure 4.3 and 4.4) to see how the fit between the observed and calculated gravity improved, and how the deep layers changed their geometry. They all give a good fit between the observed and the calculated gravity, but both the 10 and 20 iterations give an unrealistic geometry of the deeper layers. Therefore, 5 iterations were chosen as it also gave the most realistic geometry of the deepest layers for both methods.

The final result of the gravity after the Moho has been corrected for is repeated in figure 4.5. There is no significant difference of the two methods when looking at the relative gravity modeled after the Moho has been corrected for. In the constant density method, the observed and calculated gravity seems to fit slightly better. As it is the Moho that has been changed, the difference lies in the geometry of the deep structure in the geological model. Here, the grid method makes the Moho and the lower crustal body deeper than in the constant density method, especially in the north-western part of the line.

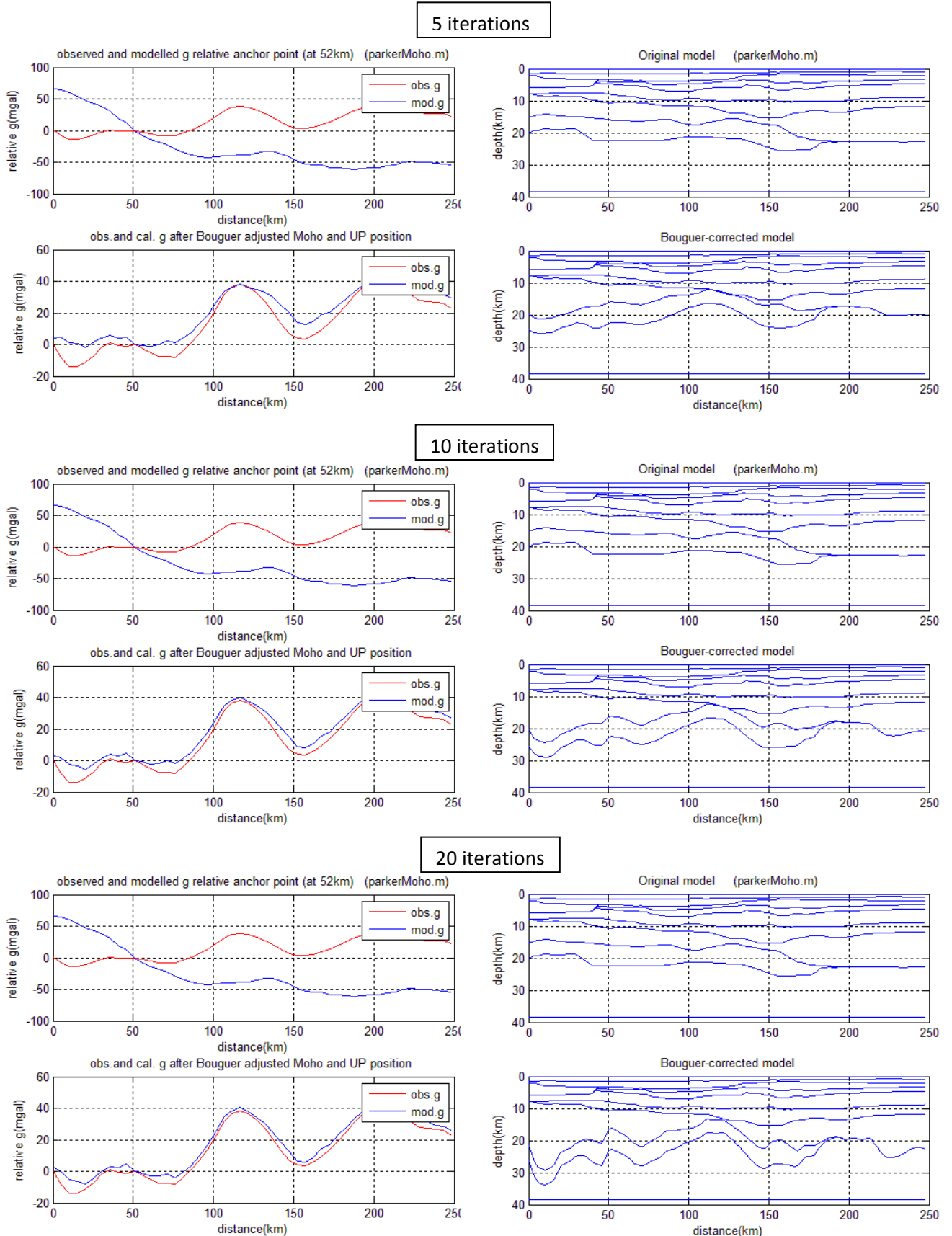


Figure 4.3: Correcting for the Moho for the constant density method, testing the number of iteration needed to make the best fit and the most realistic geometry of the deeper layers.

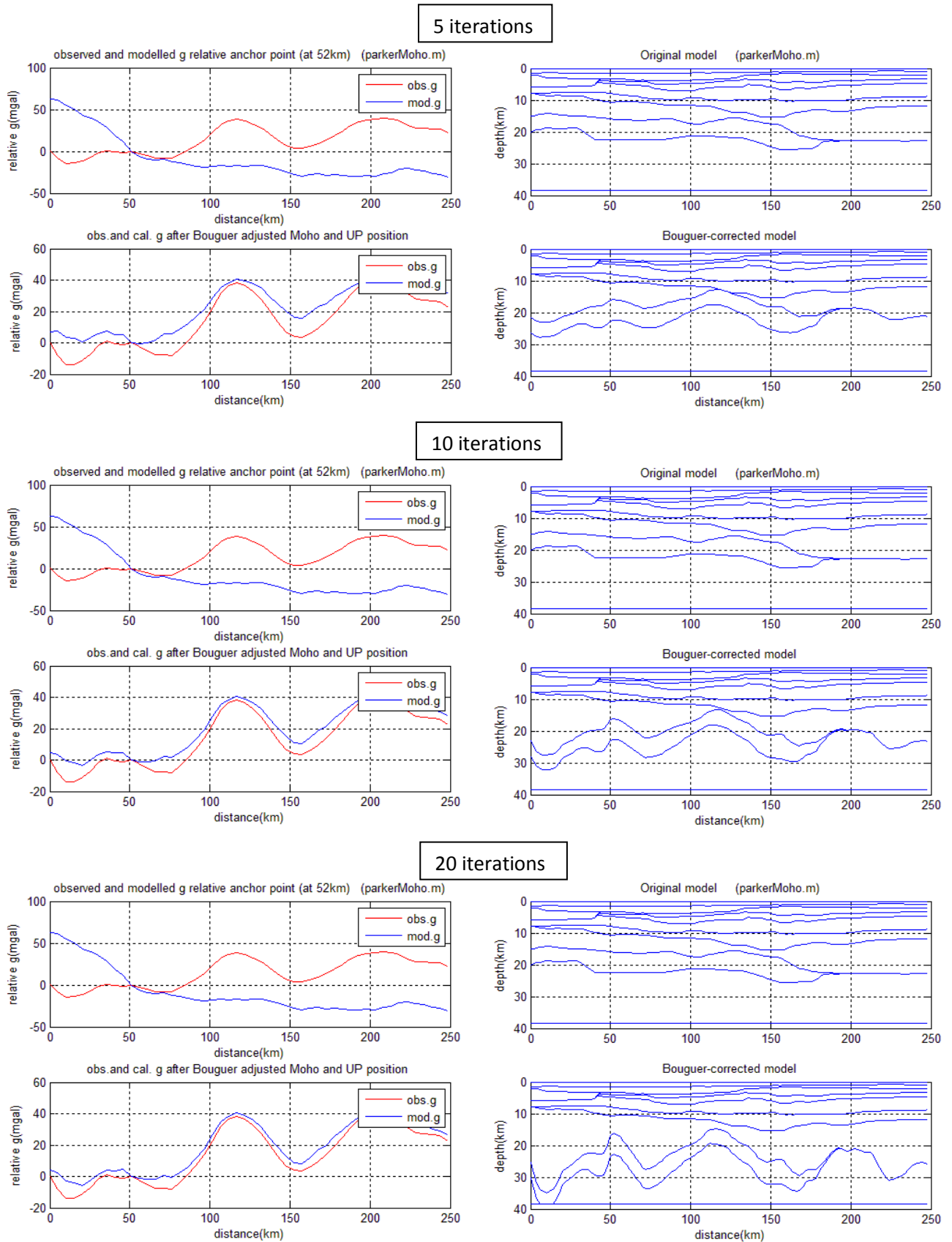


Figure 4.4: Correcting for the Moho for the grid method, testing the number of iteration needed to make the best fit and the most realistic geometry of the deeper layers.

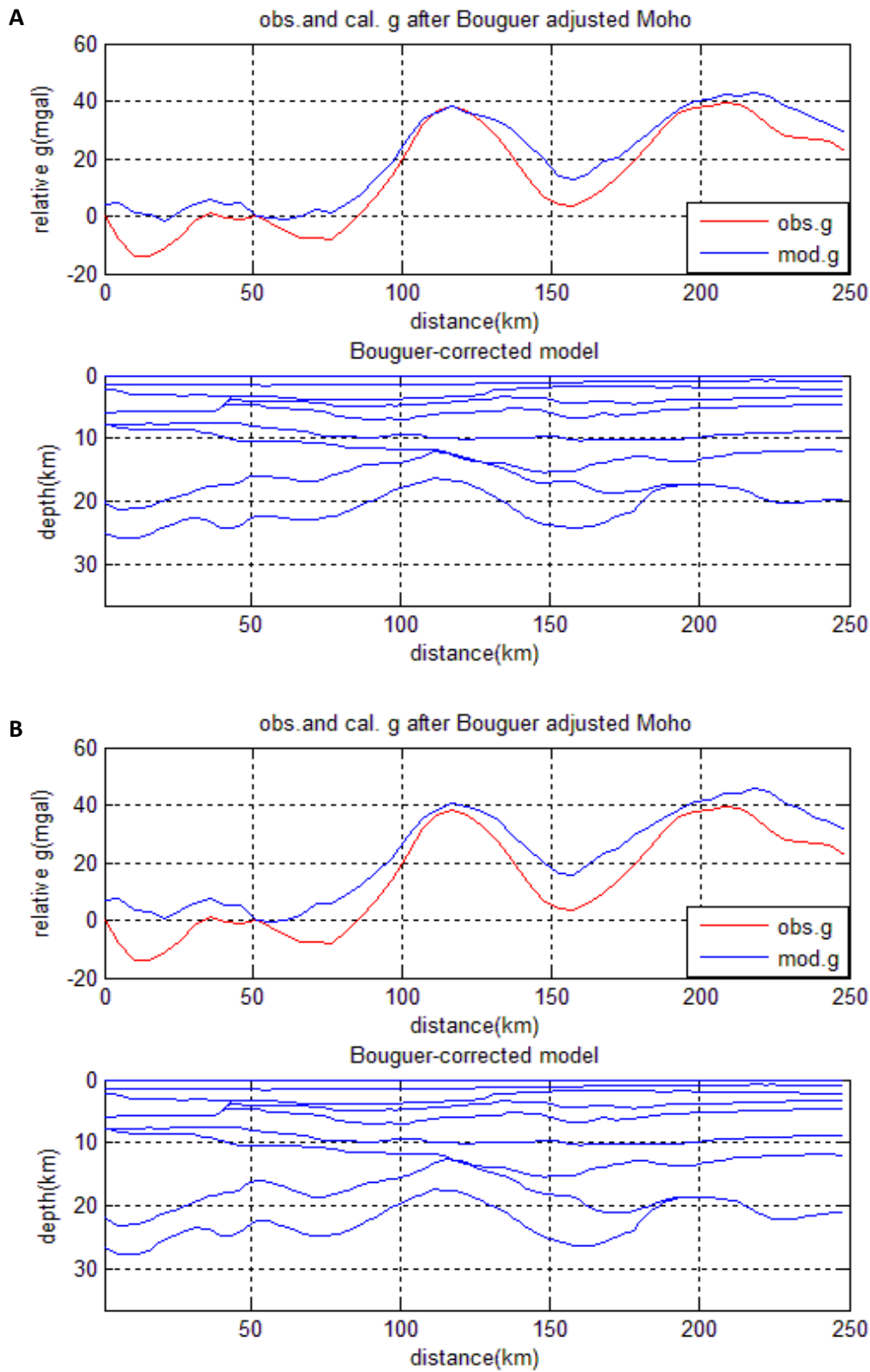


Figure 4.5: The observed and the calculated gravity after the Moho has been corrected for. A: the constant density method. B: Grid method

4.4 Other possible changes of the model that can decrease the difference between modeled and observed gravity

If changing the density in layer 3 (basaltic intrusion, figure 4.8A and table 4.2) from 2.63 g/cm³ to 2.2 g/cm³ (shallow sediments) we get a reduction of about 60 mGal of the value of the gravity in the north-western end of the line (figure 4.6A), which narrows the gap between the observed and modeled gravity. If we reduce the density in the lower crustal body (see layer 11, figure 4.8A) from 3.10 g/cm³ to 2.90 g/cm³ the gravity difference is reduced even more (figure 4.6B). The fit between the observed and calculated gravity is then already much better before the Moho is adjusted for (figure 4.7 compared to figure 4.3 and 4.4). Hence the Moho adjustment will be smaller than in the previous cases.

These examples show that the density and geometry of certain layers may have great influence on the Cordell-Henderson-corrected Moho. There is for example a big difference between figure 4.5A and figure 4.8B. The first is calculated from the original model with constant densities, while the latter is calculated from the original model after ρ_3 has been changed from 2.63 g/cm³ to 2.2 g/cm³ and ρ_{11} from 3.1 g/cm³ to 2.9 g/cm³.

Another possible change that will reduce the difference between the observed and modeled gravity is shown in figure 4.9A. Here, the mantle lithosphere down to 100 km has a change in density from 3.28 g/cm³ in NW to 3.34 g/cm³ in SE. An argument for such a change is that the northern end of the profile is close to the continent-ocean boundary. The resulting gravity curve fits the observed curve much better than if the mantle was homogeneous ($\rho=3.3$) when comparing figure 4.3 and 4.9A.

In figure 4.10 two more realistic examples show how the modeled gravity curve is changing with changing ρ -values in certain layers. First, layer 11 was divided in two (similar as figure 4.9) and the density of the NW of the layer was changed from 2.28 g/cm³ to 3.30 g/cm³ (figure 4.10A). In addition the density in layer 3 was reduced from 2.63 g/cm³ to 2.40 g/cm³ (figure 4.10B).

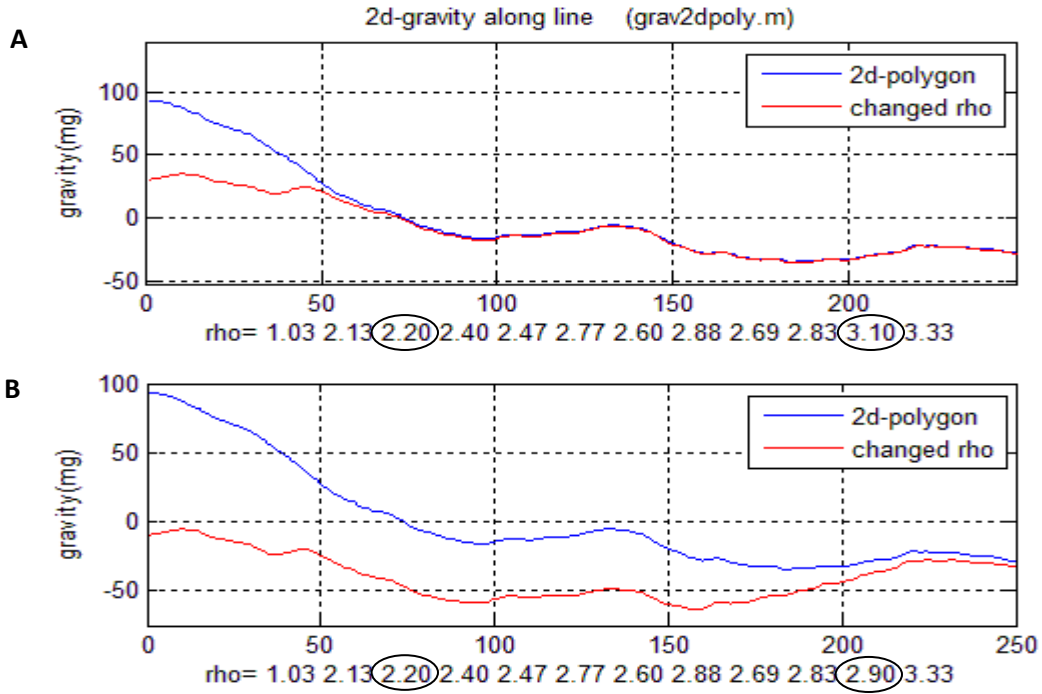


Figure 4.6: The constant density method. A: The modeled gravity of the line based on the densities from the thesis of Libak and the modeled gravity when changing the density in layer 3 from 2.63 to 2.2 g/cm³. B: Here the density in layer 3 is changed from 2.63 to 2.2 g/cm³ and the density in layer 11 from 3.1 to 2.9 g/cm³

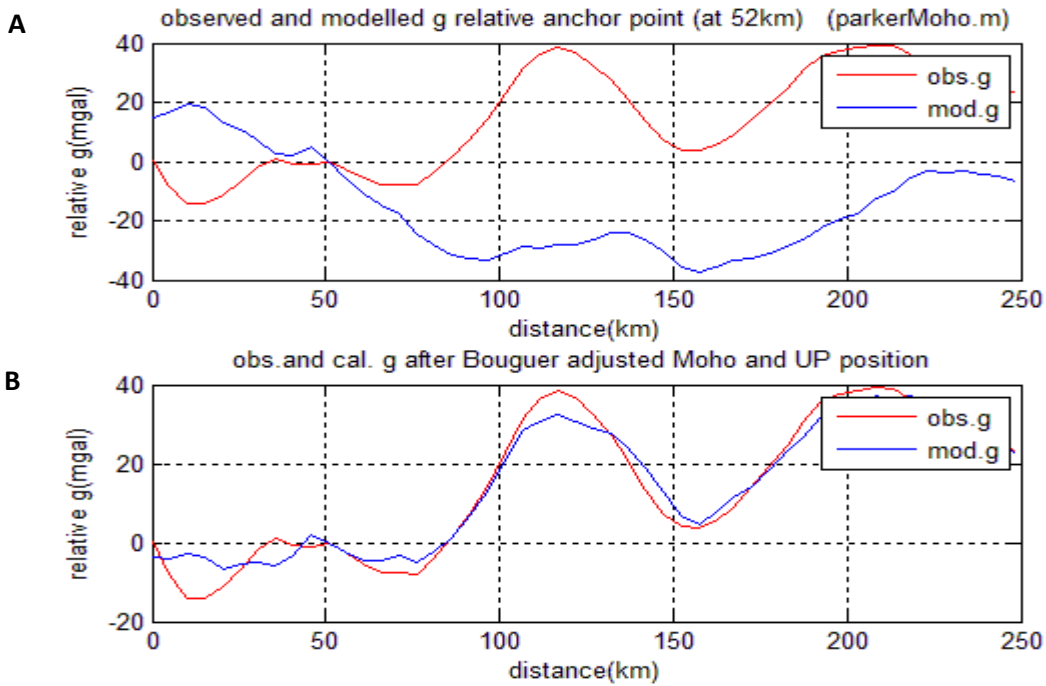


Figure 4.7: The constant density method. A: The observed and calculated relative gravity after changing the densities in layer 3 and 11. B: The observed and calculated relative gravity when after Moho has been corrected for (see figure 4.8).

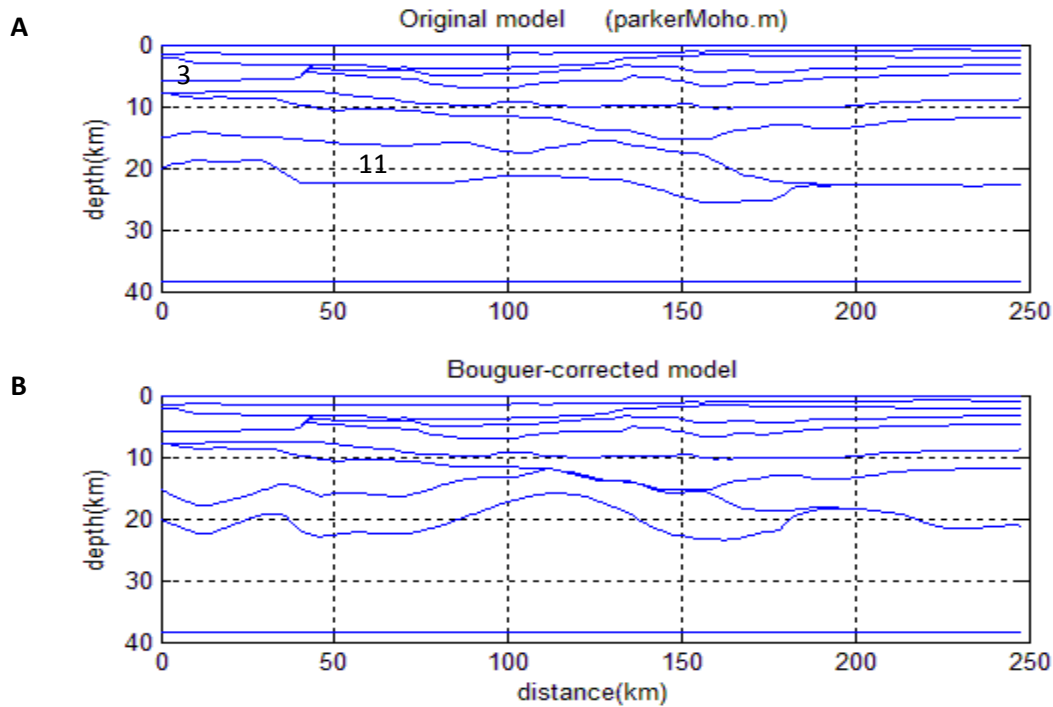


Figure 4.8: The constant density method. A: The original line L10-96. B: The Cordell-Henderson-corrected model, when the density in layer 3 and 11 has been changed.

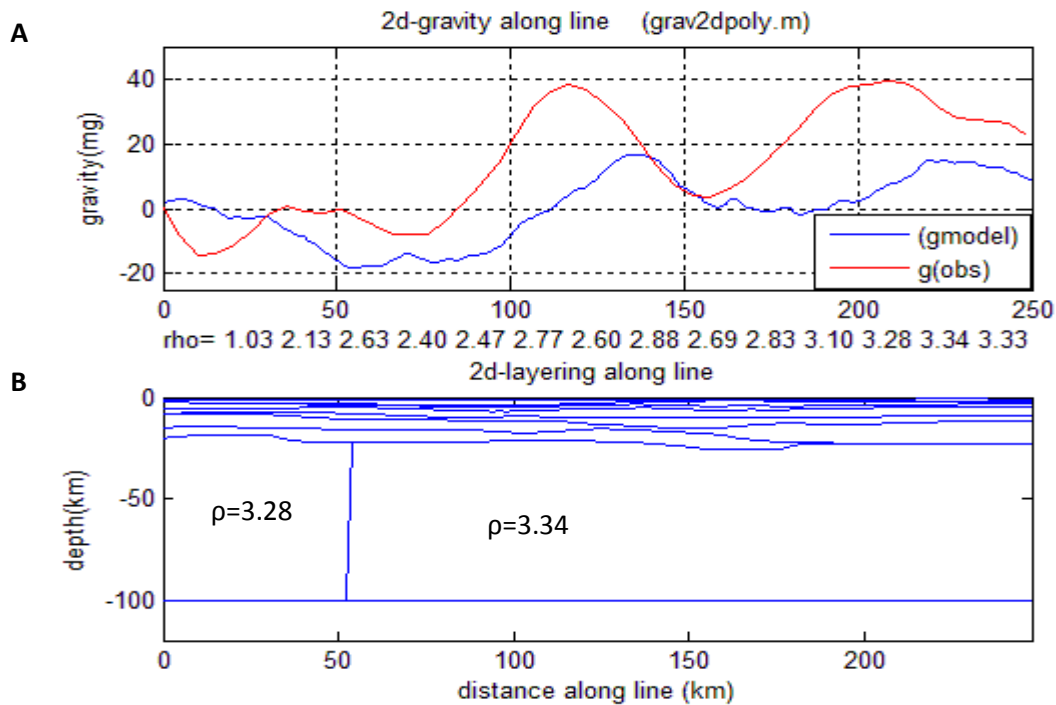


Figure 4.9: A: The modeled gravity when the mantle lithosphere down to 100 km has a change in density from 3.28 g/cm^3 in NW to 3.34 g/cm^3 in SE. B: The geological model showing that the mantle lithosphere has a change from 3.28 g/cm^3 in NW to 3.34 g/cm^3 in SE.

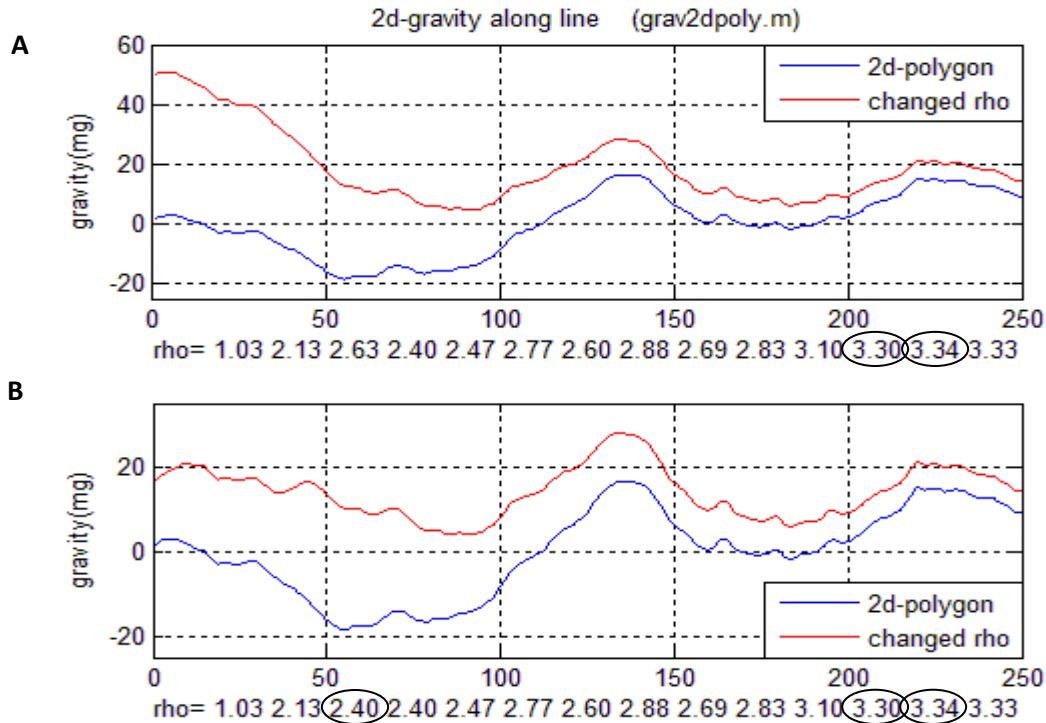


Figure 4.10: Two more examples showing the modeled gravity changes while changing densities in layer 11 and 3 (for details, see text)

In the Vøring Basin, there is presence of sill. The sill layers are relatively thin, and is absent in the interpretation of the layering of the line. The thickness of the sill is difficult to estimate as the base of the sill is a weak reflector because it is composed of a mixture of the underlying sediments together with the sill composition. Still, we have an estimate of the thickness of about 50-150 m (Raum, et al., 2002).

An extreme case of a thickness 250 m sill was modeled to see the effect of the layer when modeling the gravity. The sill-layer is modeled 50 km long and with a density of 3 g/cm³. This means that there is a density contrast from sand layer (2.65 g/cm³) to the underlying sill layer (3 g/cm³).

The result is shown in figure 4.11. The 250 m thick layer of sill give a difference of about 5 mGal compared to the gravity outside the extent of the sill. A thin sill layer will apparently give negligible contribution to the gravity field.

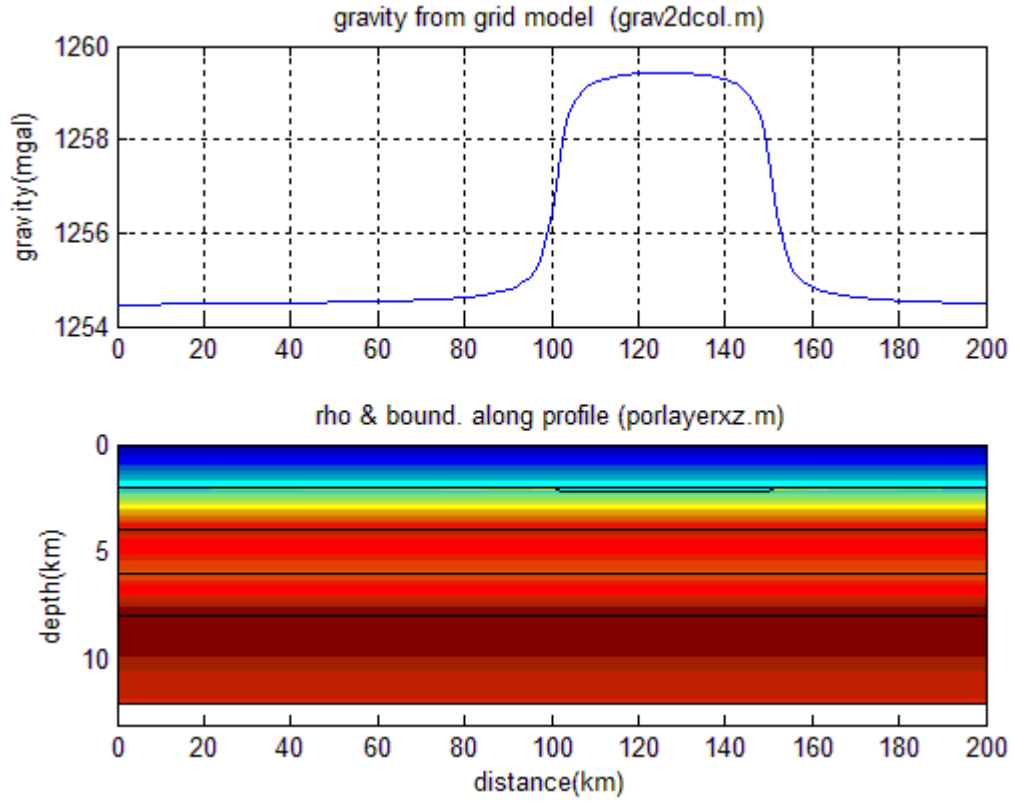


Figure 4.11: A simple flat layered model, where there is a 250 m thick and 50 km long layer of sill present, with density contrast from sand (2.65 g/cm^3) to sill (3.00 g/cm^3).

Chapter 5: Grid method applied on two seismic sections from the North Sea

5.1 General

In this chapter, two seismic profiles were picked from the North Sea by using the database Discos. Discos is a common national store base for exploration and production-related information. The discos data storage is a computer file system that has been designed to store large amounts of digital data on behalf of the companies and the public. This means that digital data from the Norwegian continental shelf is located in the national petrodata store in Stavanger. The type of data obtained from the data base are seismic and navigation data, well data and production data.

I interpreted the geological layering of the profiles and by using information from adjacent wells, a depth conversion was done and further a geological model of each profile was made. The information needed from the wells was the lithology from the different formations and time periods together with the velocity. From this information, the porosity parameters and the densities could be calculated and further be used in the modeling.

5.2 Interpretation

The study area where the seismic profiles were picked from is the North Sea. Line 1 and Line 2 extend from the Utsira High across the Viking Graben, where Line 2 is located a bit north from Line 1 (figure 5.1).

The interpretation of the layering was based on an interpretation from a paper from Myhre(1977) together with paper from the Norwegian Petroleum Society (Ziegler, 1986). The paper of Myhre(1977) includes an interpretation of the lithology in the adjacent well, no. 16/1-1, and the paper from the Norwegian Petroleum Society (Ziegler, 1986) contains a summary of the tectonic evolution of the Norwegian offshore areas and place the hydrocarbon occurrences in their tectonic habitat. Within this paper, a classic

seismic line across the Viking Graben, the Utsira high and the Stord basin is shown. This seismic line is interpreted and shows the different layers in age.

The first horizons to interpret were the ocean bottom and the base Cretaceous unconformity, which are two very strong reflectors. Then the other horizons were interpreted after what the seismic showed and the layering interpreted in the two papers. The migrated seismic profiles without and with interpretation are shown in figure 5.2 and 5.3. The interpreted layers, from youngest to the oldest, are:

- Quaternary
- Pliocene
- Miocene
- Oligocene
- Eocene
- Paleocene
- Cretaceous
- Late Jurassic
- Early to Middle Jurassic
- Triassic
- Permian
- Crystalline crust

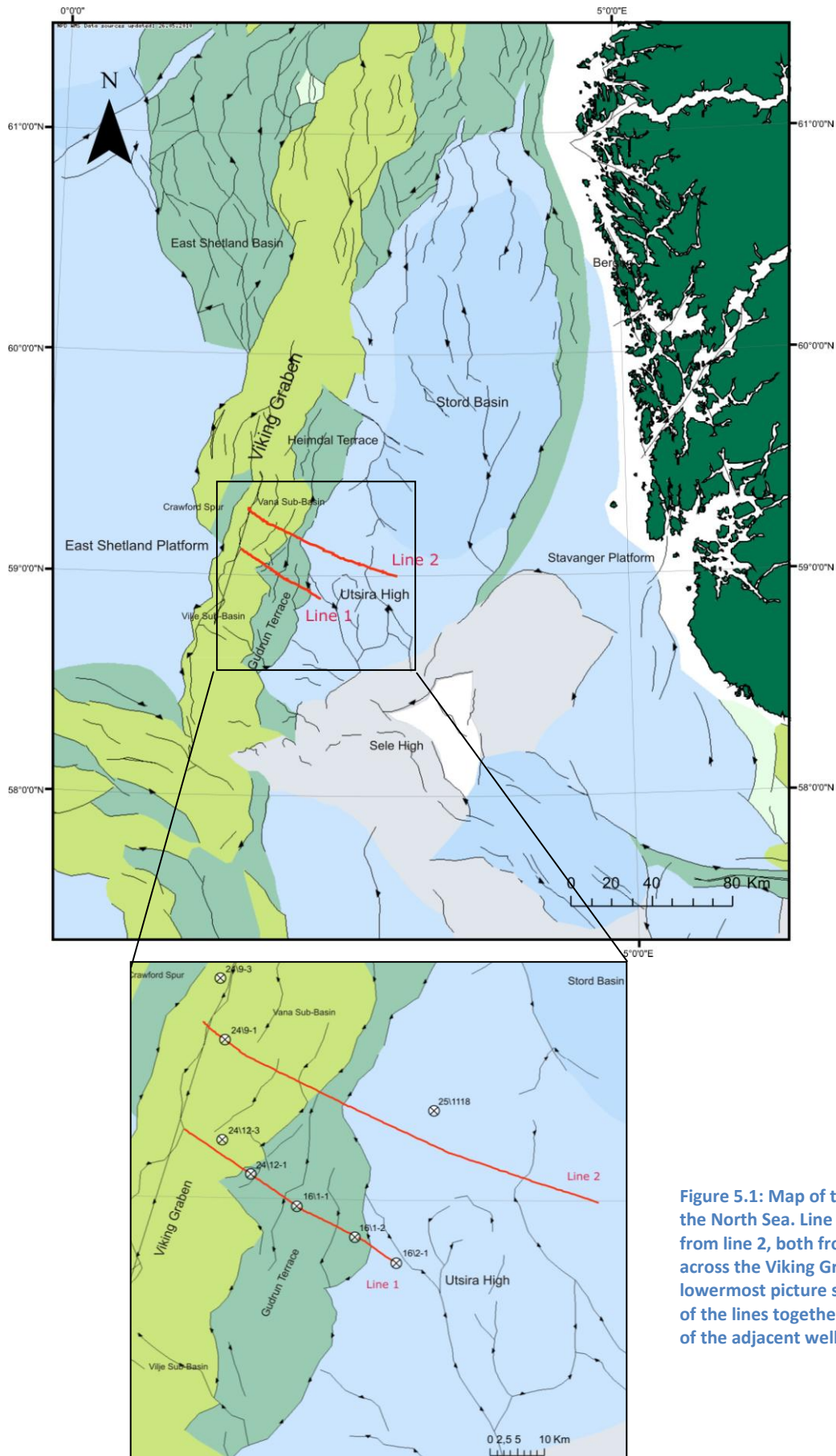


Figure 5.1: Map of the study area in the North Sea. Line 1 is located south from line 2, both from the Utsira High across the Viking Graben. The lowermost picture shows a closer view of the lines together with the location of the adjacent wells.

There are some uncertainties within the interpretation:

There is a major thinning of the Cretaceous and upper Jurassic strata on the regional seismic line over the Horda platform, where the Cretaceous layer is only a few 10's of meters thick (Sneider, 1994). This major thinning made it difficult to locate and interpret the top of Cretaceous package above the Utsira High and, as shown in figure 5.3 and 5.4, the final interpretation ended in a termination of the layer close to the top of the Utsira High. When comparing the composite logs, one located at the Viking Graben and one located at the Utsira High, one can see the major thinning (figure 5.2). However, this uncertainty does not give a significant effect in the gravity modeling, because the Cretaceous strata layer is thin and lies relatively shallow.

A more significant uncertainty is the interpretation of the deepest horizons and layers where the reflections are weaker and more difficult to interpret. Here, the layers have lower porosity and are denser, and also the velocity is higher. Hence, a misinterpretation could give a larger effect in the gravity modeling.

After the interpretation was done the profiles were digitalized into ASCII-data files, which further were used in the modeling in Matlab. The digitizing was done using a digitizing tablet. If the boundary of the layers were terminating along the profile, the lower interface was put together with the upper one and a layer thickness of zero was set. This was necessary to interpolate each interface to grid values through the entire model. In the two interpreted profiles, the water layer, Quaternary, Pliocene, Miocene, Oligocene and Eocene never have a thickness of zero.

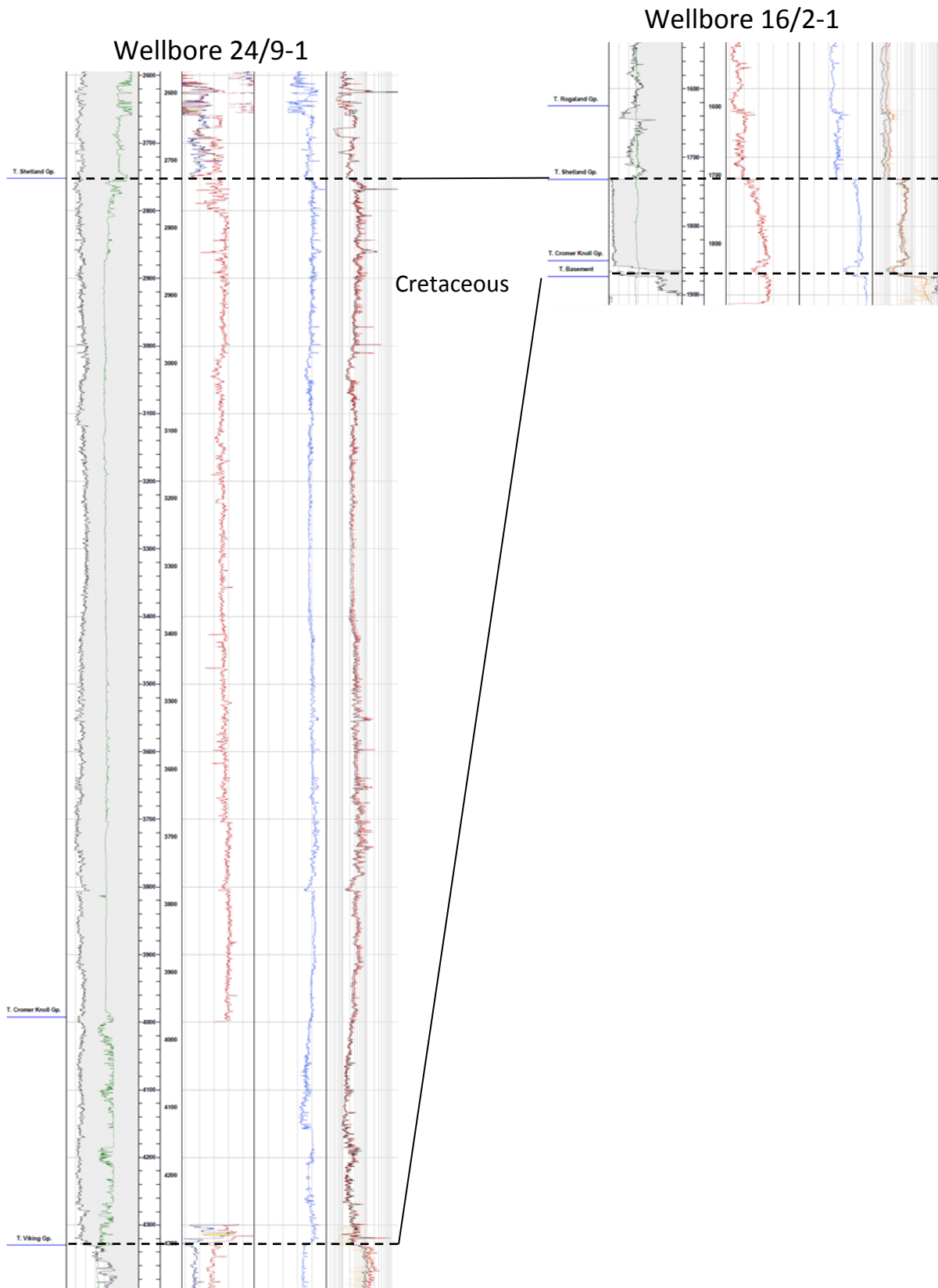


Figure 5.2: Sections from wellbore 24/9-1 and wellbore 16/2-1 showing the thickness variation of the Cretaceous strata. Well 16/2-1 is located at the western part of the Utsira High, while well 24/9-1 is located in the Vana sub-basin in the southern Viking Graben. The logs have the same length scale, but the layers are not at the same depth; in well 24/9-1 the top Cretaceous is at ca. 2740 m depth while in well 16/2-1 it is at 1730 m.

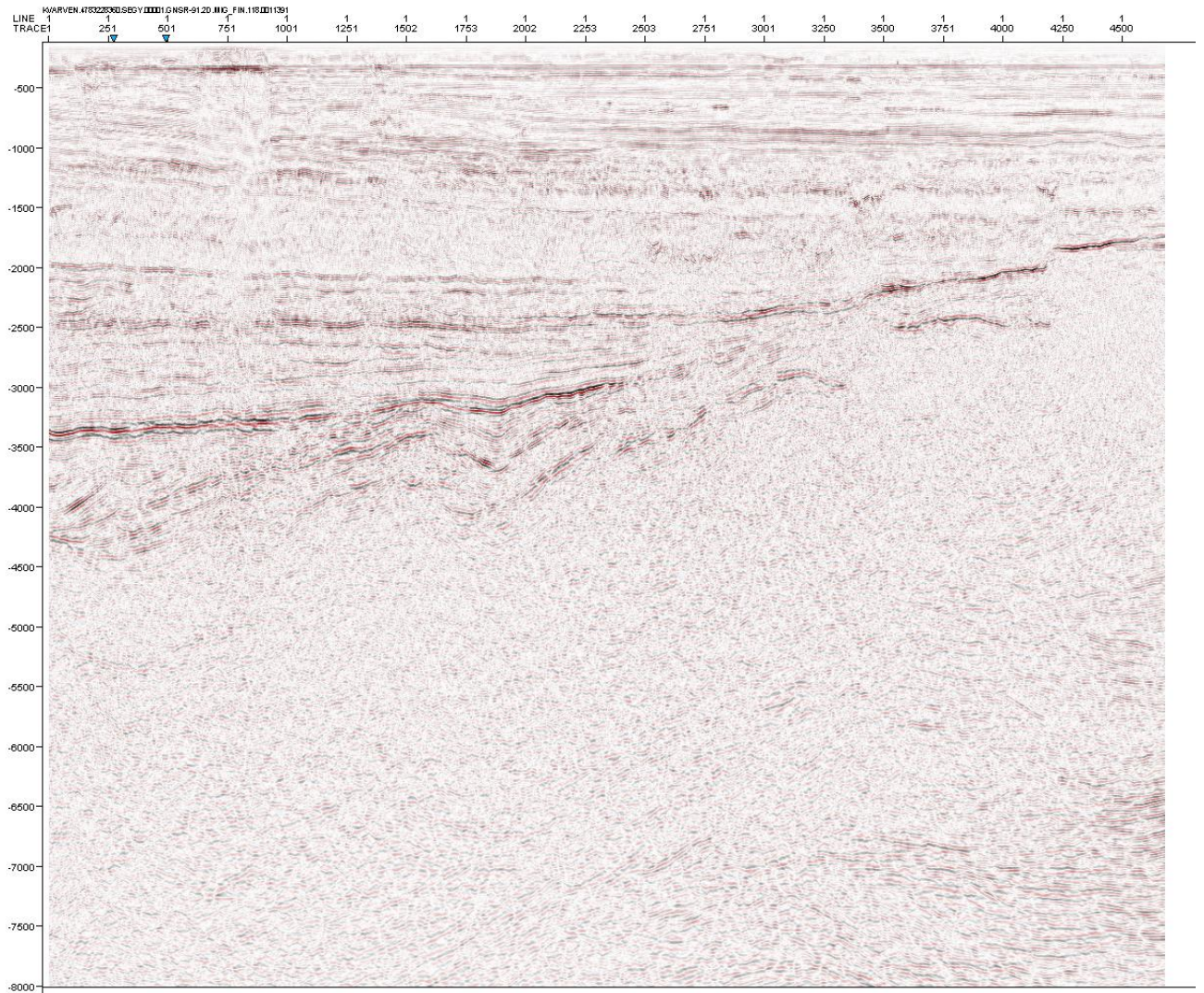


Figure 5.3A: Line 1 before interpretation

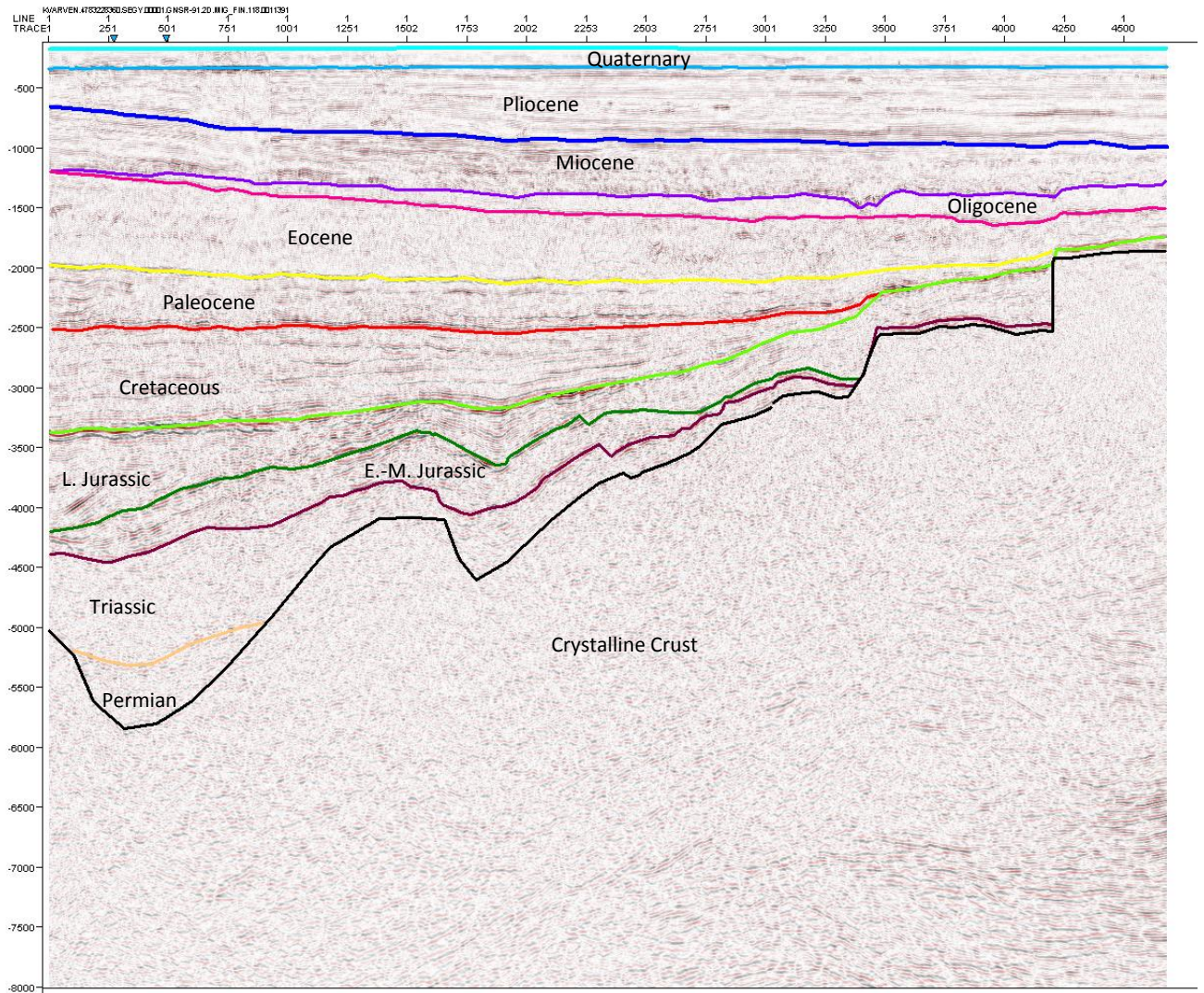


Figure 5.3B: The interpretation of line 1

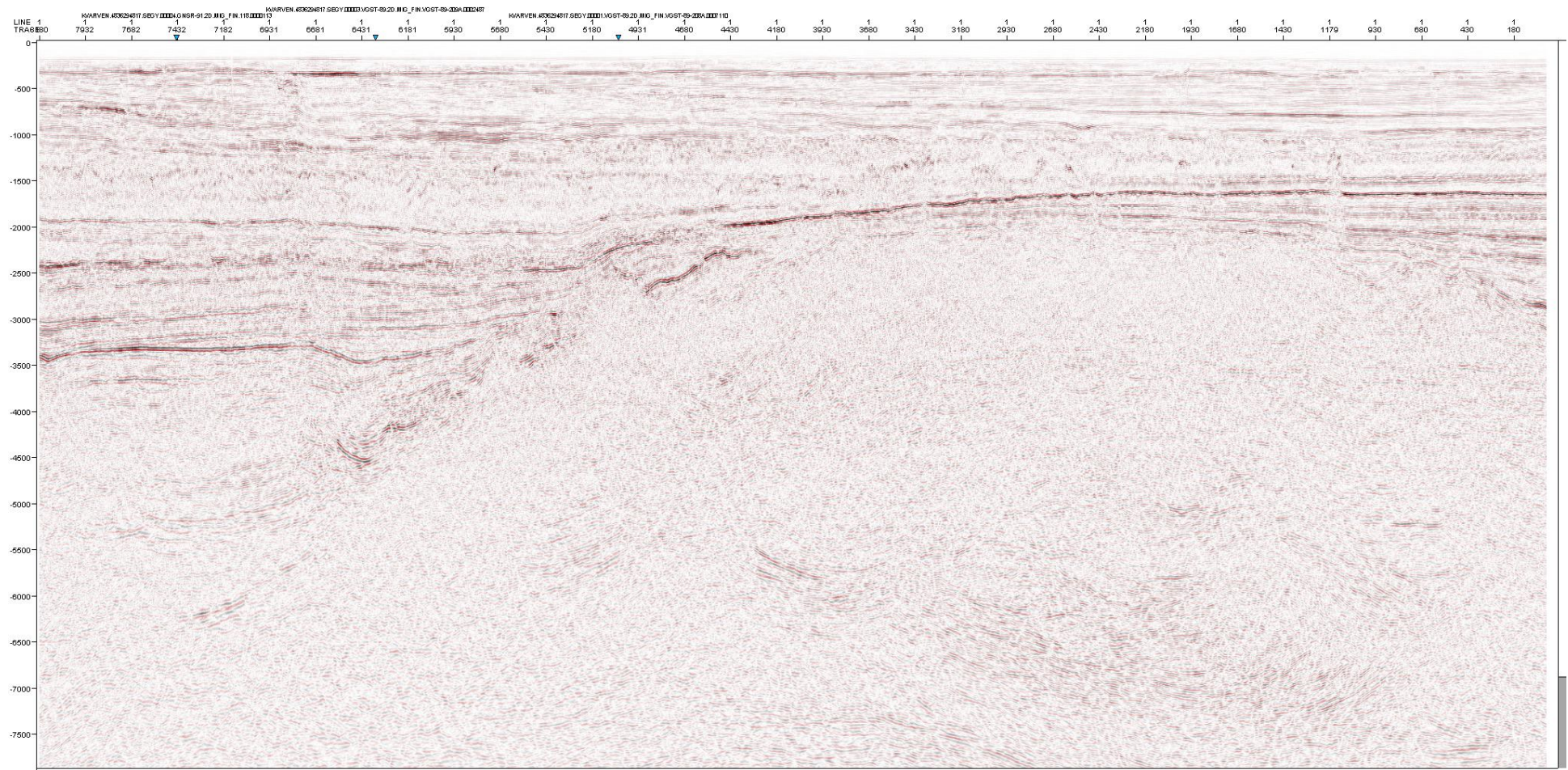


Figure 5.4A: Line 2 before interpretation

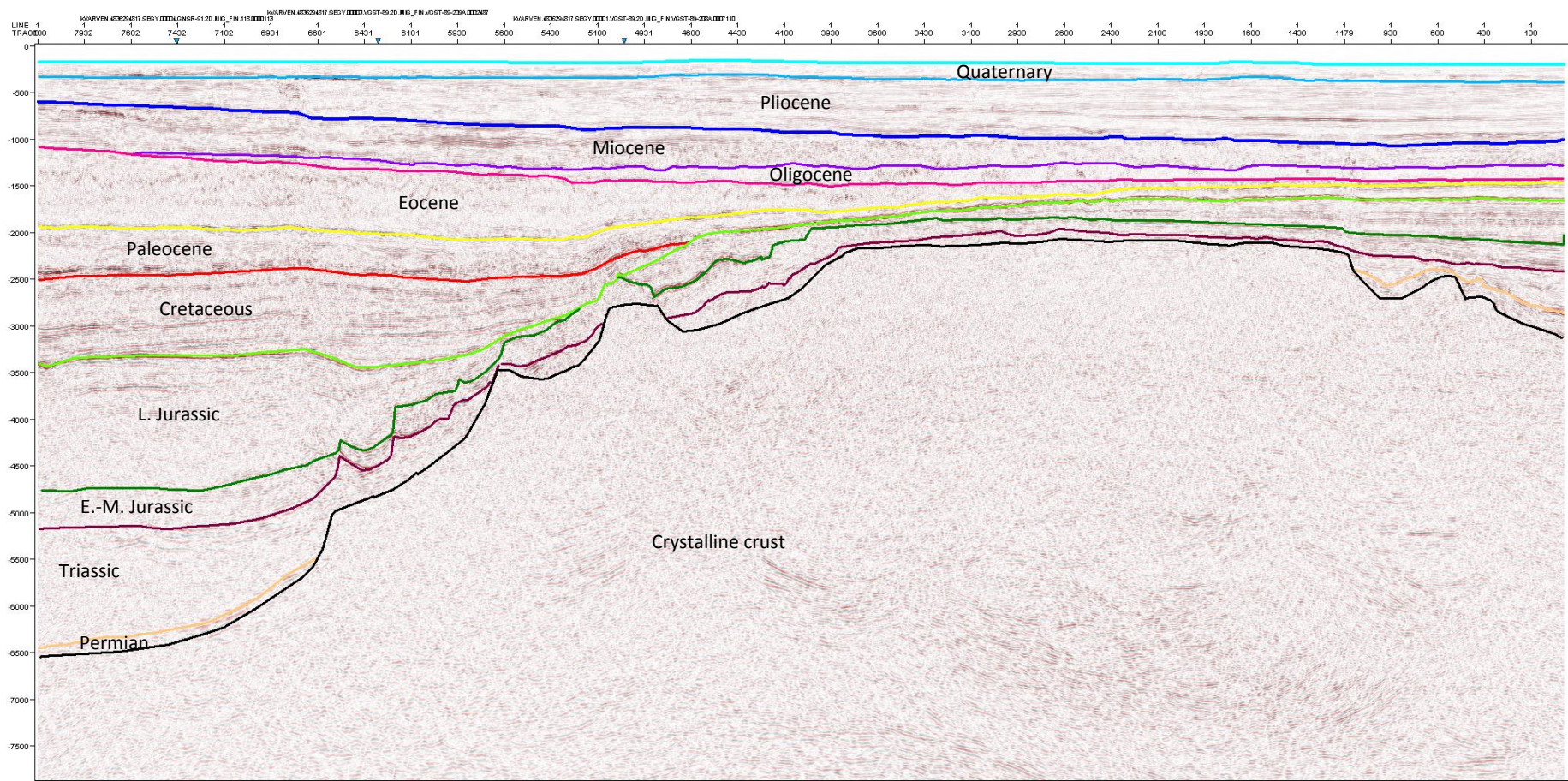


Figure 5.4 B: The final interpretation of the line 2.

5.3 Lithology and velocity

5.3.1 Lithology

The lithology of the different layers was found from reports from adjacent wells in the North Sea (NPD). Some of the reports present the percentage of the different lithologies section by section down the length of the borehole. The amount of information found from the different wells depends on the well; some wells include composite logs, several reports, cores etc., while other wells don't give any profit. The wells with the most information comprising lithology are 16/2-1 (Myhre, 1976), 16/1-2 (Esso, 1977), 24/12-1 (Statoil, 1978) and 24/9-1 (Bjørøy, 1990). On the background of these wells, the lithology from Pliocene to Permian was found. The Quaternary deposits are glacial (NPD, 1977) and the lithology was found from the report of well 16/2-1 (Myhre, 1976), where only some of the layer is presented. Hence there is some uncertainty about the lithology of this layer. The percentage of the different lithologies found from the reports were eventually compared to sand/shale ratio in the gamma-ray logs from well 24/9-1, 24/12-3 S, 16/2-1, 25/11-18 and 24/9-3 (NPD).

The similarity between the different wells was overall good, but in the layer of Triassic there was a difference of up to 44 % shale and 36 % sandstone. Also in the Cretaceous layer, a difference of up to 26 % chalk and 22 % sandstone were present. In these two layers, an average was made.

After the percentage of the lithology was set, the porosity and density parameters were calculated. This was done by the same method as in chapter 4 and as described in sub-chapter 2.4. However, the porosity and density parameters for marl, coal and cement are not included in table 2.1. The parameters for these extra lithologies used in the modeling are shown in table 5.1. There is limited published information about these parameters, hence an average was set. The porosity was assumed constant throughout these three lithologies as their percentage within the different packages are small and will give negligible influence in terms of calculating the densities.

Table 5.1: Porosity and density parameters of marl (ODP), coal (Alden, 2010) and cement.

Lithology	ϕ_0	a	Density (g/cm ³)
Marl	0.23	0	2.69
Coal	0.04	0	1.25
Cement	0	1	2.70

Table 5.2 shows the layers with the final lithology and the density and porosity parameters used in the modeling.

5.3.2 Velocity

As the seismic profiles are in TWT (two way travel time), a depth-conversion is needed before the gravity is calculated. To depth-convert, the seismic velocity of each layer must be known. As the stacking velocities were not available in Discos, composite logs including sonic logs from adjacent wells were used to find the velocities. Well 24/12-3 S, 24/9-1, 24/9-3, 25/11-18 and 16/2-1 did all have composite logs including sonic logs, and from these the average velocity in each layer could be calculated. Figure 5.6 shows the composite log of well 16/2-1 as an example; the layers are sectioned down the length of the borehole, and the average velocity was picked in each of these layers.

The sonic log is a measure in microseconds per feet, which needs to be converted into kilometers per second. The formula for converting this unit is an inverse formula:

$$\frac{km}{s} = \frac{0.3048}{\dots \frac{\mu s}{ft} \cdot 10^{-3}},$$

where the velocity read from the log, in microseconds per feet, is put at the dotted line.

As the wells with the composite log did not penetrate deeper than early Jurassic, the Triassic and Permian velocities were not found from the sonic logs. Triassic and Permian velocities were set as respectively 4 km/s and 4.5 km/s, as these layers are restricted for the main graben and lie relatively deep. The final velocities used in the modeling are listed in table 5.2.

The velocity in each layer is set constant, which is a simplification. The velocity of the layer is dependent on the depth (or porosity) at where the layer is. One could have found the velocity from Wyllie's equation;

$$\frac{1}{v} = (1 - \phi) \frac{1}{v_g} - \phi \frac{1}{v_f},$$

v_g is the grain velocity

v_f is the fluid velocity

ϕ is the porosity

Then the v_g , v_f and ϕ must be known (from the lithology), but this method was not used in this thesis.

By comparing the sonic log of the Cretaceous layer from well 16/2-1 at Utsira High with the one from well 24/9-1 in center of Viking Graben, the depth dependency was estimated (see figure 5.5). With a depth difference of about 1000 m, the difference in velocity was 0.36 km/s. This result seems significant, but because the shallower part of the layer is much thinner than the deeper part (about 100 m compared to about 1500 m), the effect of this simplification is not large. When not using constant velocity, the layer located above the Utsira High would lie a bit shallower.

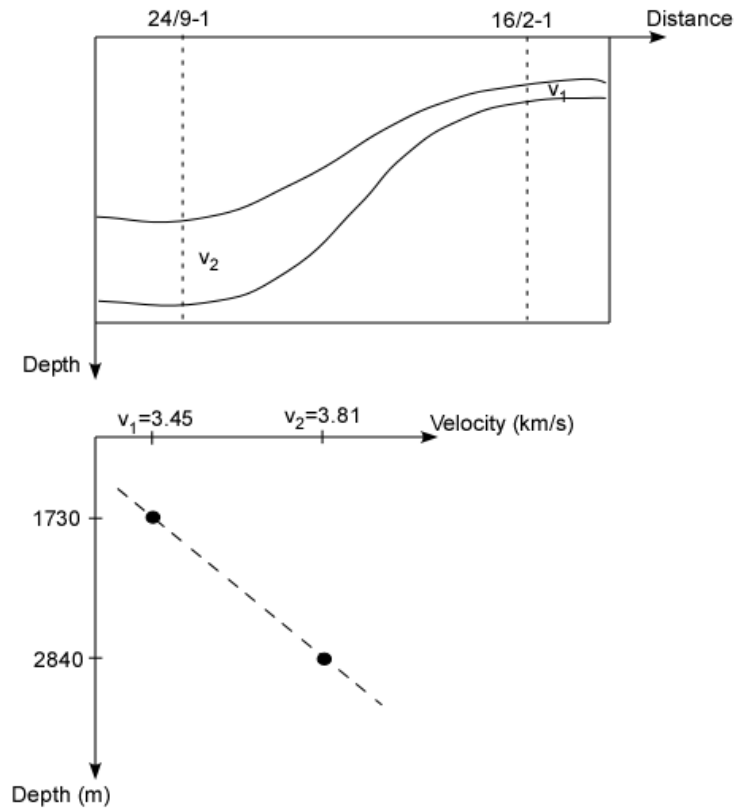


Figure 5.5: Relative depth difference of the Cretaceous layer and a velocity-depth distribution curve estimated from the velocity and depth found from the wells 24/9-1 and 16/2-1.

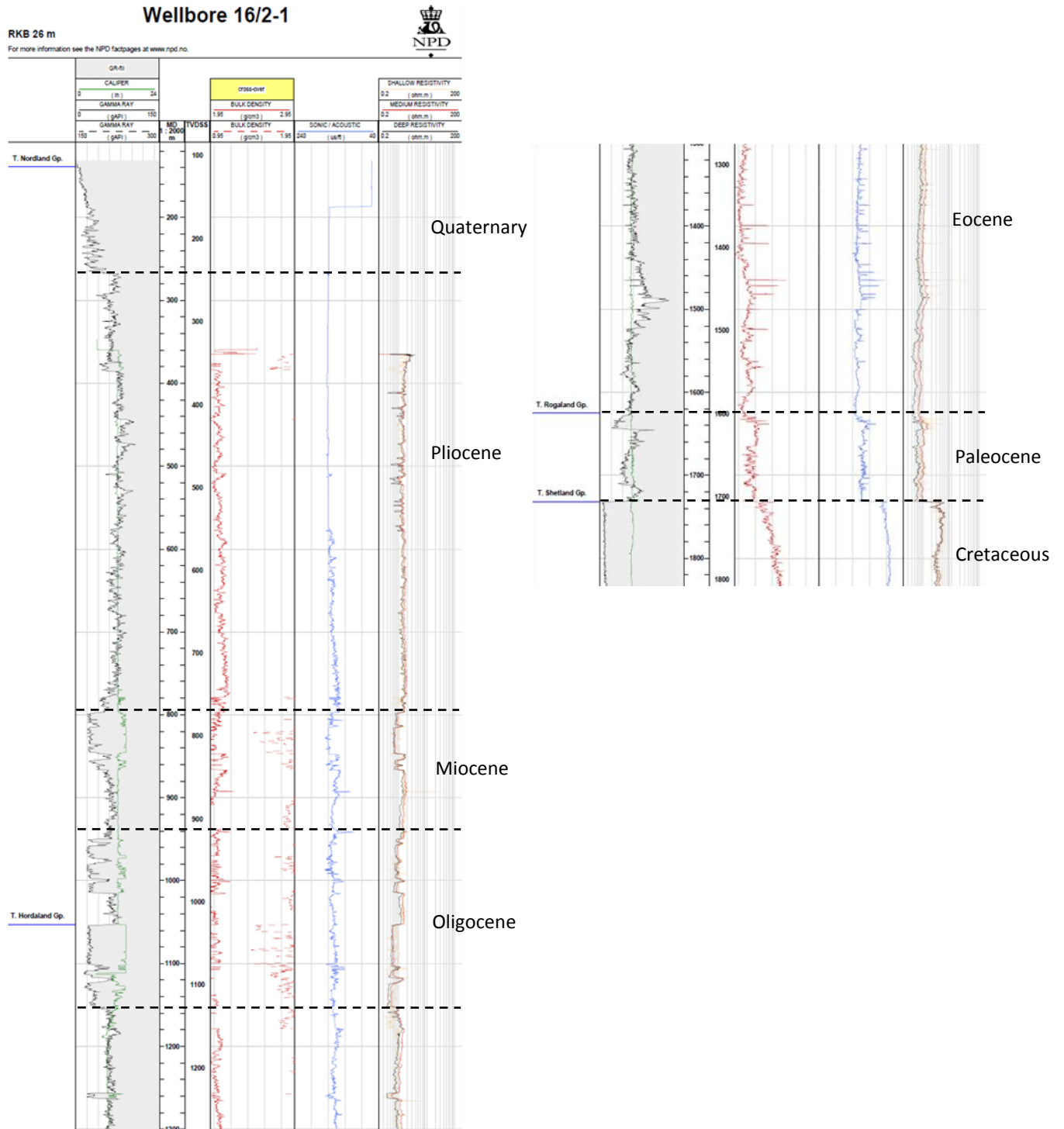


Figure 5.6: The composite log from well 16/2-1, showing the arrangement of the layers. Within each layers, the average velocity was calculated.

Table 5.2: The parameters used in the modeling.

Nr.	Layer	Lithology	% in each layer	ϕ_0	a	ρ_g (g/cm ³)	ρ_f (g/cm ³)	v (km/s)
1	Water			1	0	1.03	1.03	1.500
2	Quaternary	Shale	15	0.5110	0.3060	2.661	1.03	1.643
		Sandstone	85					
3	Pliocene	Shale	98.5	0.6279	0.5064	2.720	1.03	1.937
		Sandstone	1.5					
4	Miocene	Shale	51.4	0.4550	0.3934	2.686	1.03	2.011
		Sandstone	48.6					
5	Oligocene	Shale	71.2	0.5897	0.4409	2.700	1.03	2.140
		Sandstone	28.8					
6	Eocene	Shale	92	0.6205	0.4943	2.715	1.03	2.162
		Sandstone	7.2					
		Chalk	0.8					
7	Paleocene	Shale	70	0.5964	0.4498	2.700	1.03	2.864
		Sandstone	26					
		Chalk	4					
8	Cretaceous	Shale	56	0.5860	0.4715	2.707	1.03	3.730
		Sandstone	11					
		Chalk	22					
		Marl	11					
9	Upper Jurassic	Shale	75.8	0.6042	0.4677	2.685	1.03	3.263
		Sandstone	18.2					
		Chalk	4.5					
		Coal	1.5					
10	Middle-Lower Jurassic	Shale	40	0.5617	0.4151	2.658	1.03	3.810
		Sandstone	44					
		Chalk	13					
		Coal	2					
		Marl	1					
11	Triassic	Shale	46	0.5548	0.3948	2.657	1.03	4.000
		Sandstone	47.5					
		Chalk	4.5					
		Coal	2					
12	Permian	Shale	2	0.4791	0.5295	2.678	1.03	4.500
		Sandstone	51					
		Chalk	30.5					
		Cement	16.5					
13	Crystalline crust	Granite	100	0	0.05	2.900	1.03	6.100

5.4 The depth model, density grid and calculated gravity

The digitized time models of the two seismic profiles were depth-converted using a Matlab script. The result of the depth-conversions of the two lines is shown in figure 5.7.

After the depth models were made, the density grid and hence the gravity was calculated. This was done by using two other Matlab scripts. The density and porosity along the two profiles are shown in figure 5.8 and the calculated gravity is shown in figure 5.9.

The gravity modeling gives realistic results. The gravity shows a higher value at the Utsira High, where the denser crystalline crust is shallow and a lower value in the Viking Graben, where the crystalline crust lies deeper. The denser crystalline crust makes the main trend of the modeled gravity and the sedimentary basin make some small attributes to the trend of the gravity.

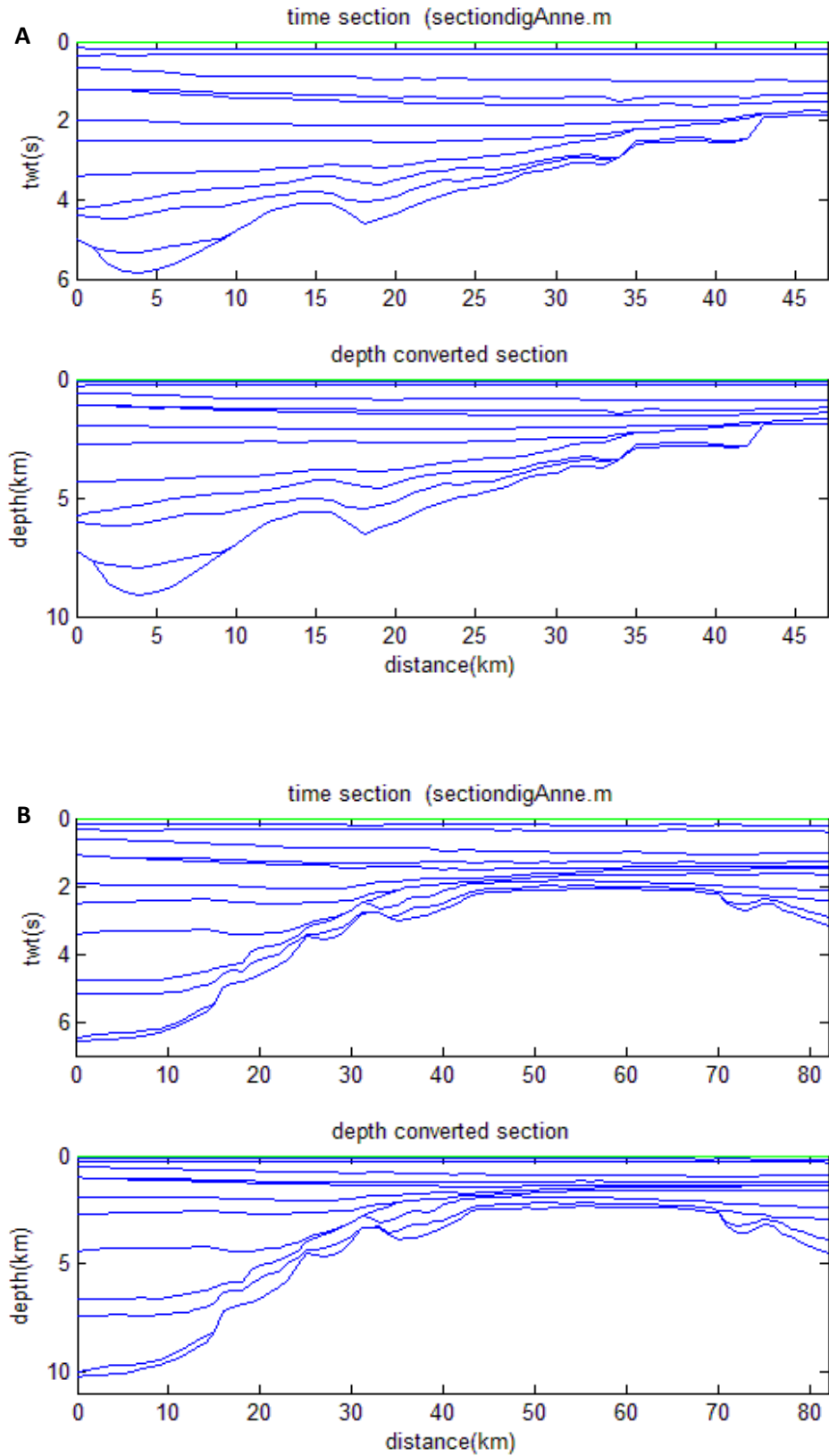


Figure 5.7: Time model versus depth model of the two lines. A: Line 1, B: Line 2.

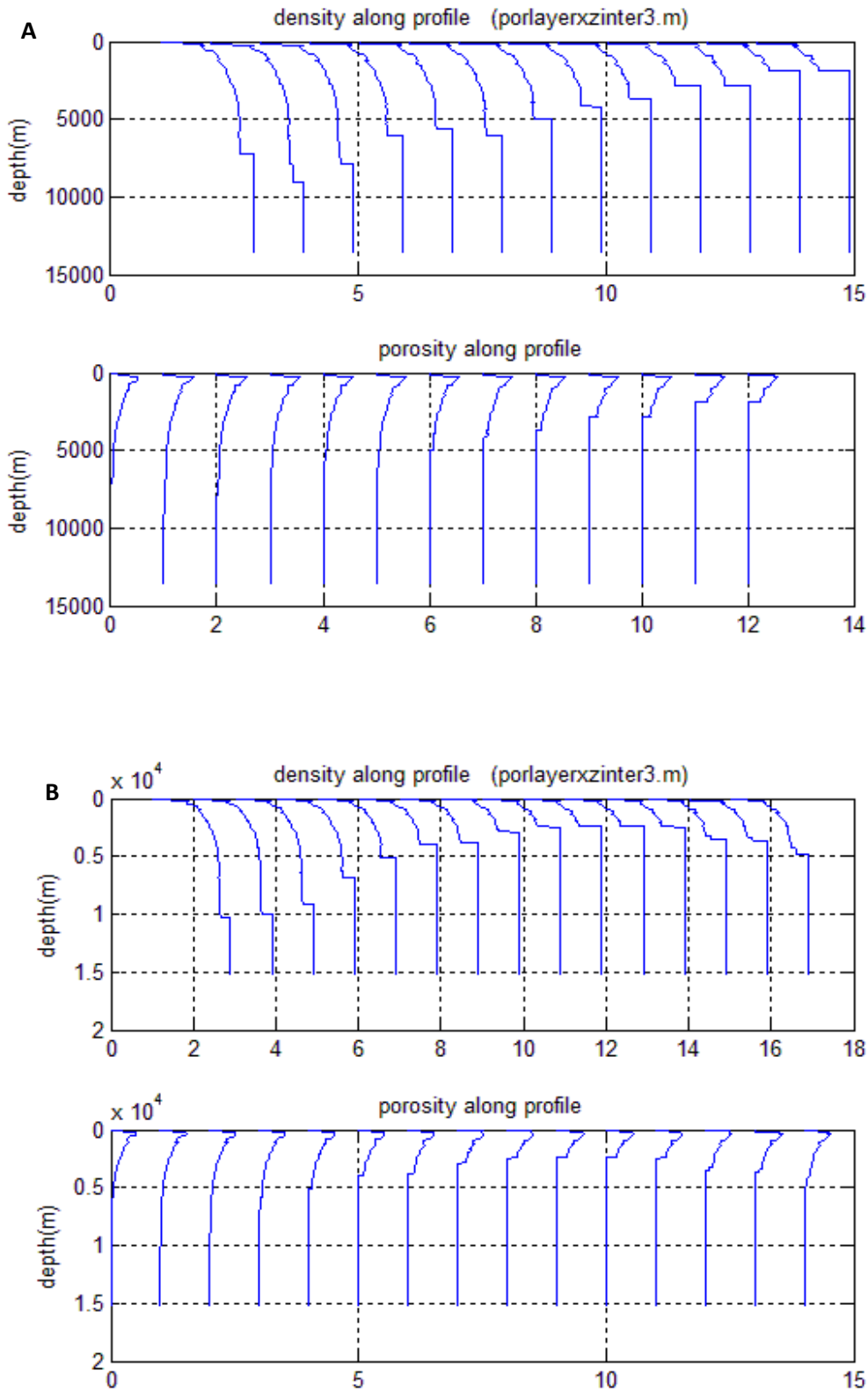


Figure 5.8: The density and porosity along the models. A: Line 1, B: Line 2

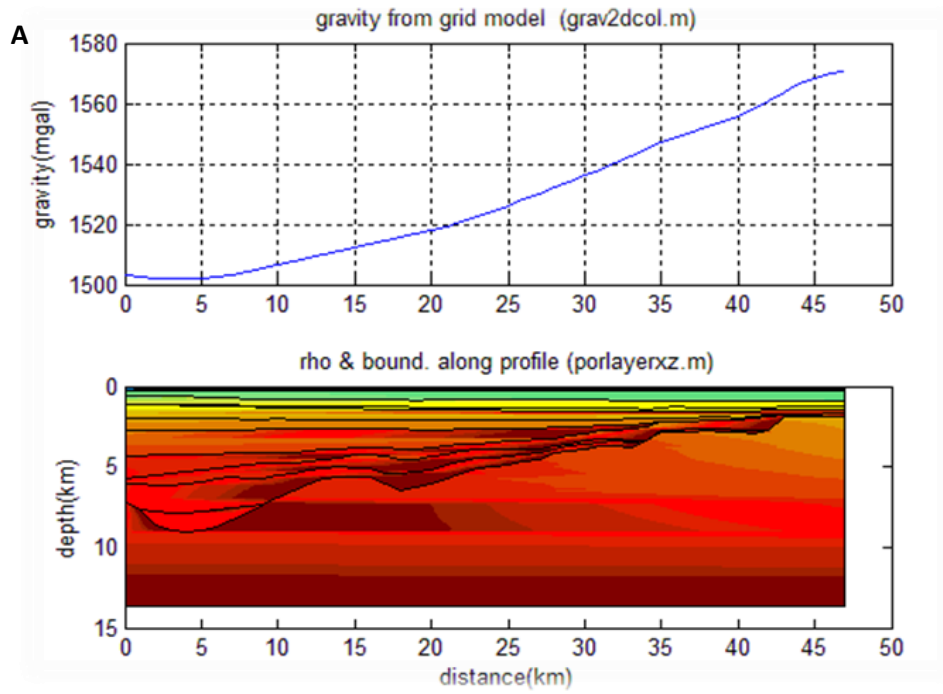


Figure 5.9: The calculated gravity of the models. A: Line 1, B: Line 2

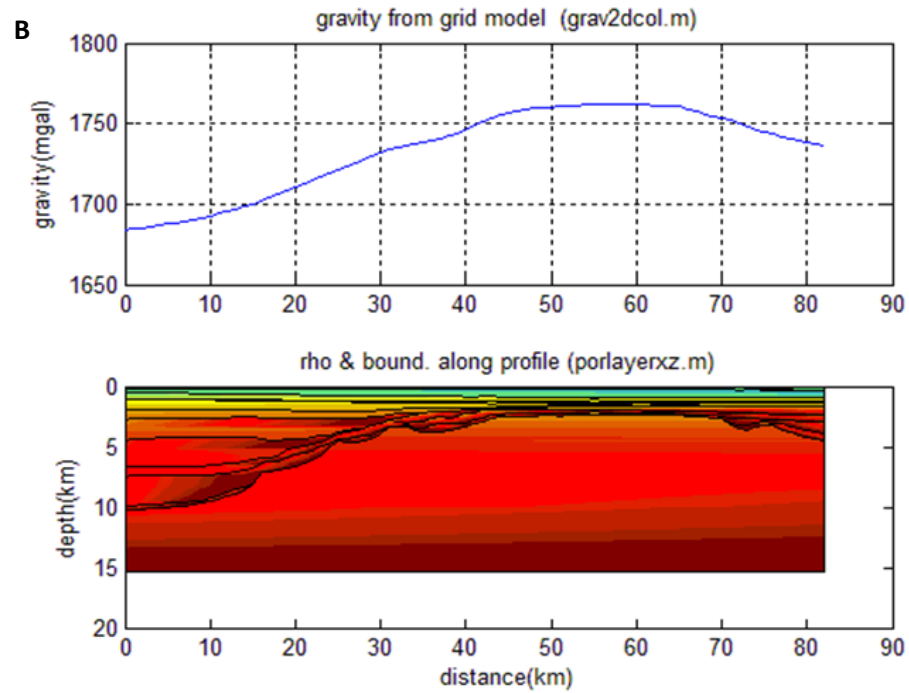


Figure 5.7: The porosity and density along the models. A: Line 1, B: Line 2

5.5 The observed gravity

Sandwell and Smith (1997, 2009) have constructed a global marine gravity field model from Geosat and ERS-1 altimetry, and more recently they used three approaches to reduce the errors in the anomalies. First, the raw waveforms from the ERS-1 and Geosat/GM missions was retracked, which improved the range of precision of 40 % and 27 %. Second, they used the EGM2008 global gravity as a reference field to make the transition of the gravity from continent to ocean seamless. Third, biharmonic spline interpolation method was used to construct residual vertical deflection grids.

The map of the global marine gravity field is put out on the internet (SIO, 2009), where one can download ASCII data-files of the gravity anomaly from the area of interest. In this thesis, the area from 58.5°N to 60.0°N and from 0.5°E to 3.5°E was picked, since it is within this area the seismic lines are located. The end-coordinates of Line 1 and Line 2 are used to place the lines in the map, and to find the observed gravity of each of the lines. The gravity, together with the location of the lines, is shown in figure 5.10 and 5.11. The end-coordinates are listed in table 5.3.

Table 5.3: The end-coordinates of Line 1 and Line 2

		Longitude	Latitude
Line 1	Start	1.66°E	59.12°N
	End	2.39°E	58.88°N
Line 2	Start	1.73°E	59.33°N
	End	3.05°E	58.99°N

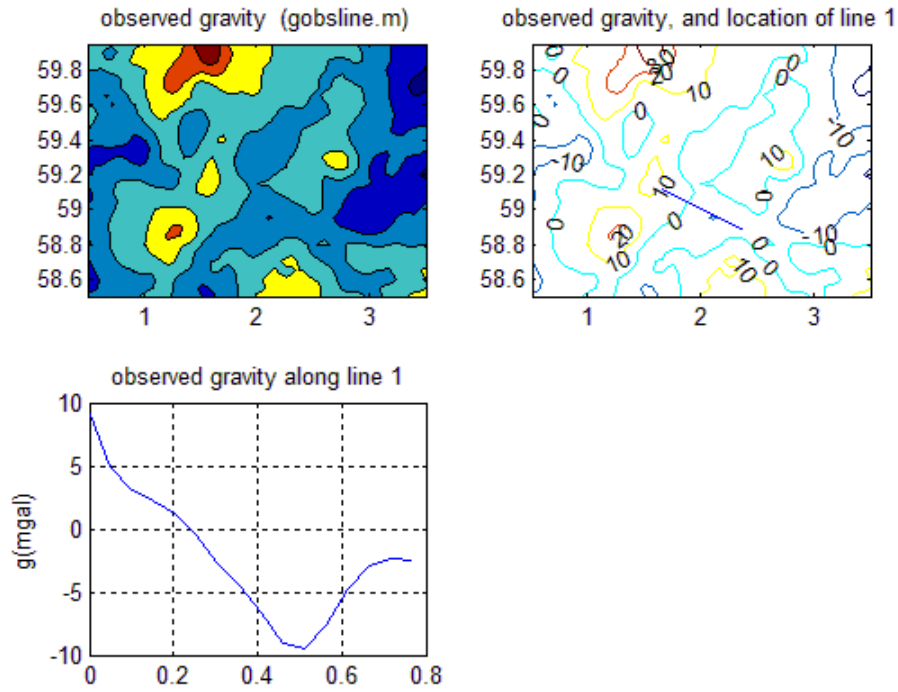


Figure 5.10: The observed gravity of Line 1 and the location of the line

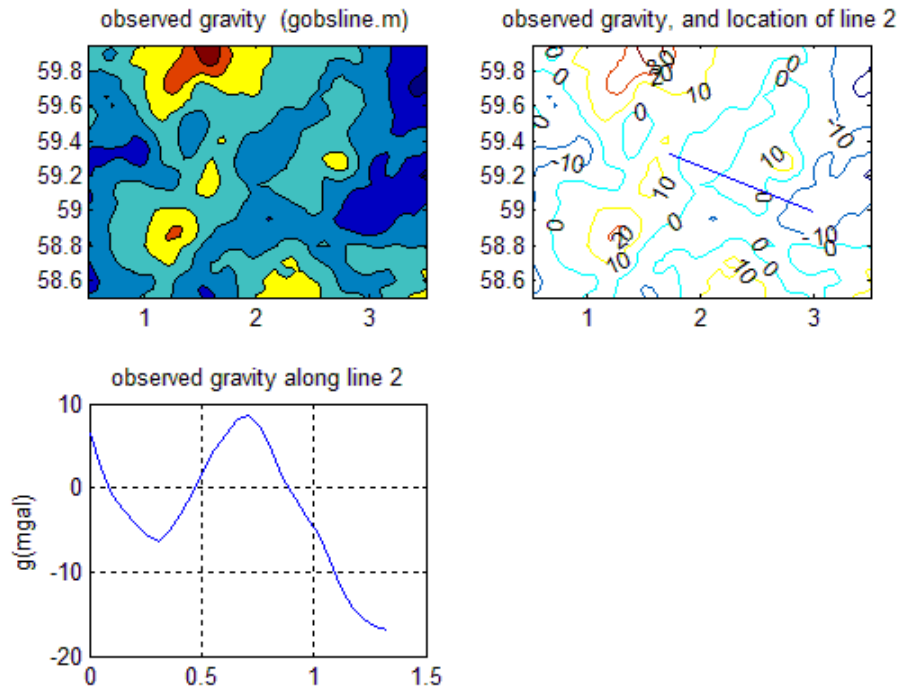


Figure 5.11: The observed gravity of Line 2 and the location of the line

5.6 Cordell & Henderson-calculated Moho and comparison with published Moho in the area

To calculate the Moho another Matlab script was used. The script determines the Moho by using Cordell & Henderson's method, described in chapter 3, to make the observed gravity field to fit with the calculated gravity field. An anchor point of the depth of the Moho was assumed. This anchor point was found from published data (Fichler & Hospers, 1990), where they made a contour map of the Moho. The location of the two seismic lines within this contour map is shown in figure 5.16. The anchor point coordinates and the values used in the modeling are listed in table 5.4, the anchor points are also marked in figure 5.16. The modeling was performed by changing the model in the areas outside the anchor point so that the calculated field was in compliance with the observed.

Table 5.4: The coordinates and values of the anchor points.

Line nr.	Longitude	Latitude	Distance (km)	Moho-depth (km)
1	1.9°E	59.1°N	20	23
2	1.85°E	59.3°N	15	23

When calculating the Moho, one could choose the number of iterations to make the best fit. Figure 5.12 and 5.13 show the result choosing different number of iterations. Finally, the model with 15 iterations was chosen to further model the gravity of both the deep and shallow structures. The one with 5 iterations made a good fit to the left of the profiles, but to the right it did not make a good enough fit. 50 iterations made a very good fit, but then the Moho doesn't look realistic. When comparing with the published Moho depth map (Fichler & Hospers, 1990), the calculated result with 15 iterations give the same trend as the contour map (figure 5.16), but the deepest part of the calculated Moho depth is up to 6 km deeper to make it fit better with the observed gravity.

The final geological model of line 1 and 2 when Moho has been added are shown respectively in figure 5.14 and 5.15. These models are based on the Moho calculation with 15 iterations on both lines. The fit between the observed and calculated gravity is good.

Then the gravity of the final profiles was modeled. The two lines were modeled with a grid size in x-direction of 2 km and z-direction of 20 m. The modeling was done in two different ways like in chapter 4, one where the density is constant (mean density) within the layers and one where the density varies within the layers. This gives two different results of the modeled gravity of each line. The result of the gravity modeling is shown in the figures 5.17 and figure 5.18 together with the observed gravity of the lines.

Figure 5.17 shows the results of the modeled gravity of line 1. The two results have the same trend of the relative gravity, but a difference of about 2-3 mGal is present to right of the profile. Figure 5.18 shows the result of the modeled gravity of line 2. The difference is the same here as for line 1. When modeling with constant densities for line 2, however, the depth of the mantle became larger and hence the thickness of the mantle became larger. As the mantle is the densest layer, one may expect the mantle to contribute in a higher value of the gravity.

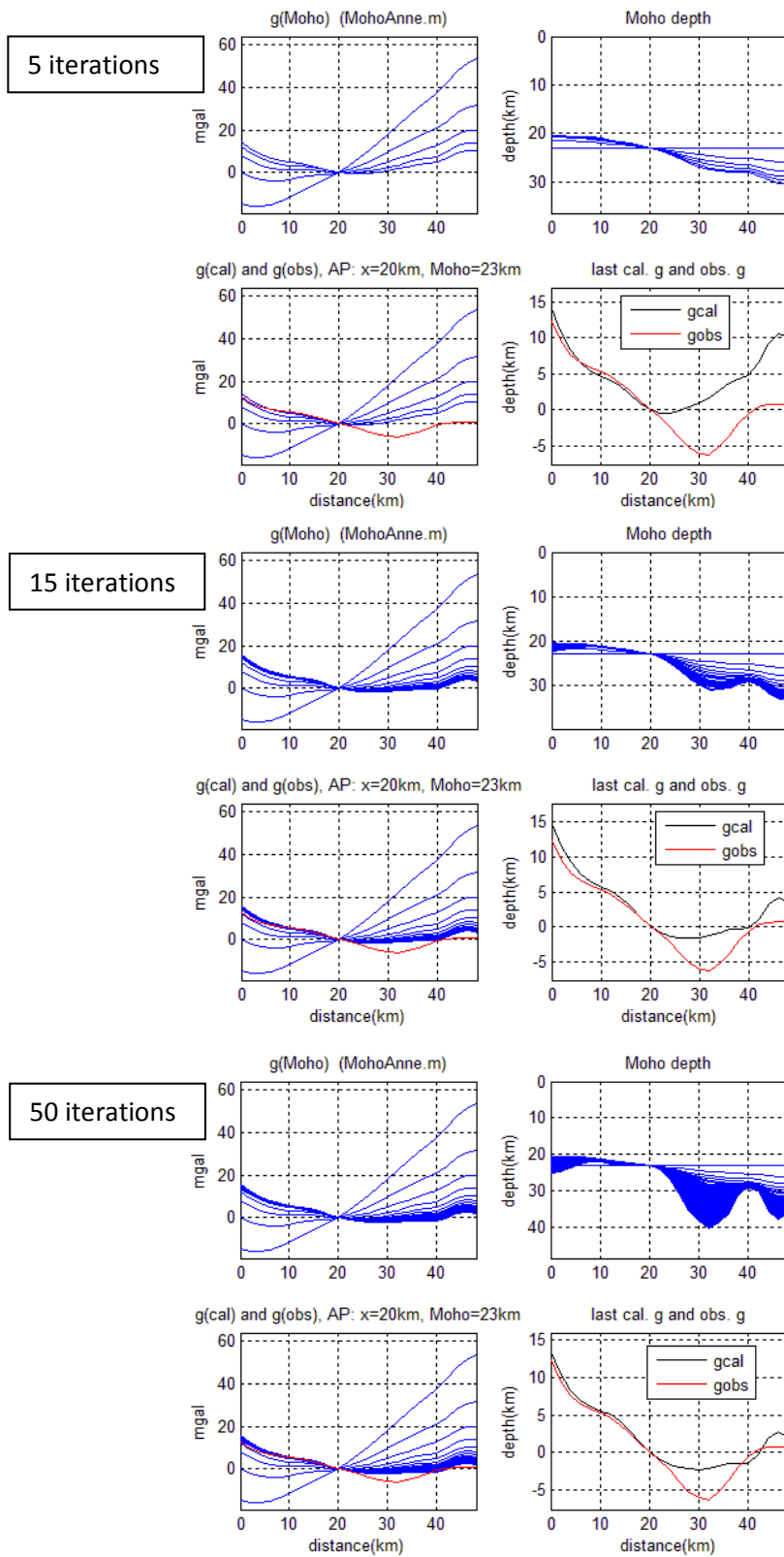


Figure 5.12: Correcting for the Moho for line 1, testing the number of iteration needed to make the best fit and the most realistic geometry of the deeper layers.

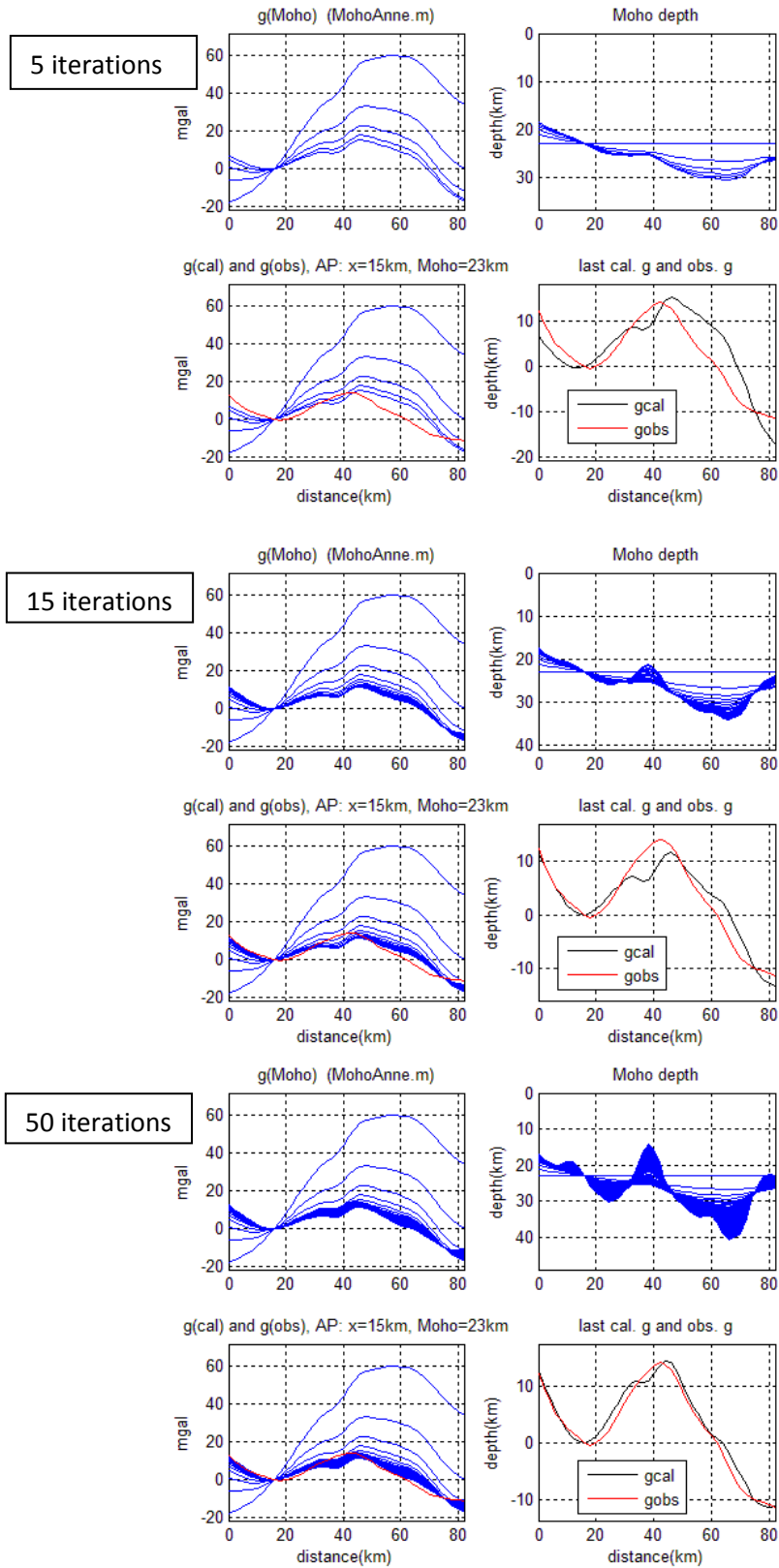


Figure 5.13: Correcting for the Moho for line 2, testing the number of iteration needed to make the best fit and the most realistic geometry of the deeper layers.

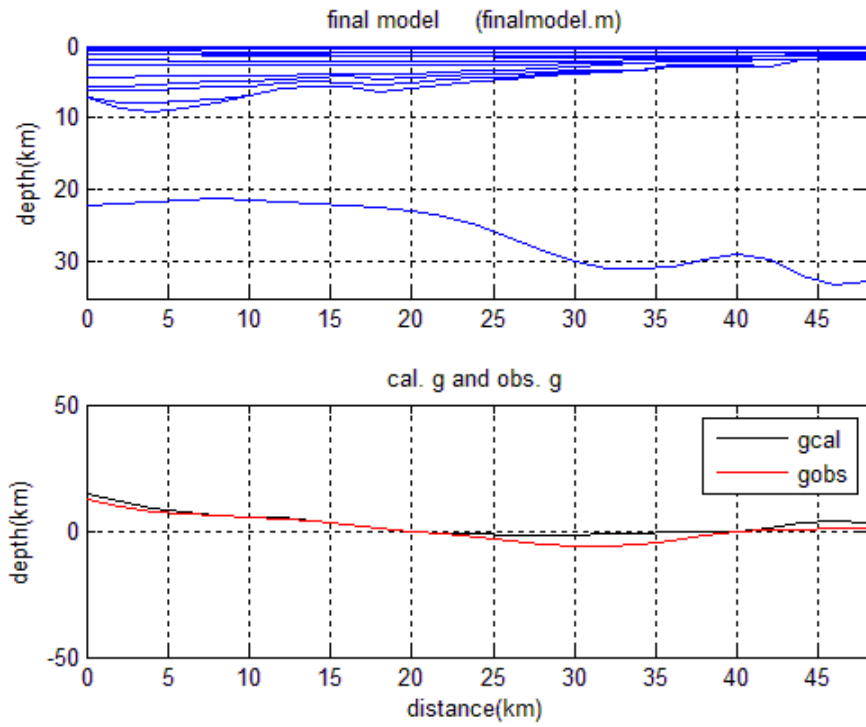


Figure 5.14: The final geological model of line 1 after the Moho has been added.

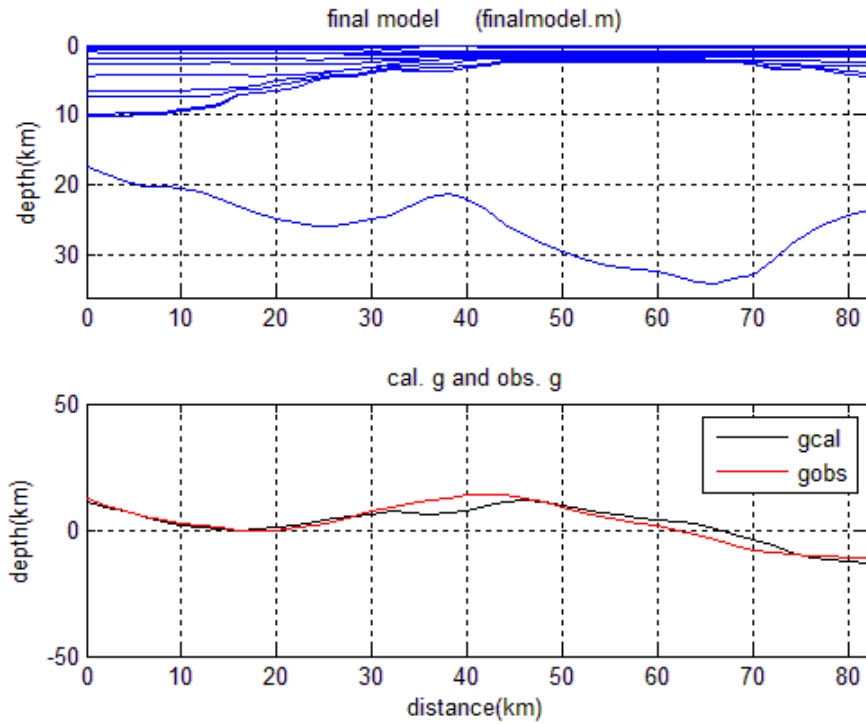


Figure 5.15: The final geological model of line 2 after the Moho has been added.

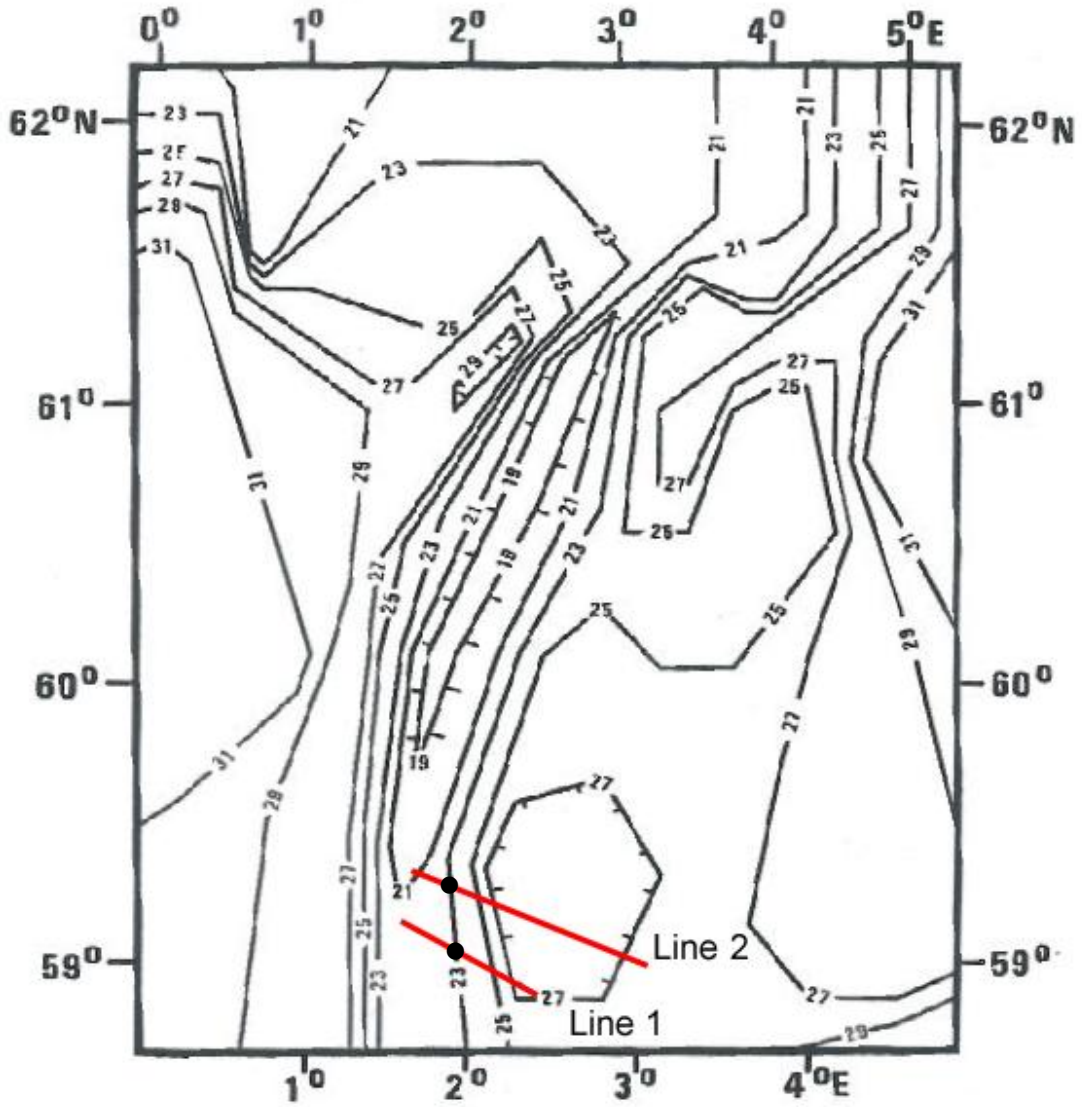


Figure 5.16: Contour map of the Moho modified from Fichler and Hospers (1990), with the location of line 1 and 2. The anchor point used in the modeling are marked as black dots on the line.

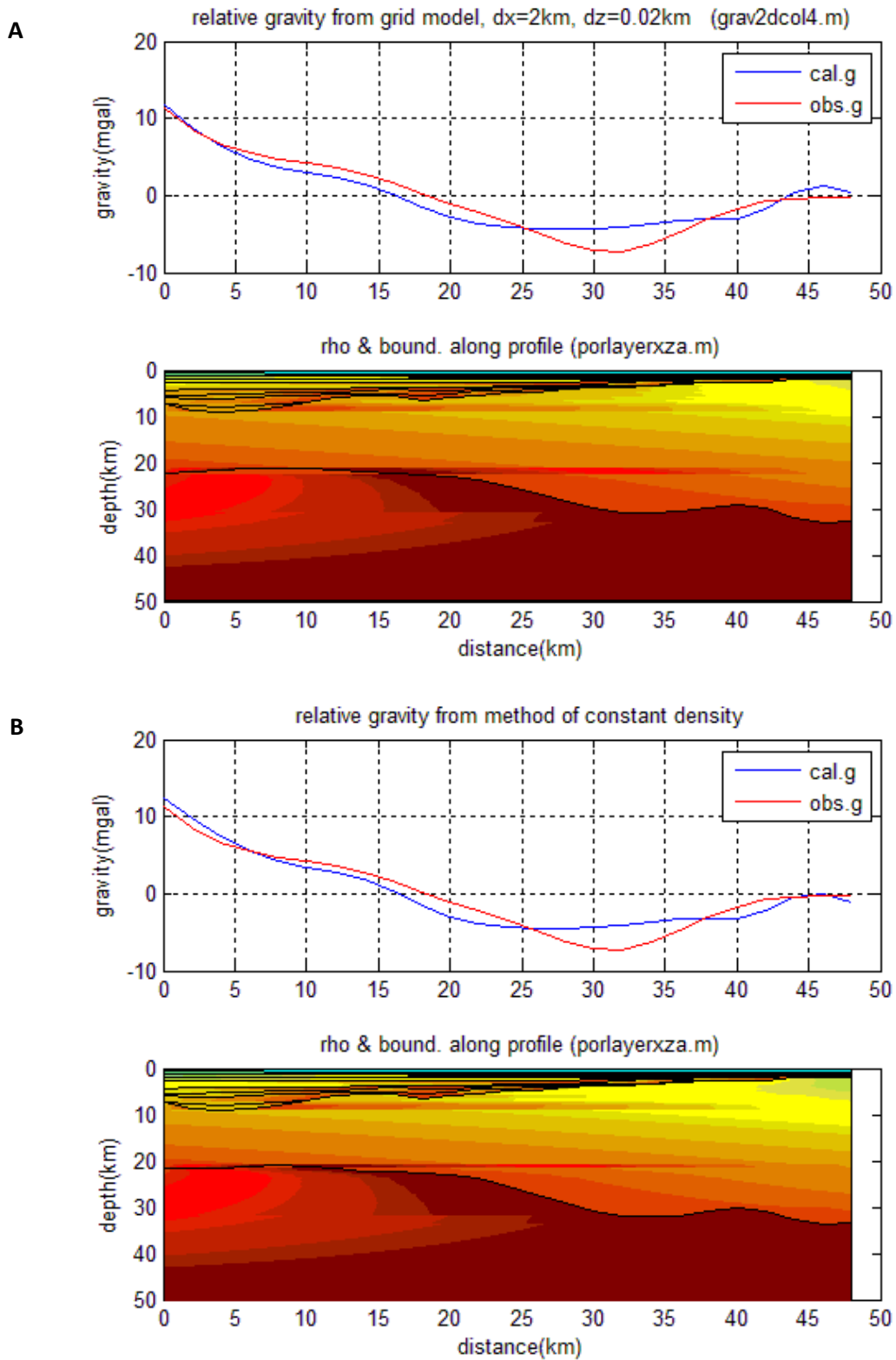


Figure 5.17: The modeled gravity of the final geological model and the observed gravity of line 1. A is modeled with varying density, and B is modeled with constant density.

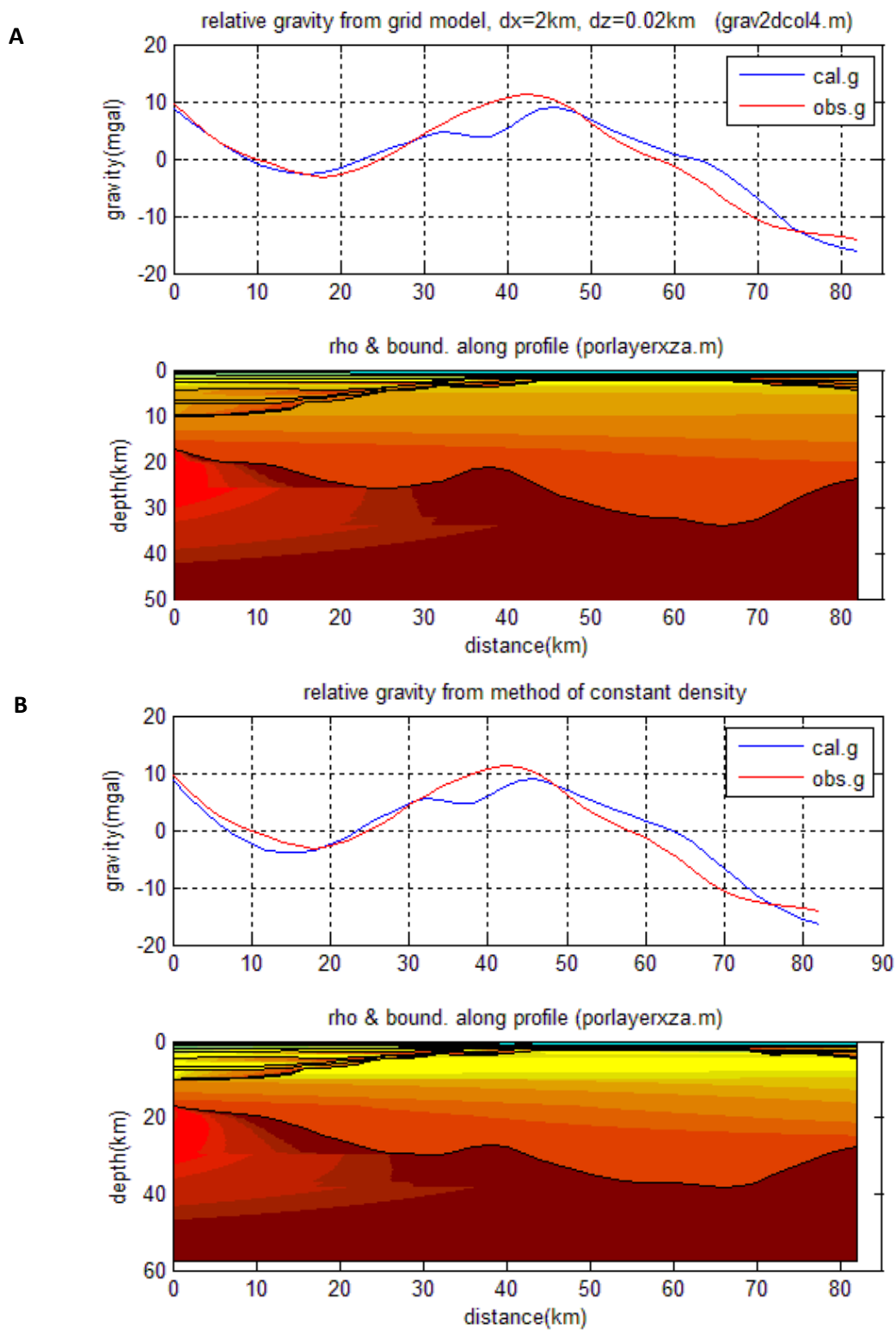


Figure 5.18: The gravity modeled of the final geological model of line 2. A is modeled with varying density, while B is modeled with constant density.

After the gravity was modeled, another Matlab script was used to calculate the total pressure at a depth of 50 km. The vertical pressure at a depth (z_s) equal to the deepest basement along the line was calculated using the interpreted model (figure 5.19). The pressure from the lower part (z_s to 50 km) was added for each Moho-iteration to find the total pressure for each iteration (figure 5.19). The green curve in the figures show the iteration giving least variation in total pressure, and thus the solution that best fits Airy isostasy.

If Airy isostasy prevails exactly, then the pressure at a depth equal to Moho's deepest point should be the same (I assume that $\rho(\text{crust})$ and $\rho(\text{mantle})$ do not change laterally). Knowing the structure and densities above z_s , the pressure ρ_s at $z=z_s$ can be calculated, and the depth to Moho that gives Airy isostasy can be estimated when an anchor point is given. This is illustrated in figure 5.20. Using the symbols in the figure and equalizing Airy's columns at anchor point and at x , we get

$$P_s(AP) + z_{AP} \cdot g \cdot \rho_c + (H - z_{AP} - z_s) \cdot g \cdot \rho_m = P_s(x) + z(x) \cdot g \cdot \rho_c + (H - z(x) - z_s) \cdot g \cdot \rho_m$$

Then the "Airy" depth of Moho ($z_M(x)$) may be written as

$$z_M(x) = z(x) + z_s$$

where

$$z(x) = z_{AP} + \frac{P_s(x) - P_s(AP)}{g(\rho_m - \rho_c)}$$

z_s is the depth of deepest basement

z_{AP} is the depth of the Moho under z_s at anchor point

$P_s(x)$ is vertical pressure at depth z_s at x

$P_s(AP)$ is vertical pressure at depth z_s at anchor point

ρ_m is the density of the mantle

ρ_c is the density of the crust

Figure 5.21 shows the “Airy Moho” depths of line 1 and 2. These depths are very similar to those published by Fichler and Hospers(1990), see figure 5.16.

Then the gravity of the models of Airy isostasy calculated Moho was modeled. The result is shown in figure 5.22 together with the observed gravity of the profiles. When comparing figure 5.22 with figure 5.17 and 5.18 one can see that Cordell & Henderson’s method of calculating the depth of Moho make a better fit between the modeled and observed gravity than if the Moho was calculated by Airy isostasy method. This indicates that the crust is not in local isostatic equilibrium in the area.

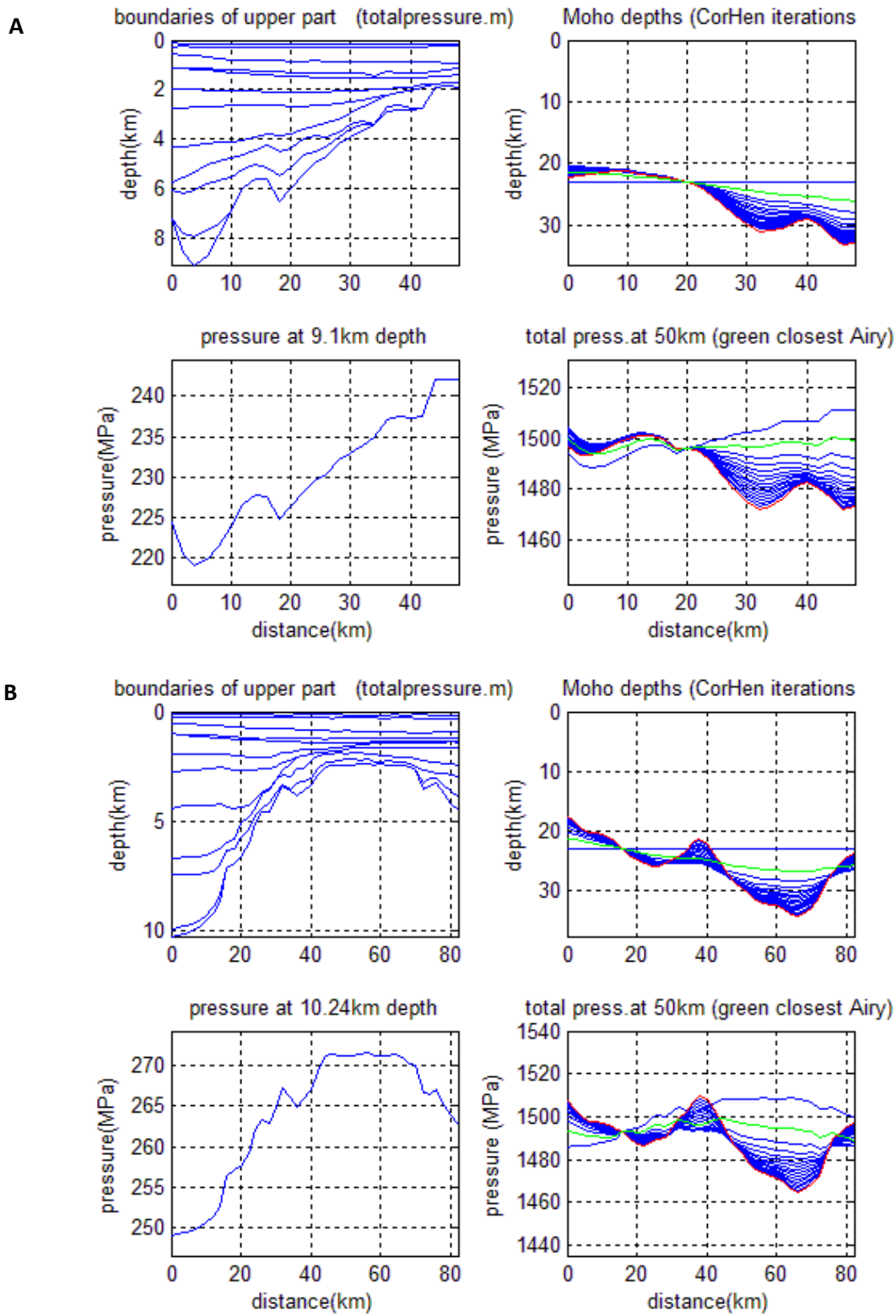


Figure 5.19: A: The total pressure at 50 km depth along line 1 for different iterations. B: The total pressure at 50 km depth along line 2 for different iterations

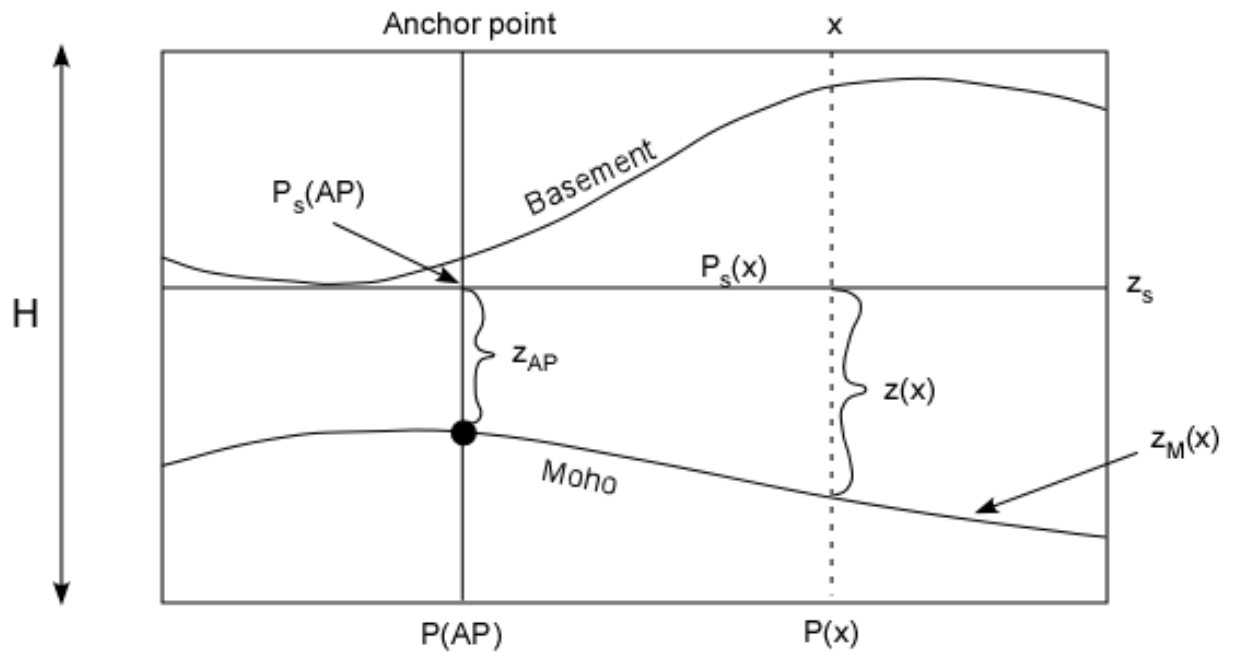


Figure 5.20: Showing the symbols and structure if Airy isostasy prevails. The depth to Moho can then be calculated if an anchor point is given.

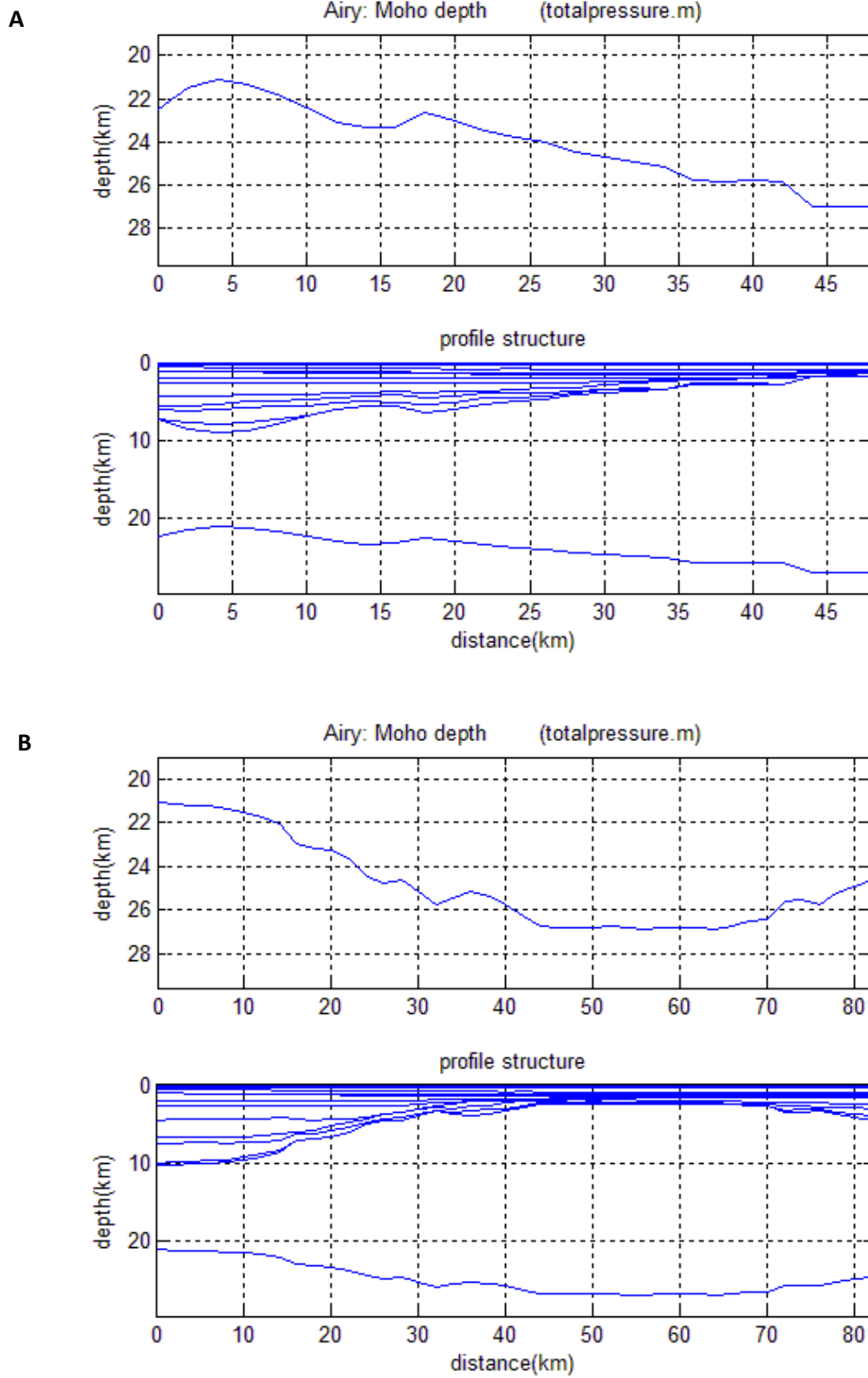


Figure 5.21: A: Moho depth of line 1 based on Airy isostasy. B: Moho depth of line 2 calculated based on Airy isostasy.

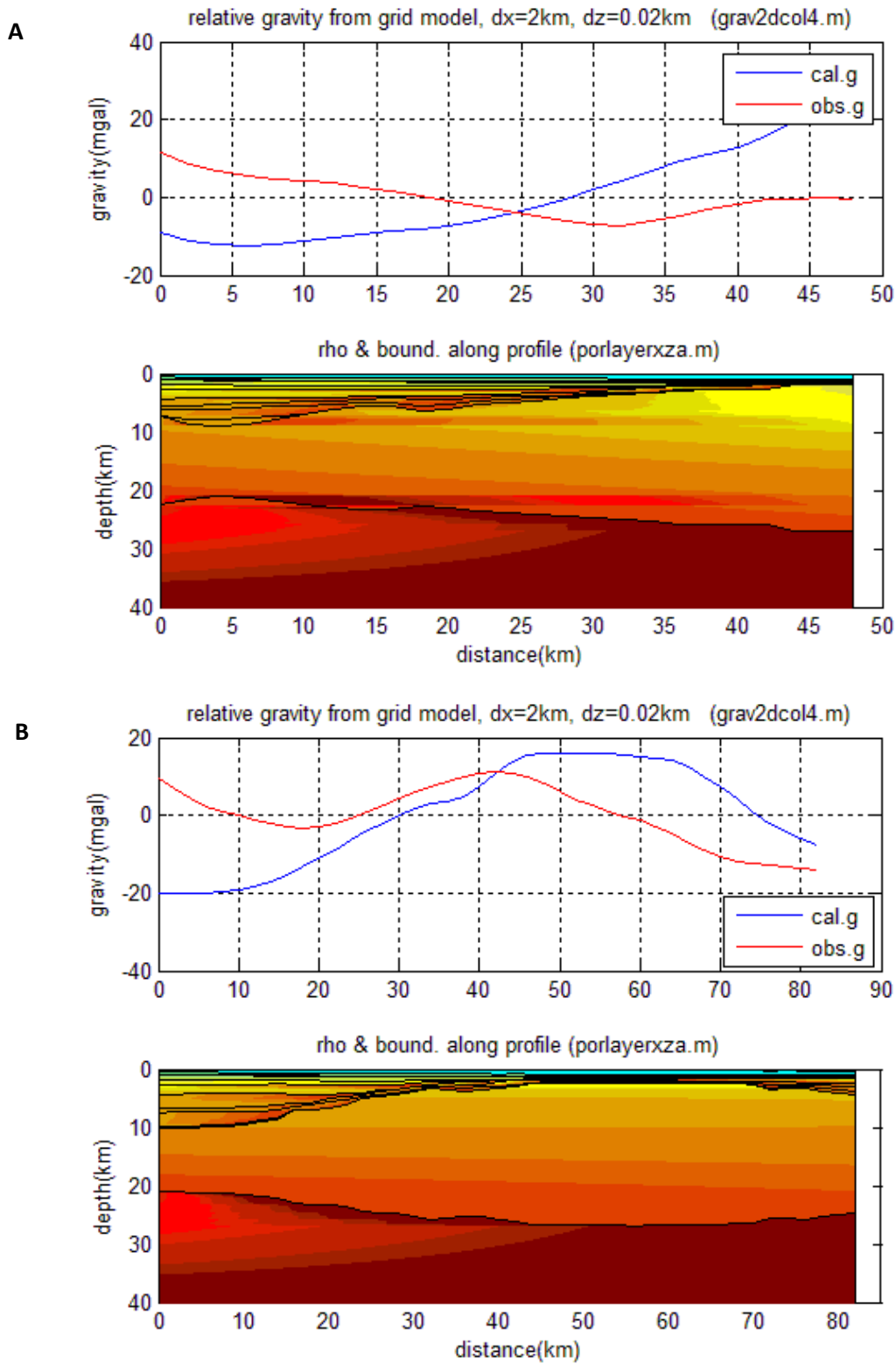


Figure 5.22: The modeled gravity when Airy isostasy calculated Moho versus the observed gravity. A: Line 1. B: Line 2

Chapter 6: Summary and discussion

- A grid method based on lithology parameters, such as porosity and density was applied to calculate the gravity of some synthetic models, an OBS-line from the Vøring margin and two seismic sections from the North Sea. The results were compared with other methods.
- The gravity modeling of the synthetic models show that when comparing with a method with constant densities within the layers, the trend of the relative gravity may differ much, mainly due to the weight of the vertical columns vary differently along the profile in the two cases.
- The size of the grid is important, as the result of the modeling may miss out on some information if the grid-size is too big. A cell size $\Delta x, \Delta z$ of 2 km x 20 m gave accurate gravity-calculations and short computing time.
- Athy's law for porosity was used in the modeling. By compensating for effective pressure at the top of each layer we achieve a better and more realistic density result than using Athy's curves uncompensated.
- In case of overpressure, the value of the gravity will decrease in the area of overpressure. The amount of decrease is dependent on the depth and the extension of the overpressured layer.
- Wrong interpretation of erosion may have great effect of the modeled gravity.
- Gravity modeling of the OBS-line gives a similar trend when using the grid method as using constant layer densities derived from seismic velocities.
- The difference between the modeled and the observed gravity is significant. Cordell & Henderson's iterative method of correcting the Moho was done to make a better fit. 5 iterations made a good fit and a realistic geometry of the Moho.
- By changing the density in certain key layers, the difference between the observed and calculated gravity may be considerably reduced.
- Thin sill-layers (50-100m) may locally give up to 2 mGal contribution to the gravity field.

- The modeled gravity of the two interpreted sections from the North Sea shows a regional gravity field that mimicked the depth to basement.
- A comparison of the observed and calculated gravity was made to calculate depth to Moho. By using Cordell & Henderson's iterative method with a given anchor point and 15 iterations, a good fit with the observed gravity and a realistic geometry of the Moho was obtained. Using constant layer densities instead of lithology predicted densities the modeled Moho along the two lines was changed vertically by less than ± 4 km.
- Moho was also calculated based on Airy isostasy, but the Cordell & Henderson's method made a significantly better fit between the calculated and observed gravity than the Airy method.

The method

In this thesis a proposed grid method for calculating the gravity field along an interpreted seismic line is given. The advantage of the method is that it theoretically is very accurate and may include models with rapidly varying densities both vertically and horizontally. It is quick to perform, and may be applied when lithology and porosity parameters are well known. It is, however, dependent on how closely the porosity is following Athy's law, and may give significant errors if neglecting present overpressure zones or erosions.

Results from line 1 and line 2

These results are showing a Moho-trend that is similar to other published Moho-depths in the area(Fichler & Hospers, 1990), but has greater topography. The modeled gravity field is dependent on several factors, for example:

- Interpretation of the seismic lines
- Time to depth conversion
- Identification of lithology and relationship between lithology and porosity.
- Localization of Anchor point.
- Computing parameters (grid size, number of iterations).

- 3D effects (observed gravity field is a 3D-field, while the modeled field is a 2D-field).

Therefore the accuracy of the results is difficult to estimate.

The results indicate, however, that the lithosphere in the area is not in Airy-equilibrium, but has an elastic thickness, T_e , greater than zero. This implies regional isostasy in the area, see figure 6.1.

Modeling the deflection due to stretching and sediment loading using different T_e may give an estimate of T_e in the area.

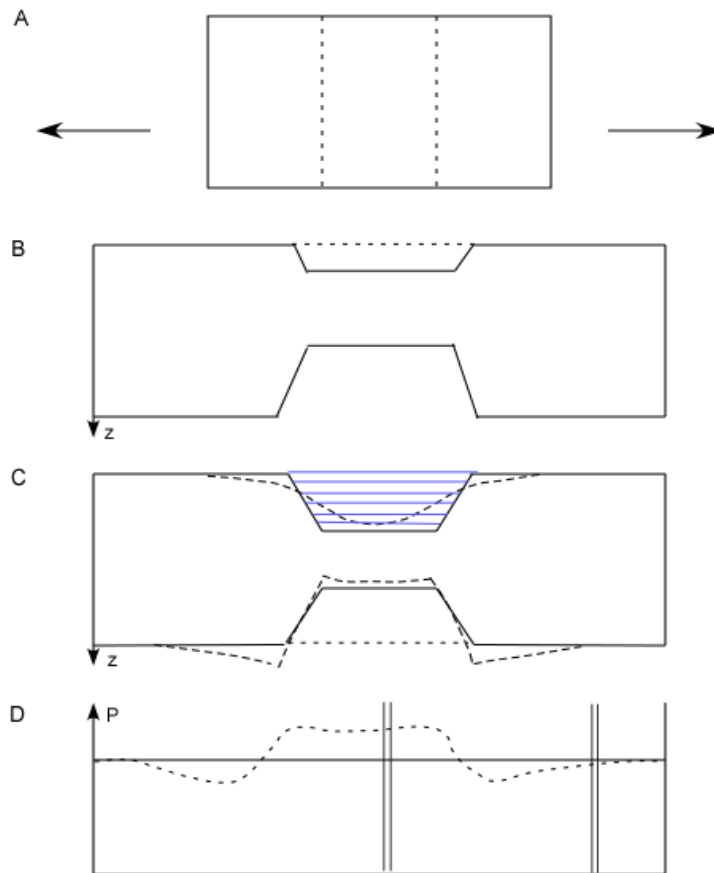


Figure 6.1: Cartoon showing the lithological pressure for local and regional isostasy. A and B: Stretching of the model, C: Additional subsidence due to sediment infill, D: Lithostatic pressure at compensation depth. Solid curve in figure C and D is local isostasy (Airy), while the dotted curve is regional isostasy ($T_e > 0$). The area between the double lines in figure D represents roughly the two interpreted seismic lines.

References

- Alden, A. (2010). Densities of Common Rock Types from http://geology.about.com/cs/rock_types/a/aarockspeggrav.htm
- Bjørøy, M., Buxton, L., Ferriday, I. L., Hall, P. B., Bakken, K. A. (1990). *Regional Petroleum Geochemistry Block 24/12 and Surrounding Areas, Well nos. 24/9-1*. Trondheim: Geolab Nor A/S.
- Blystad P., B. H., Færseth R. B., Skogseid J., Tørudbakken B. . (1995). Structural elements of the Norwegian continental shelf: Part 2. The Norwegian Sea Region. *NPD Bulletin 8 (Norwegian Petroleum Directorate)*, 2-44.
- Brekke, H. (2000). The tectonic evolution of the Norwegian Sea continental margin, with emphasis on the Vøring and Møre Basins. In A. Nøttveit (Ed.), *Dynamics of the Norwegian Margin* (Vol. 167, pp. 327-378). London: Geological Society Special Publication.
- Cordell, L., & Henderso.Rg. (1968). Iterative 3-Dimensional Solution of Gravity Anomaly Data Using a Digital Computer. *Geophysics*, 33(4), 596-&.
- Dyrelius, D., & Vogel, A. (1972). Improvement of Convergency in Iterative Gravity Interpretation. *Geophysical Journal of the Royal Astronomical Society*, 27(2), 195-&.
- Esso. (1977). *Geological completion report 16/1-2*. Stavanger: Esso Exploration & Production Norway inc.
- Fichler, C., & Hospers, J. (1990). Deep Crustal Structure of the Northern North-Sea Viking Graben - Results from Deep Reflection Seismic and Gravity-Data. *Tectonophysics*, 178(2-4), 241-254.
- Hubbert, M. K. (1948). A line-integral method of computing the gravimetric effects of two-dimensional masses. *Geophysics*, 13, 215-225.
- Jensen, H., Hall, P. B., Bharati, S., Ferriday, I. (1992). *Geochemical Report for NOCS 6506/11-2*. Trondheim: Geolab Nor A/S.
- Jung, A. (1961). *Schwerkraftverfahren in der angewandten Geophysik*. Leipzig: Akademische Verlagsgesellschaft Geest & Portig K.-G.
- Kearey, P., Brooks, M., & Hill, I. (2002). *An introduction to geophysical exploration* (3rd ed.). Malden, MA: Blackwell Science.
- Libak, A. (2008). *Tredimensjonal gravimetrisk modellering på Vøring marginen*. University of Bergen, Bergen.
- Lindberg, P., Riise, R., Fertk, W. H. (1980). *Occurrence and distribution of overpressures in the Northern North Sea area*. Paper presented at the 55th Annual Fall Technical Conference and Exhibition of the Society of Petroleum Engineers of AIME.
- Mjelde, R., Faleide, J. I., Breivik, A. J., & Raum, T. (2009). Lower crustal composition and crustal lineaments on the Voring Margin, NE Atlantic: A review. *Tectonophysics*, 472(1-4), 183-193.

- Mjelde, R., Raum, T., Digranes, P., Shimamura, H., Shiobara, H., & Kodaira, S. (2003). V-p/V-s ratio along the Voring Margin, NE Atlantic, derived from OBS data: implications on lithology and stress field. *Tectonophysics*, 369(3-4), 175-197.
- Musset, A. E., Aftab Khan, M. (2000). *Looking into the Earth - An itroduction to Geological Geophysics*. New York: Cambridge University Press.
- Myhre, L. (1976). *Lithology Well no. 16/2-1*. Stavanger.
- Myhre, L. (1977). *Lithology Well 16/1-1*. Stavanger.
- NPD, N. P. D. (06.05.2010). NPD's Fact pages. from <http://www.npd.no/engelsk/cwi/pbl/en/index.htm>
- NPD, N. P. D. (1977). A standard lithostratigraphic nomenclature for the central and northern North Sea. *Bulletin 1*, 39.
- ODP, O. D. P. Average wet bulk density, porosity, and velocity of each lithologic unit and each lithology, calculated from discrete sample measurements. from http://www-odp.tamu.edu/publications/185_IR/chap_04/c4_t17.htm#583463
- Parker, R. L. (1973). Rapid Calculation of Potential Anomalies. *Geophysical Journal of the Royal Astronomical Society*, 31(4), 447-455.
- Raum, T., Mjelde, R., Digranes, P., Shimamura, H., Shiobara, H., Kodaira, S., et al. (2002). Crustal structure of the southern part of the Voring Basin, mid-Norway margin, from wide-angle seismic and gravity data. *Tectonophysics*, 355(1-4), 99-126.
- Raum, T., Mjelde, R., Shimamura, H., Mural, Y., Brastein, E., Karpuz, R. M., et al. (2006). Crustal structure and evolution of the southern Voring basin and voring transform margin, NE Atlantic. *Tectonophysics*, 415(1-4), 167-202.
- Sandwell, D. T., & Smith, W. H. F. (1997). Marine gravity anomaly from Geosat and ERS 1 satellite altimetry. *Journal of Geophysical Research-Solid Earth*, 102(B5), 10039-10054.
- Sandwell, D. T., & Smith, W. H. F. (2009). Global marine gravity from retracked Geosat and ERS-1 altimetry: Ridge segmentation versus spreading rate. *Journal of Geophysical Research-Solid Earth*, 114, -.
- Sclater, J. G., & Christie, P. A. F. (1980). Continental Stretching - an Explanation of the Post-Mid-Cretaceous Subsidence of the Central North-Sea Basin. *Journal of Geophysical Research*, 85(Nb7), 3711-3739.
- SIO, S. I. o. O. (2009, 12.09.2009). Radar Altimetry. *Satelite Geodesy*, from http://topex.ucsd.edu/WWW_html/mar_grav.html
- Skar, T., Van Balen, R.T., Arnesen, L., Cloetingh, S. (1999). Origin of overpressure on the Halten Terrace, offshore Mid-Norway: the potential role of mechanical compaction, pressure transfer and stress. In A. C. Aplin, Fleet, A.J., Macquaker, J.H.S. (Ed.), *Muds and Mudstones: Physical and fluid flow properties* (Vol. 158, pp. 137-156): Geol. Soc. Spec. Publ.
- Smith, J. E. (1971). The dynamic of shale compaction and evolution of fluid pressure. *Math.Geol.*, 3, 239-269.
- Sneider, J. S., de Clarens, P., Vail, P. R. (1994). Sequence stratigraphy of the middle to upper Jurassic, Viking Graben, North Sea. In J. S. Steel, Felt, V. L., Johannessen, E. P., Mathieu, C. (Ed.), *Sequence stratigraphy on the Northwest European margin: Proceedings of the Petroleum Society Conference* (Vol. 5, pp. 167-197). Stavanger: NPF Special publication.
- Statoil, T., Norsk Hydro, Saga. (1978). *Completion Report Well 24/12-1*.

- Talwani, M., Worzel, J. L., & Landisman, M. (1959). Rapid Gravity Computations for 2-Dimensional Bodies with Application to the Mendocino Submarine Fracture Zone. *Journal of Geophysical Research*, 64(1), 49-59.
- van Balen, R. T., & Skar, T. (2000). The influence of faults and intraplate stresses on the overpressure evolution of the Halten Terrace, mid-Norwegian margin. *Tectonophysics*, 320(3-4), 331-345.
- Ziegler, W. H., Doery, R., Scott, J. (1986). Tectonic habitat of Norwegian oil and gas. In A. M. e. a. Spencer (Ed.), *Habitat of Hydrocarbons on the Norwegian Continental Shelf* (pp. 3-20). Stavanger: Graham & Trotman for the Norwegian Petroleum Society.

Appendix A: Some MATLAB programs used in the modeling

Figure A1 shows the workflow of modeling a seismic line, and below, some of the programs used in this thesis are described in more detail.

- Interpret seismic line
- Digitize the interpretation to an ascii-file, e.g. line1a.asc

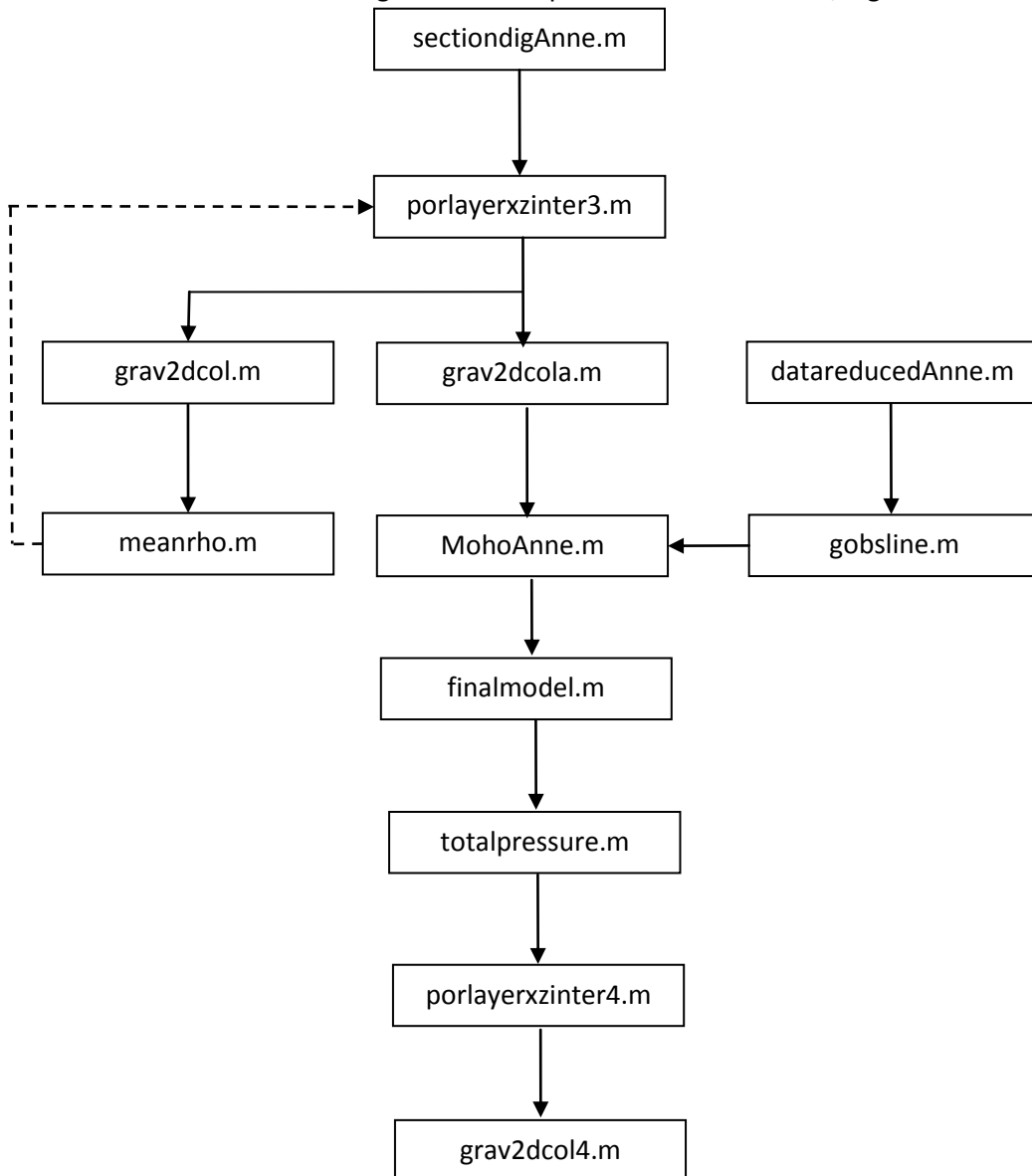


Figure A1: The workflow of modeling the seismic lines in chapter 5

Appendix A: Some MATLAB programs used in the modeling

Some details about the programs in figure A1:

- ***sectiondigAnne.m***

The program plots an interpreted and digitized seismic profile and transforms it (after equispacing) to a depth profile using given layer velocities.

- ***porlayerxzinter.m***

These programs estimates the density in the model from given lithology and porosity parameters. The porosity is corrected for changing overburden pressure.

- ***grav2dcol.m***

These programs calculate the gravity from the gridded density method.

- ***MohoAnne.m***

The program calculates the depth to Moho using the iterative Cordell and Henderson's method. The observed gravity is loaded from gobslines.m, see flow-diagram, figure 7.1.

- ***finalmodel.m***

This program plots the final crustal model, and the observed and calculated gravity field.

- ***totalpressure.m***

The program calculates the lithological pressure and Moho depth using Airy.

Description of some other MATLAB-programs used in this thesis:

- ***porlayer.m***

These programs calculate the porosity-depth curve for a multilayered model. Correct for effective pressure at top of layers.

- ***vertcol.m:***

The program calculates the gravity from vertical 2D columns.

- ***grav2dparker.m***

The program calculates the gravity from a multilayered model, using Parker's Fourier-method.

- *grav2dpoly.m*

The program calculates the gravity from a multilayered model, using the polygon method (Talwani et al.1959).